Eidgenössische Technische Hochschule Zürich
Swiss Federal Institute of Technology Zurich

Master of Advanced Studies (MAS)
In Hydraulic Engineering

ÉCOLE POLYTECHNIQUE
FÉDÉRALE DE LAUSANNE

MAS practical research project

Hydrology and check dams analysis in the debris flow context of Illgraben torrent (VS)

Hydrological analysis, evaluation of the check dams stability and their role on the debris flow dynamic

Hydrologie et barrages de consolidation dans le contexte des laves torrentielles du torrent de l'Illgraben (VS)

Analyse hydrologique, évaluation de la stabilité des barrages de consolidation et leur rôle dans la dynamique des laves torrentielles

Technical report

Candidate

Glassey Thierry
Av. de Tourbillon 58
1950 Sion
076/204.72.73
thierry.glassey@epfl.ch

Responsible for the follow-up

Dr. Brian W. McArdell
Swiss Federal Institute WSL
Zuercherstrasse 111
CH-8903 Birmensdorf
Tel. +41-44-739-2442
brian.mcardell@wsl.ch

Dr. Peter Molnar
ETH Zurich, HIL G 28.2
CH-8093 Zurich
Tel. +41-44-633-2958
molnar@ifu.baug.ethz.ch

Dr. Eric Bardou
Rue de l'Industrie 45
1950 Sion
Tel. +41 27-324-0384
eric.bardou@crealp.vs.ch

Management representative

Prof. Dr. Paolo Burlando
ETH Zurich, HIL G 33.1
CH-8093 Zurich
Tel. +41-44-633-3812
Fax +41-44-633-1061
paolo.burlando@ifu.baug.ethz.ch

ACKNOWLEDGEMENTS

I’m very grateful to my supervisors, Dr. Brian McArdell, head research group at WSL, Dr. Peter Molnar from the chair of hydrology and water resources management at the Institute of environmental engineering of ETHZ and Dr. Eric Bardou, scientific collaborator at CREALP for their support and precious advices throughout the thesis work. They devoted a lot of time to answer my questions and discuss the main issues on the work. They also allow me to familiarize with the very interesting topic of debris flow and numerical models.

I am very thankful to all the WSL/SLF staff and especially Mélanie Raymond-Pralong, Christoph Graf, Marc Christen, François Dufour and Albert Böll for all their essential comments, advices and explanations.

Thanks to Giovanni de Cesare for his patience and answers during this MAS.

I would also like to thank all the people working at CREALP for their support and pleasant coffee breaks, and especially Pascal Ornstein, for the data and infrastructures he put at my disposal.

Special thanks go to Romain Minoia for his fruitful collaboration and discussion about hydrological issues.

And last but not least thanks to my family for their encouragements throughout this MAS formation and a very last but very special thanks for my girlfriend Aline who helps me so much in the elaboration of this thesis, who had the patience and the strenght to support me during all the paintful periods; thanks for everything.

SUMMARY

The Illgraben catchment, due to its particular geological and geomorphological features, is one of the most active debris torrent in Switzerland. An hydrological analysis was performed through a frequency analysis of the surrounding ANETZ (Meteoswiss) stations and rainfall interpolation with GIS methods to finally get the IDF curve for the area (assuming several hydrological behaviour). Flood peak discharges were calculated with the software HAKESCH and flood hydrograms, based on an empirical method, allowed to define the resulting flood volumes for several return period.

Check dams installed across the whole Illbach channel were also studied to get an overview of their functions; geomorphological and sediment transport interactions were analysed in order to understand the trumps and weaknesses of these structures. Numerical model AVAL-1D was used to look at the behaviour of debris flow at the vicinity of check dams and assess its reliability to reproduce the reality. Finally a trial was done with the model RAMMS to confirm the previous results and test an experimental bed erosion module.

RESUME

Le bassin versant de l'Illgraben est un des torrents à laves torrentielles les plus actifs de Suisse. Une analyse hydrologique, comprenant une analyse fréquentielle des stations ANETZ entourant l'Illgraben (Meteosuisse) ainsi que l'utilisation des SIG pour l'interpolation des données pluviométriques au bassin versant de l'Illgraben, a permis de construire la courbe IDF de la zone étudiée. Les débits de crues ont été calculés à l'aide du logiciel HAKESCH ainsi que les volumes de crue, basé sur des méthodes empiriques, pour différentes périodes de retour.

Une étude a également été menée sur les barrages de correction torrentielle installés le long de l'Illbach afin de faire un inventaire de leurs différentes fonctions; sur la base de considérations géomorphologiques et de charriage, on a pu établir leurs points forts et leurs faiblesses. Le modèle AVAL-1D a servi à étudier le comportement des laves au droit des seuils et leur propension à reproduire la réalité. Finalement, des tests ont été effectués avec le modèle RAMMS pour confirmer les résultats précédents et évaluer un module expérimental d'érosion du lit du torrent.

TABLE OF CONTENTS

TABLE OF FIGURES

TABLE OF TABLES

1 INTRODUCTION

1.1 General context

The Illgraben is a well-known steep headwater catchment prone to very frequent debris flow activity. It is located near the village of Susten, canton Wallis, in the southwestern part of the Swiss Alps and extends from the summit of Illhorn (elevation 2716 m a.s.l.) to the confluence of the Illbach and the Rhone River (610 m a.s.l.). Compared to its relative small area (~10km^2), the Illgraben catchment has developped, since the Rhône glacier started to retreat (~15’000-10’000 years ago), a very important fan (~7km^2) that forced the Rhône river to deviate its path to the toe of the north flank of the Rhône valley (Figure 1). The fan increased in size as debris flows deposited material along its way down to the Rhône. The unusual size of the fan could be explained by the geological and morphological features of the catchment.

Protection measures have been built following the catastophic event of 1961 and a general safety concept has been elaborated at the beginning of the 21th century in order to assess the potential hazards that might threaten the Susten village and cantonal infrastructures. A monitoring system was set up (including three raingauges, a radar device, two video cameras, and a force plate) with the goal to warn the authorities, the people in charge of security as well as the population for coming debris flows.

Figure 1. Situation of Illgraben and Illbach catchments (Google Earth™)

1.2 Historical review of Illgraben debris flow processes

1.2.1 Historical records

The Illgraben is well-known over Switzerland for its recurrent debris flow activity and the size of its fan tends to prove it. Appendix 3 lists all recorded events since the beginning of historical records in 1932. The biggest debris flow ever recorded occurred in 1961. This event is described in detail in section 1.2.2. From this event, the historical records were divided into 4 parts:

- 1961 to 1965: 21 events are listed (rockfall debris source for debris flows).
- 1965 to 1982: no event recorded
- 1982 to 2000: 13 events recorded
- 2000 until now: 31 events recorded

The temporal varability of the results is strikening: sometimes many events occur per year and sometimes, over a long period, there were no events recorded. If the 1961 rockfall event provided an important sediment source for debris flow and thus consequently high frequency of debris flow are understandable, the distribution of events over ~80 years leads to the following comment: either there are processes in the catchment that increase debris flow frequency during some periods (1961-1965, 2000-2008) and the remaining time the processes are less actives, or there are others factors which play a role, like anthropic ones.

The former is hardly defensible because the two period cited above correspond to an exceptionnal event and to the installation of measurement devices respectively; moreover, for the 2001-2008 period, a study have shown there seems to exist a cycle of wet and dry years, leading to more or less frequent events; but this approach is based on only 7 years of measurements (Berger & al., in prep).

The second hypothesis formulated above is much more realistic for several reasons: until 1961, excepted for 1945, the scarce records might be due to a relative unconsciousness of the potential hazard and small events might have been 'forgotten'. Since 1961, this hazard became a reality and a cautious attention felt on the following events. When the retention dam (check dam n°1) was built, the hazard decreased and people felt in security; as debris flow started again, records started too, with less than one event/year on average and since the measurement devices were installed, numerous events per year were recorded. These assumptions lead to believe that anthropic factors (i.e. accuracy of recording all events) might mislead the interpretations; results from historical data should be taken cautiously when assigning return period to events.

1.2.2 The 1961 event: the awareness of hazard and protection measure concept

In April 1961, a huge rockfall of ~3.5 millions cubic meters of stones and fines occured at the back of Illgraben catchment. It spread until the actual location of check dam n°1 and blocked the Illgraben torrent, creating a natural dam which collapsed in June 1961. The lake outburst triggered a huge debris flow (estimated volume of 500'000 m^3) that filled the channel, overflowed in many places, destroying houses in Susten and the cantonal's road bridge. This event blocked the main valley road for several weeks. In 1962 the canton allowed credits to start the correction of the torrent, in order to protect people and infrastructures against the destructive force of debris flows.

In autumn 1963, boreholes were undertaken for geological investigations and studies were conducted until July 1965. In August 1967, the correction works started and lasted until end of 1969 for the first step, which included a concrete dam and 2 check dams. During the 1970's, 27 other check dams were built (Appendix 1 and 2).

Between 1965 and 1982 (see also Appendix 3) no debris flow were related; there are two reasons that could explain this fact: the first one is that the book in which alla data were recorded was lost; the second reason is that maybe there were debris flow, but of unsignificant importance (or they stopped on the upper part of the fan); this is due, at least for the first year (s) to the construction of the check dam n°1 (a 50m-high retention dam which was built to stabilize the huge unstable mass remaining from the 1961 rockfall). This dam, situated at ~1000 m a.s.l., filled up in one or a few events but at least prevented for 17 years big debris flows to occur. From 1982, debris flows started again and occurred almost every year from this date [28]. From the 30 check dams built about 1/3 are actually burried or destroyed.

1.3 Geological and geomorphological features

Geological and geomorphological studies were conducted in Illgraben to determine the potential triggering area as well as the kind of material that could be delivered. Geomorphological studies were performed to understand the processes and potential future developments.

1.3.1 Geology

The deep and steep Illgraben valley is incised at the border between two tectonic units: on one side the thrust contact of the Siviez-Mischabel sheet and on the other side, the Pontis sheet (Figure 2, Figure 3 and Figure 4). This thrust has been refolded and verticalized (Figure 4). On the northern side, the whole Gorwetsch crest (see Figure 3) is composed of triasic marble limestones and dolomites, both making up the cover of the Pontis sheet. At the contact between the sheets, we find breccias as well as 'rauwackes'. On the southern sideslopes, the permo-triasic cover of the Siviez-Mischabel thrust forms the whole northern flank of Illhorn and is composed almost entirely of quartzites. One has to distinguish between two types of quartzites: the white, massive ones, of inferior Trias age and the green ones, sericitic and frequently conglomeratic, given to Permo-Trias. The latter contain brown, ankerit-rich layers, that are interpreted as paleosoils [65]. Decametric layers of vacuolar and pulverulent quartzites (called Zucker-Quartzit in German) are found at the border of pinched synclines of 'rauwackes', dolomites and triasic limestones. All these rocks are intensively fractured, due to their belonging to the Rhône-Simplon fault system.

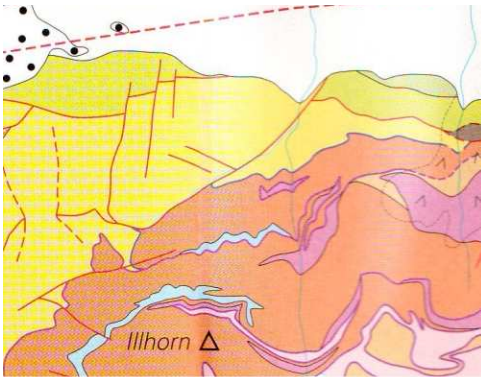

Figure 2. Tectonic map of Illgraben area (Geological atlas of Switzerland©swisstopo). The cover of the Siviez-Mischabel sheet is shown in pink-red and the cover of the Pontis sheet in yellow-green. Legend in Appendix 5

Figure 2 shows the contact zone between the two tectonical sheets, with the fault running along the Illbach and Illgraben torrent. This fault is at the origin of the erosion process. Indeed, a torrent finds its way on areas where it can erode the most easily. Faults and tectonical weaknesses are totally appropriate location fur such purpose. The contact of two cover sheets as well as the large fault (i.e. ramification of the major Rhône–

Simplon fault system) induced a heavy fracturation of rocks and created easy erodable layers like breccia, kakyrites,etc.

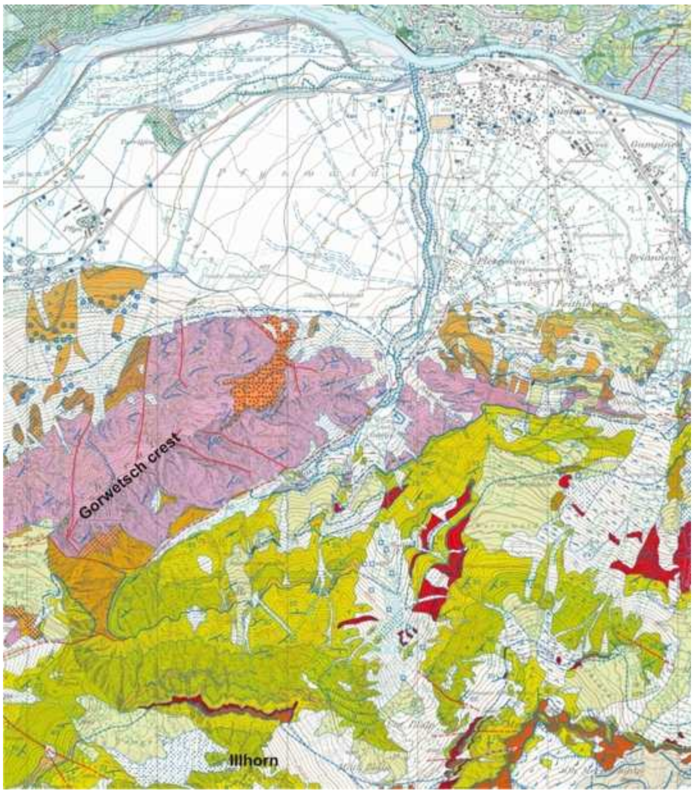

Figure 3. Geological map of the Illgraben area (Geological atlas of Switzerland©swisstopo). Legend in Appendix 6

The dolomite is unusually susceptible to weathering and provides a large amount of silty material. The calcareous deposits and dolomites are strongly jointed and repeatedly cause landslides. The petrographic composition of the deposits was determined from several samples taken in the fan in order to detect the sediment sources and their percentage within the sediment output [56].

Table 1. Petrological composition and distribution of the rocks in Illgraben [56]

Quartzite	**Quartzite with rose-Qz**	**Greywacke**	**Dolomite**	**Calcite**	**Schist and Gneiss**
Southern slopes	Southern slopes	Northern slopes	Northern slopes	Northern slopes	Channel bed
43.7%	16.8%	1.9%	3.0%	20.5%	14.2%

A petrographic analysis in the coupled system (i.e. areas directly linked with the channel) was performed and it showed that more than 60% of the sediment output comes from approximatively 6% of the entire catchment (southern flanks, under Illhorn). The dolomites represents 25% of the entire sediment budget. The 1961 event was triggered in these dolomites walls. The channel bed (schist and gneiss) provides only 15% of the entire sediment supply.

Figure 4 shows clearly the imbrication of the two sheets and the vertical fault related to the Rhône-Simplon fault system.

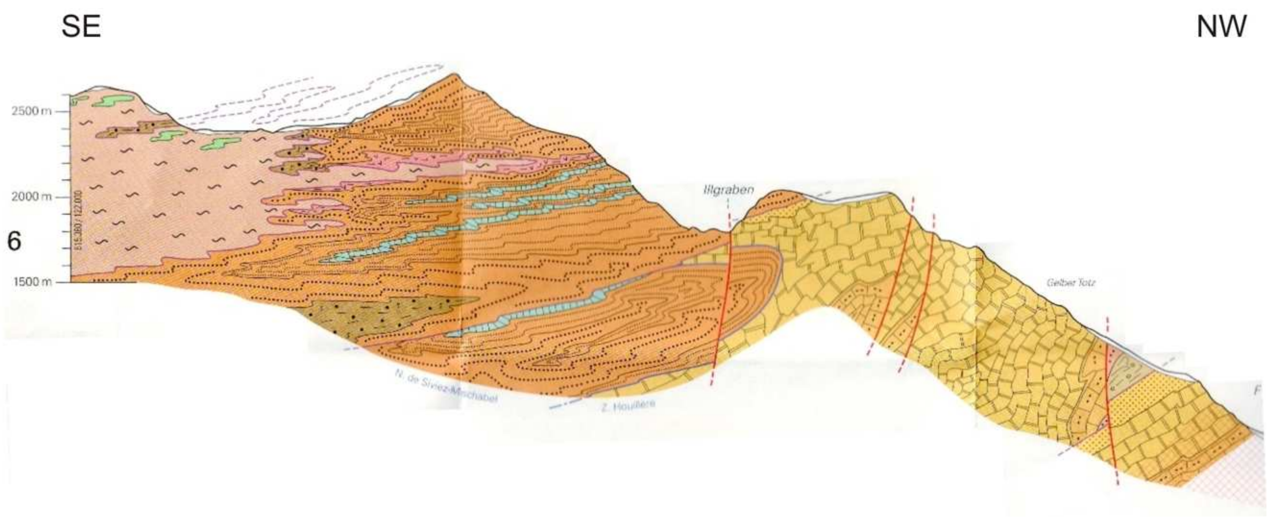

Figure 4. Geological cross-section of the Illgraben area (Geological atlas of Switzerland©swisstopo). Legend in Appendix 7

1.3.2 Geomorphology

The Illgraben area is divided into two catchment: the Illbach catchment (whose Illsee hydropower reservoir catchment were removed from the study) and the Illgraben catchment which is the source of debris flow. The latter (4.7 km^2) is characterized by very steep slopes (100% on average) whereas the former (3.7 km^2) reaches an average of 75%. The channel itself has mild slopes (compare to other mountain torrents) ranging from 20% at the back of the Illgraben catchment to ~10% on the fan. Figure 5 shows the distribution of slopes over Illgraben and Illbach catchments.

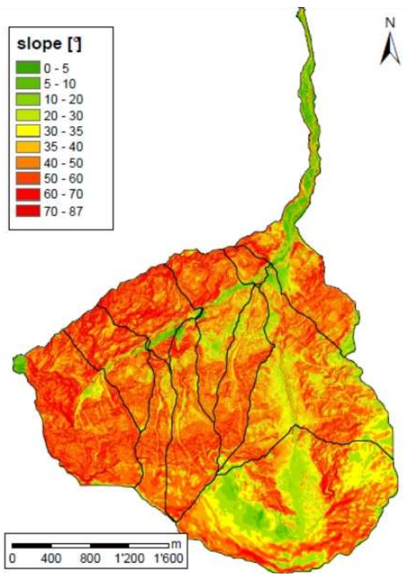

Figure 5. Distribution of the slopes in the Illgraben and Illbach catchment [45]

1.3.2.1 Triggering areas

Geomorphological and aerial photography analysis were performed in previous studies to determine the areas prone to provide material for debris flows initiation [23],[45],(pers. communication Bardou and Figure 7). Results delineate four active to very active zones in debris flow processes (Figure 6): the big gully at the back of the catchment composed of highly weathered rocks, without any vegetation; the big channel, eroded and without vegetation too; the Vanoischigraben, a very active gully and the Steinschlaggraben, whose debris flows sometimes overflow check dam n°1 without going through its spillway (pers. communication Bardou).

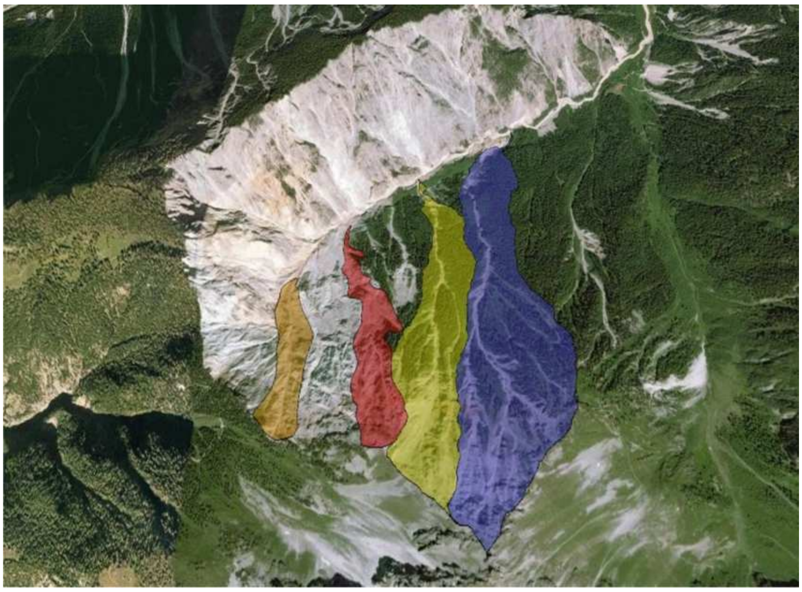

Figure 6. Location of the four most active zones in Illgraben catchment (orange: gully very active at the most back of Illgraben; red: big channel; yellow:Vanoischigraben; blue: Steinschlaggraben). Google Earth™

These four zones are presently very active and with global warming, the permafrost layer conditions at high altitude would certainly change, resulting in a probable increase of soil destabilization and debris flow frequencies and magnitudes.

Snow avalanches seem to play an important role in the triggering mechanism of debris flows: indeed, as the catchment is very incised and rockfalls important, snow firns are protected from melting until quite late in the season and act as a potential additionnal source of water; they also keep the soil saturated: this feature leads to a shorter response of the catchment on a rainfall event and thus increase the runoff coefficient.

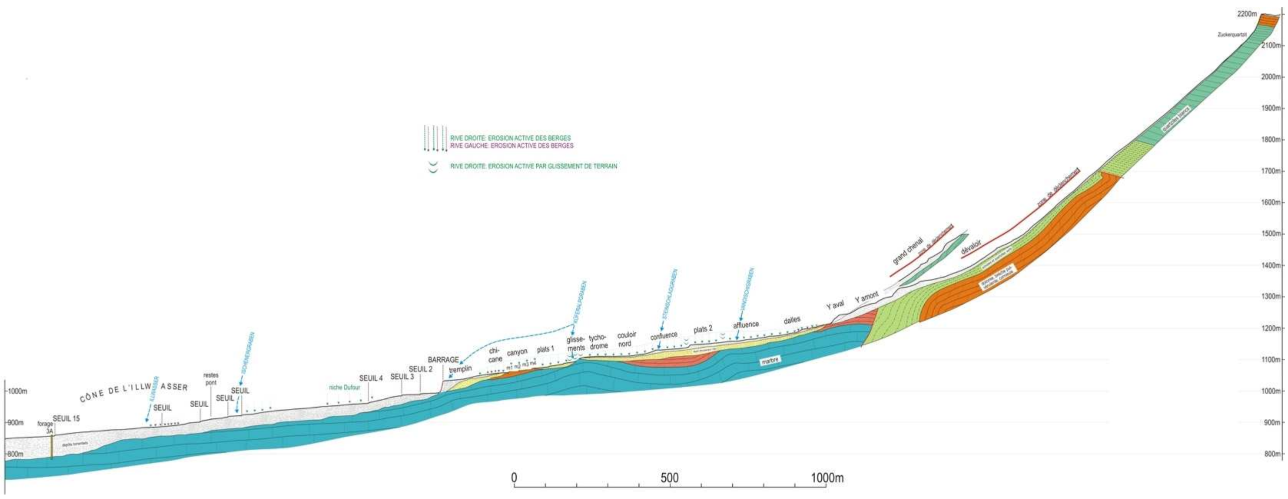

Figure 7. Longitudinal geological profile of upper Illgraben catchment (Sartori, 2001)

1.3.2.2 *Sediment balance*

The sediment volumes delivered by Illgraben into the Rhône are estimated to be around 22% of the total yearly Rhône sediment budget.

A study [56] was conducted on the bulk sediment volumes tranferring through Illgraben (only the part coming from the southern flank of Illhorn was calculated, this zone being considered as the main source for debris flows), both on annual records (2000 to 2006) and on a time span of 45 years. The conclusions are:

- an average sediment loss of 80’000 m^3/year for the 45 years analysed (in fact this volume corresponds to a analysis done with images from 1959 and 2004 from which the mass balance was derived)
- an average annual volume of 120’000 m^3 is assessed to transit to the Rhône river (estimations 2000-2006); considering that ~60% of the channel bed is composed with material coming from the southern flanks of Illhorn, a volume of ~72’000 m^3 was assessed as coming from this area. This is in the same order of magnitude than the previous calculation.

This study, if providing satisfying results, has the disadvantage not to take into account the bedload transport, which is a major sediment transfert process in Illgraben.

1.3.2.3 Illbach fan morphology

The fan of a torrent usually shows its activity. The Illgraben fan is unusually large in comparison with similar catchments in the region. After a rough estimation of deposited material, the radius and volumes were estimated to be 2 km and 500’000’000 m^3 respectively. The left bank, mainly covered with forest, show numerous debris flow traces (gully, levee, flow front). The right bank is much more urbanized and lots of traces have been erased, but the local appellations are significative of debris flow past activities [72].
A geomorphological analysis of the fan [19] has shown that its evolution during the last 500 years could be divided into 3 phases: an active building phase from 1412 to 1880, followed between 1880 and 1970 by a phase where sedimentary dynamics was positive (accretion of terraces) and from 1970 up to now, a stable phase, where the Illgraben fan seems to be in an equilibrium, which is not the case for the fan apex zone.

1.3.2.4 Landuse and coupled/decoupled systems

The Illgraben catchment is composed to 44% of rocky area, 42% of forest area and 14% of grassland area.
In [23] the distinction is made between coupled and decoupled system, where the coupled system consists only of erosion areas that are connected to the channel network; 27 to 45% of total catchment is considered as connected, depending on the intensity of a rainfall event; the coupled system provide more than 99% of the sediment leaving the catchment [23]. The decoupled system was divided into three subsystems: grassland, forest and decoupled erosion. The decoupled system showed almost no correlation with precipitation as in the coupled system, where every precipitation event with an intensity larger than 2mm/10min was associated with a debris flow occurrence [23].

1.4 Instrumentation

The global protection concept and warning system for Illgraben started in 1999. In this frame, a complete monitoring system was installed between 2000 and 2003. It includes 3 geophones, a force plate, 2 video cameras, a radar device and 3 automatic rain gauges.

The geophones measure the ground vibrations produced by a passing debris flow and log the data as impulses if the amplitude of the vibrations, transmitted as voltage, exceed a threshold magnitude of 200mV. The geophone data represents the vibration intensity as integrated information since the sensors record the number of exceedings during 1 seconde.

Except for the raingauges, all devices are situated along the channel on the debris fan (Figure 8). The radar device, mounted at the cantonal road, measures the flow depths. Its also provides the debris flows hydrograms. The three geophones were installed in the middle and lower part of the fan within about 500m. The geophones trigger the measuring devices and velocity can be calculated from the time difference between the geophones and the radar device. The three rain gauges are located in the southern part of the drainage basin (n°1 is located at 2200 m a.s.l, n°2 at 1630 m a.s.l. and n°3 at 950 m a.s.l), which is the primary debris flows initiation zone [28].

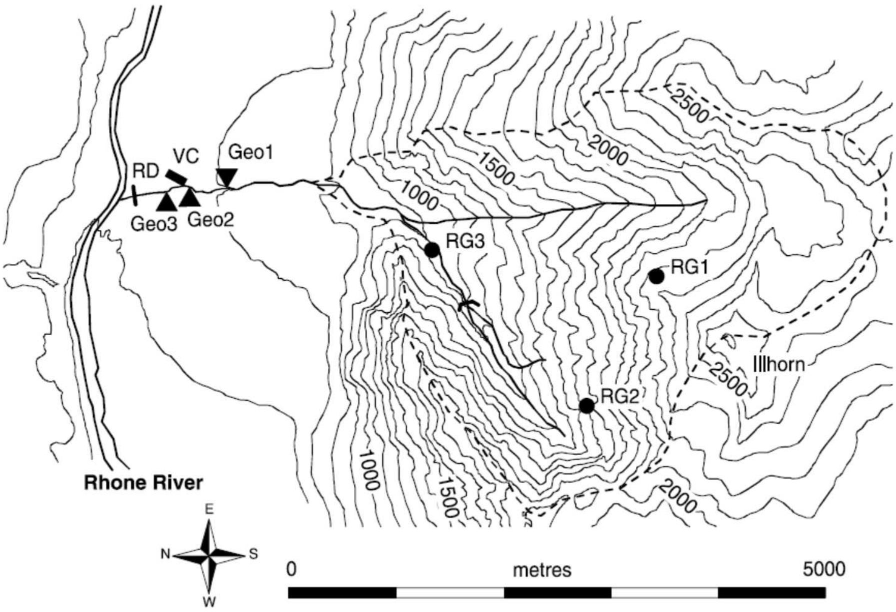

Figure 8. Monitoring system of Illgraben in 2001 (RD: radar device; VC:video camera; GEO;geophone; RG:rain gauge) [28]; the force plate, situated at the same location than the radar device, was mounted in 2003.

1.5 Objectives of the work

The main objectives of this work are:

(I) to perform an hydrological analysis based on a frequency analysis of rainfall data in order to get an IDF curve for Illgraben; to estimate peak discharges for several return periods with their corresponding hydrograms (Chapter 2 and 3).

(II) to understand the effects and interactions of the check dams on debris flows and floods from field data (Chapter 4).

(III) to perform numerical simulations of debris flows with the models AVAL-1D and RAMMS to evaluate the performance of these models in reproducing the flow behaviour close to the check dams, as well as checking the actual limits of these models (Chapter 5).

2 HYDROLOGICAL ANALYSIS

2.1 General setting and objectives

The climate in Illgraben is strongly influenced by its location in an alpine valley: a mild climate and a low annual precipitation [28]. The mean annual precipitation ranges from 700mm in the lower part of the drainage basin to 1700mm at the Illhorn (BAFU, 1999).

The Illgraben torrent is prone to many research studies mainly focus on the behaviour and particularities of the debris flow events (several events/year) rather than on the triggering mechanisms. In 1999, the canton ordered a complete study of the catchment in order to assess the potentially hazardous areas and establish a warning system concept; theses studies treated the different topics related to steep headwater basin: geomorphology, geology, hydrology, erosion and sediment transfer as well as debris flow activity monitoring [23],[28],[29],[30],[40],[45],[56].

The objectives of the first part of this work are numerous:

- rainfall analysis with recent datasets and comparison with other documents (HADES, IDF curves made by WSL)
- elevation influence on precipitations
- rainfall interpolation methods
- construction of DDF and IDF curves for the Illgraben basin
- design discharge calculation
- design hydrograms creation

2.2 Short literature review on hydro-meteorological studies in Illgraben

Several authors have shown that often there exists a rainfall intensity threshold above which debris flows occur. Caine (1980) and Zimmermann & al. (1997) have suggested the following relations between the critical intensity and the duration of a rainfall event:

$I_{crit} = 14.82\ D^{-0.39}$ (Caine, 1980) Eq.1

$I_{crit} = 21\ D^{-0.72}$ (Zimmermann and al, 1997) - for internal Alps areas Eq.2

where

I_{crit} = critical rainfall intensity [mm/h]

D = rainfall duration [h]

Several critical intensities have been calculated [72], following Eq.1 and Eq.2 and are given in Table 2.

Table 2. Critical rainfall intensity related to rainfall duration

Rainfall duration	Rainfall intensity (Caine, 1980)		Rainfall intensity (Zimmermann & al., 1997)	
[h]	[mm/h]	Total [mm]	[mm/h]	Total [mm]
1	14.82	14.8	21.0	21.0
3	9.65	28.9	9.5	28.5
6	7.36	44.2	5.7	34.7
24	4.29	102.9	2.1	51.1

It was attempted to establish a correlation between rainfall and debris flow events (Figure 9). Unfortunately, to perform this study, the pluviometric distribution in the Illgraben catchment was not known very accurately. Only raingauges surrounding the Illgraben (Sierre, Grimentz and Hérémence) were used to establish the relation triggering factor – debris flow event. The dataset were composed of 24h-rainfall depth records measured from the beginning of the 20th century to the end of the 20th century. The 24h-rainfall records do not reflect accurately the stormy events (generally those that trigger debris flows). The intense, short-duration storms rainfall data are smoothed by daily records.

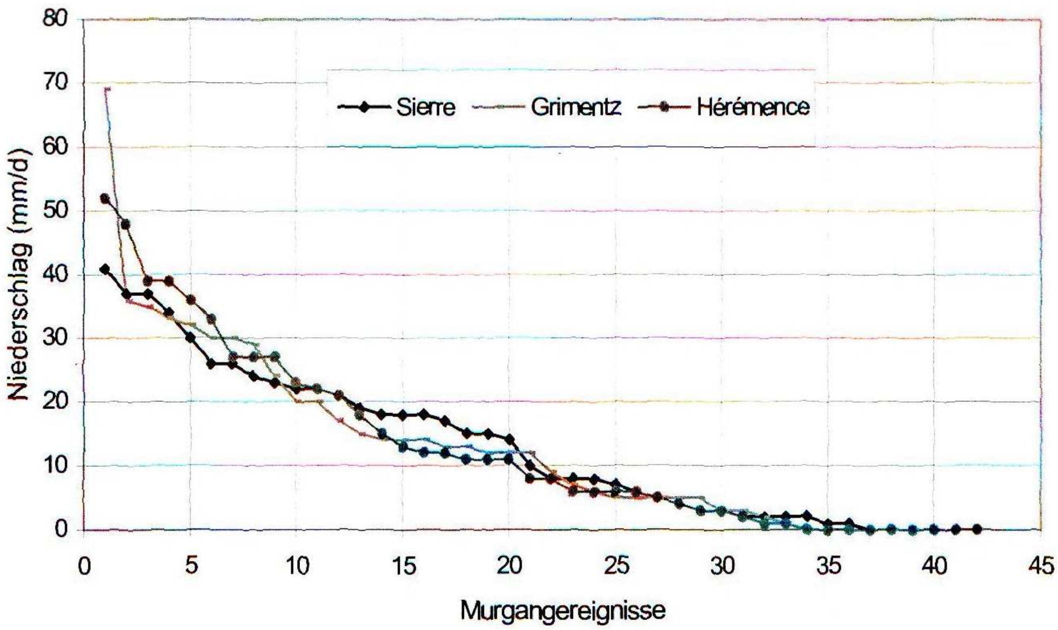

Figure 9. Relation between rainfall depths (stations of Sierre, Grimentz and Hérémence) and debris flow events (Zimmermann & al., 2001)

From the 3 stations used for the analysis (Sierre, Hérémence, Grimentz), it was said that the daily rainfall depths are similar; this assessment was extended, maintaining that the behaviour of precipitations in the main Rhône valley is quite similar to those on the side valleys (which is in fact fairly wrong). When analyzing the relation between precipitations and debris flow occurrence, no clear trend could be extracted from the results and has led to the following comments [72]:

- for almost half of the debris flow events, the daily rainfall sum was 10mm or less.
- for a few events, no rainfall was recorded at the 3 stations.
- what is the role of snowmelt in the debris flow initiation process?
- no rainfall threshold could be given for debris flow initiation.
- no event-volume could be found in comparison to precipitations volume.

As those results let some unsolved questions, we decided to conduct an analysis of the spatial and temporal distribution of the precipitations based on recent and accurate rainfall records coming from the 5 nearest ANETZ stations (automatic raingauges belonging to the MeteoSwiss network) around Illgraben.
At present, 3 raingauges are installed in the Illgraben catchment [28] to better catch the stormy rainfall patterns (raingauge timestep=10min) and the hydro-meteorological behaviour of the area.

2.3 Hydrological frequency analysis

The aim of a frequency analysis is to analyse the distribution of measured data in order to find theoretical distribution laws that fit as best as possible the empirical values. By this procedure, we are able to obtain interpolated/extrapolated rainfall values for any duration and return period (but the smaller the measurement period, the higher the uncertainties for high return period); such an analysis leads to the creation of the Intensity-Duration-Frequency curves (IDF), useful tool to characterize and predict the precipitations of a given area.

For this work, the frequency analysis was performed on the 5 ANETZ stations surrounding the Illgraben catchment. These stations are listed in Table 3. The frequency analysis could have been done with the data coming directly from the Illgraben raingauges, and results would have been highly improved, but unfortunately, records are available only since 2001, which is too short to perform a useful frequency analysis; even with 25-30 years of records, the extrapolations to 100-, 300 years return period are quite rash.

Table 3. Characteristics of ANETZ stations surrounding the Illgraben area

ANETZ station	X-coordinate	Y-coordinate	Elevation	Distance from Illgraben catchment centroid	Available records (10min-data) / period of operation
[-]	[m]	[m]	[m.a.s.l]	[m]	[year]
Sion	592200	118625	482	22860	1981-2008
Visp	631150	128020	640	17230	1979-2007
Montana	603600	129160	1508	11470	1981-2008
Zermatt	624300	97575	1638	29080	1982-2007
Evolène	605415	106740	1825	20120	1986-2007

The elevation ranges and distances from Illgraben catchment are very heterogenous (see Figure 10). For this reason, we have used several methods to look whether a consistency in the data exists or not.

2.3.1 Description of the data used for the frequency analysis

The ANETZ stations used in our study (10min. timestep records) are operating since 25-30 years (Table 3). The resolution is very high, making the size of the datasets huge (~53000 data per year). We received 2 datasets. The first one included the maximal annual precipitations for 1h, 3h, 6h, 12h and 24h and the second one the complete record (in order to get the 10-, 20- and 30min. annual maxima). Due to measurements and probably technical problems, some data are missing (especially in the first years after installation of the stations) and others are inconsistent. This led to a careful attention given to the data: all data showing a value of 32767 indicate an error in the dataset. These values were deleted. All the maxima were then checked (the hypothesis was that a peak value had to be included in a storm event, (i.e. with increasing or decreasing rainfall depth before and after the peak intensity) and not be an outlier among no or weak precipitation rainfall values).

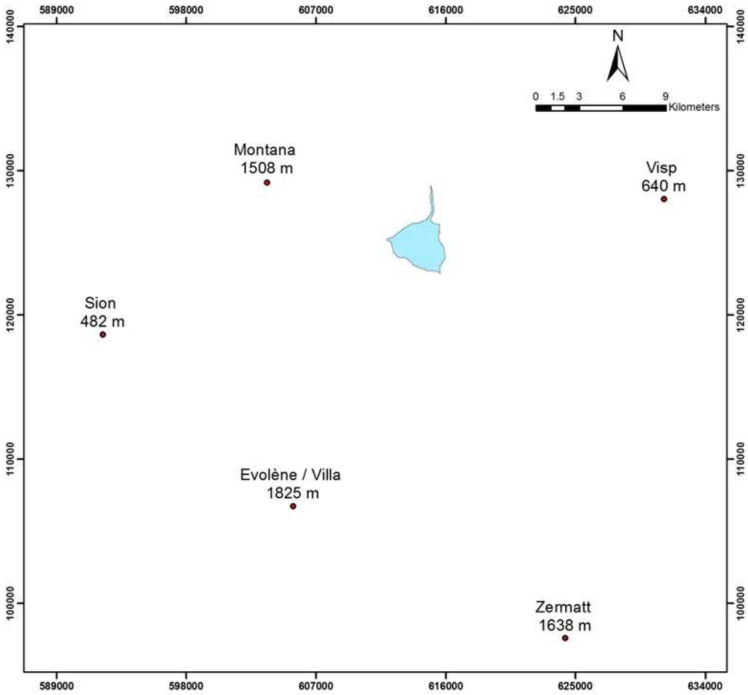

Figure 10. Situation of the ANETZ stations surrounding the Illgraben catchment (in blue)

2.3.2 Frequency analysis process

2.3.2.1 Empirical frequency functions and probability distribution functions

The 10min. data were mainly used to refine the IDF curves below 1h duration; the reason behind this is that the rainfall that triggers debris flows are often of stormy pattern, with maximum intensities lasting closer to 10min. than 1h.

The 10-, 20-, 30min., 1h, 3h, 6h, 12h and 24h maximum intensities were sorted from minimum to maximum. A rank n_i was given to each variable x_i, going from the smallest to the biggest value. Then for each rank n_i, a relative frequency was assigned with the relation:

$$f_s(x_i) = \frac{n_i}{n} \qquad \text{Eq. 3}$$

where n = sample size

From these discrete values, we calculated the cumulative frequency function, given by:

$$F_s(x_i) = \sum_{j=1}^{i} f_s(x_j) \qquad \text{Eq. 4}$$

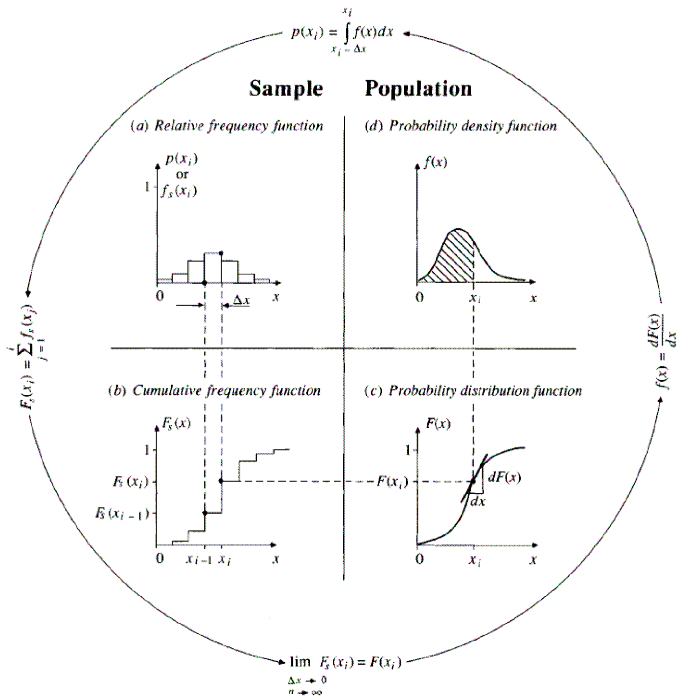

Figure 11. Empirical frequency functions and probability distribution functions (extract from [9])

By this way, we get the frequency of occurrence assigned for each of the observed value. These cumulative frequency functions are sometimes called plotting positions; a probability is then assigned to the observations, with:

$$P(X \geq x_m) = \frac{m}{n} \qquad \text{Eq. 5}$$

where m = rank of the observed value
n = sample size

There exist many empirical distribution functions, and almost all can be summarized in a general expression, which guarantees symetry around the median [43]:

$$F(x_{(m)}) = \frac{m-c}{n+1-2c} \qquad \text{Eq. 6}$$

where m = rank of the observed value
n = sample size
c = coefficient contained between 0 and 0.5

The existing formula was reviewed by Cunnane [16] who came to the conclusion that the choice depends on the related population. He recommands to use Gringorten formula for a Gumbel distribution, but according to [43], the best compromise should be Hazen formula.

In order to decide which one fits the best our data, we used the following relations:

Weibull : $\frac{i}{n+1}$ Eq. 7

where i = rank of the observed value
n = sample size

Gringorten: $\dfrac{i-0.44}{n+0.12}$ Eq.8

Hazen : $\dfrac{i-0.5}{n}$ Eq. 9

We assigned a return period T to each empirical distribution. This was calculated with:

T(x) = 1/(1-F(x)) Eq.10

Following the process, the next step is the calculation of a probability distribution function (theoretical function based on a population) that can best fit our data. As one aim of the study is to look at a wide range of return periods, our choice turned on the GEV (Generalized Extreme Value) distribution functions, whose general form is:

$$F(x) = \exp\left[-\left(1-k\frac{x-u}{\alpha}\right)^{1/k}\right]$$ Eq.11

where k, u and α are parameters to be determined

Type I: Gumbel (k=0)

Type II: Frechet (k<0)

Type III: Weibull (k>0)

The common use in Switzerland for extreme values is the Gumbel distribution function.

Gumbel distribution (EV1) is given by: $F(x)=\exp\left[-\exp\left(-\frac{x-\alpha}{\beta}\right)\right] \quad -\infty < x < \infty$ Eq. 12

where: $\hat{\beta}=\frac{\sqrt{6}}{\pi}\cdot\hat{\sigma}$

$\hat{\alpha}=\bar{x}-\hat{\beta}C$;

C = Euler constant = 0.5772
α and β = parameters of the law

There must be as many independent moments as the number of parameters to be estimated; generally, the moments of low-order are chosen, like mean and variance (that are estimates, taken from the sample).

A few relations has been used to get the probability for each value, attribute a return period to each probability and finally calculate a rainfall depth for a chosen return period (in order to build the IDF curves). These relations, derived from Eq.12 are the following:

$$F(x)=\exp[-\exp(-u)]$$ Eq.13

$$u=-\ln[-\ln(F)]$$ Eq.14

$$u=\frac{x-\alpha}{\beta}$$ Eq.15

$$x=\alpha+\beta u$$ Eq.16

The frequency for each value of the distribution law is computed from the reduced variable u (as obtained from Eq.15). The return period T for each probability was calculated according to Eq.10. Finally Eq. 16 was used to obtain the rainfall depth for a given return period T.

At this stage, we are able to build the empirical (sample) frequency function and probability (population) distribution function.

2.3.2.2 Testing the goodness-of-fit

A test procedure (most often goodness-of-fit test) is used solely to accept or reject the null hypothesis H_0, which is, in our case: 'the distribution function (i.e. Gumbel) fits the observed values'. The goodness-of-fit constitutes an internal check of the model.

One of the test comprises the visual examination of the ajustements (graphically); this method seems quite basic, but still remains one of the best tool to judge to the quality of the fit. However, this method requires a long experience in the domain and is quite a subjective approach.

The other, more objective way of checking a fit, is to use a statistical test. The two more common are the Chi-square test (χ^2) and the Kolmogorov-Smirnov test. The former is used to compare the theoretical and the sample values of the relative frequency function and the latter is used to compare the theoretical and the sample values of the cumulative frequency function [9].

By using the Chi-square test, the following problems were encountered:

- Due to the small number of data, the division of the sample led to a reduced number of classes. Gibbons & Chakraborti [21] recommand that the theoretical size of values for each class should be five at minimum. They also demonstrate that the strenght of the test is maximal when the theoretical sizes within classes are the same. In our dataset, with ~20-25 values per sample, we get maximum five classes, which is very few.
- When calculating the score of χ^2_{obs} , we obtain really high values compared to the one calculated with a quantile at 90% or 95% confidence level of a Chi-square law.
- Due to a very low freedom number (which depends on the number of classes), the differences between the score calculated and the quantile obtained from Excel were huge and led us to reject systematically the null hypothesis (i.e. to consider the probability distribution function used to fit the empirical function as not appropriate).

The Kolmogorov-Smirnov test consists to measure, for a continuous variable, the maximum gap between the theoretical frequency and the empirical frequency.

We have first to define our null hypothesis H_0, then to calculate the d_{max} (which is the maximum difference between two points lying on the theoretical and the empirical frequency function). We then have to choose a check value c (which corresponds to 1-alpha, i.e. the confidence interval); we observed that this interval decreases as the sample size increases (see Appendix 21); this is in fact logical because the bigger the sample size is, the bigger the range of values we get, and thus the confidence interval 1- α decreases. This interval also diminishes as the significance level α increases (considering the fact that there are complementary).

We chose a significance level of 10%. We get the c-value and compare it with the test-value d_{max}. If d_{max} is smaller than c, then the null hypothesis (here the theoretical distribution function fits the observed data) is

accepted, and so the fitting distribution is correct. If not, H_0 has to be rejected and we have to use another distribution function.
In this study, we used both the visual ajustement method and the Kolmogorov-Smirnov test. Results are described in §2.4.

2.3.2.3 Interpolation and extrapolation values

After checking the probability distribution function is appropriate, we interpolated the rainfall depth for 2.33- 30-, 100- and 300 years return period (i.e. the most often used return period in Switzerland in term of probability of occurrence of an event). Results are listed in Appendices 8 to 13.

2.3.2.4 DDF and IDF curves

The last stage of this analysis was to build the Depth-Duration-Frequency (DDF) and Intensity-Duration-Frequency (IDF) curves. We used the 10-, 20- and 30min. (when suitables), 1h, 3h, 6h, 12h and 24h and 2.33-, 30-, 100- and 300 years return period to build them. Results are shown in §2.4.

2.4 Results of the frequency analysis

The results are displayed for the four ANETZ stations: Sion, Visp, Montana and Evolène (Zermatt was not used further on in the process as explained in §2.6 and results are displayed in Appendix 12). The graphs were done with rainfall depth on the X-axis and return period on the Y-axis, in a semi-logarithmic scale. The time-consuming analysis to extract the 10-, 20- and 30min. maxima led to results which could not be used for many of them because of inconsistencies between the complete dataset and the annual maxima dataset given (see §2.3.1); the way the data were treated probably varied from one dataset to the other.

2.4.1 ANETZ station : Sion

The 10-, 20- and 30min. values were not analysed for this station. By checking the results visually, one could assert that if for 3h, 6h and 12h, the fits look quite good, this is not the case for 1h and 24h (the extremes empirical values look quite far for the Gumbel distribution curve). The Kolmogorov-Smirnov test was applied and the results showed that all the Gumbel distribution fits has to be accepted as representative of the population.
The DDF and IDF curves are shown in Figure 12 and Figure 13, whose tables are listed in Appendix 8.

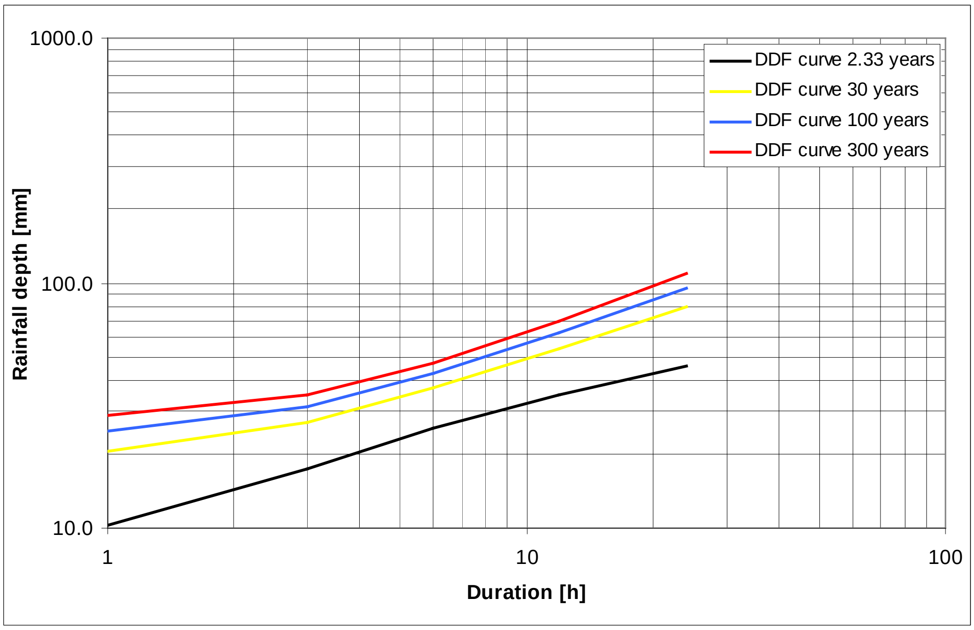

Figure 12. Depth-Duration-Frequency curve for Sion

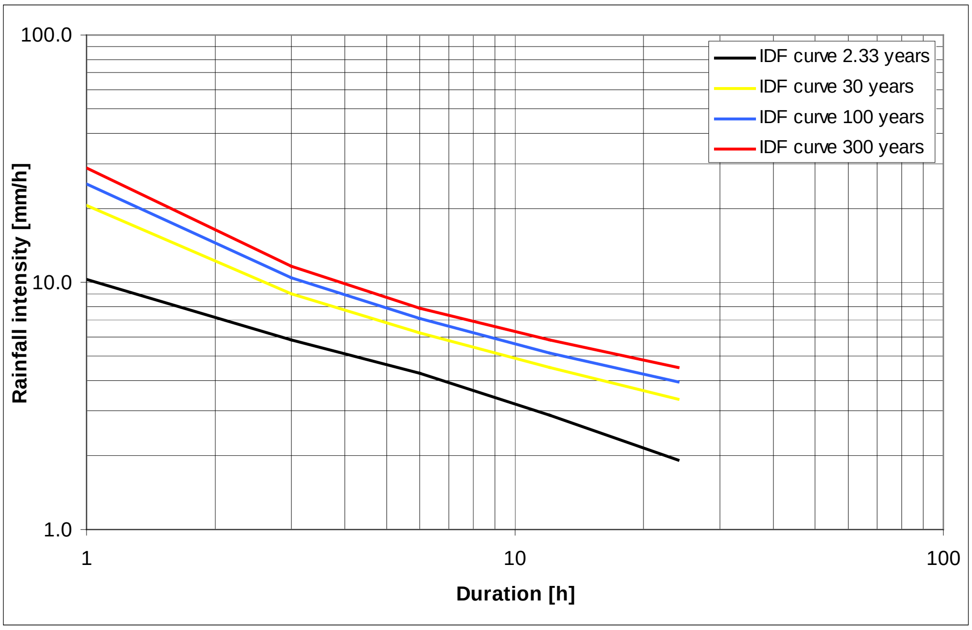

Figure 13. Intensity-Duration-Frequency curve for Sion

2.4.2 ANETZ station : Visp

Visual check for 10-, 20- and 30min., 1h, 3h, 6h, 12h and 24h shows pretty good adjustments for all the timesteps considered. The Kolmogorov-Smirnov test was applied and the results showed that all the Gumbel distribution fits has to be accepted as representative of the population.

The total dataset could be used to build the DDF and IDF curves. Results are shown in Figure 14 and Figure 15, whose tables are listed in Appendix 9.

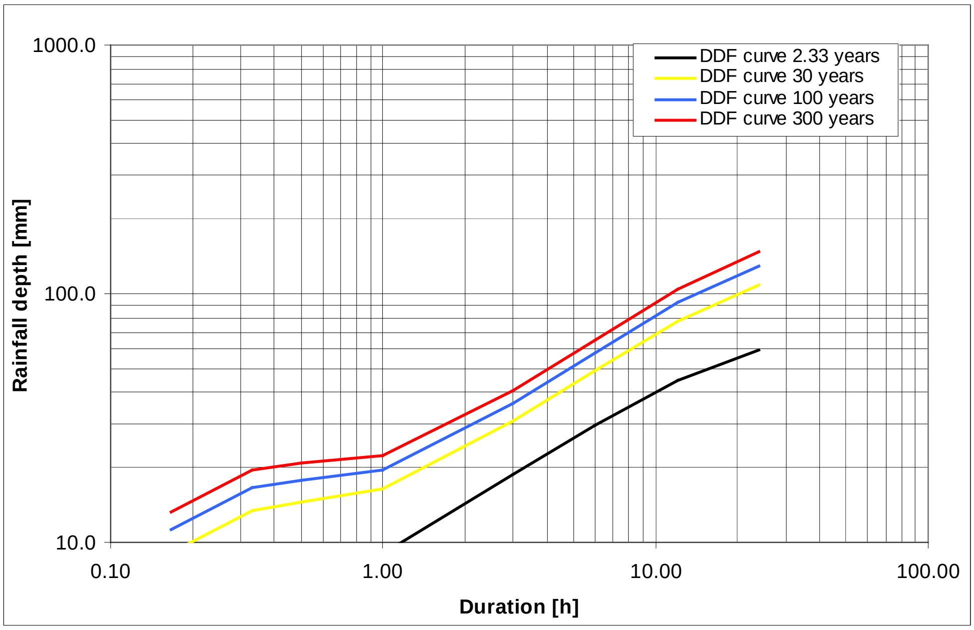

Figure 14. Depth-Duration-Frequency curve for Visp

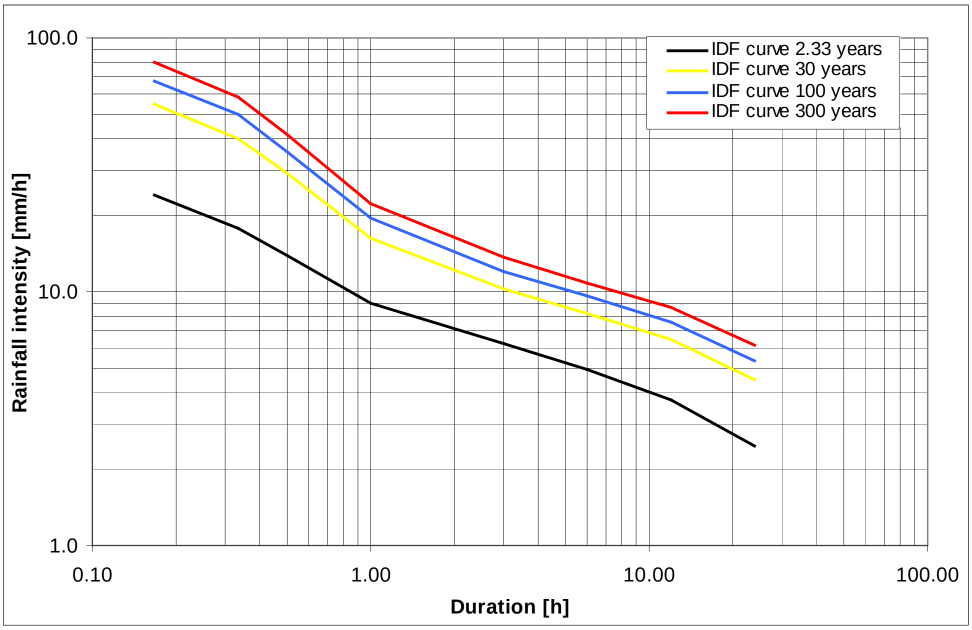

Figure 15. Intensity-Duration-Frequency curve for Visp

2.4.3 ANETZ station: Montana

The 10-, 20- and 30min. values were not analysed for this station. Visual monitoring reflects that for 3h, 6h, 12h and 24h the fits looks quite good, but not for the 1h (the extremes empirical values look quite far for the Gumbel distribution curve). The Kolmogorov-Smirnov test was applied and the results showed that all the Gumbel distribution fittings has to be accepted as representative of the population.

The DDF and IDF curves are shown in Figure 16 and Figure 17, whose tables are listed in Appendix 10.

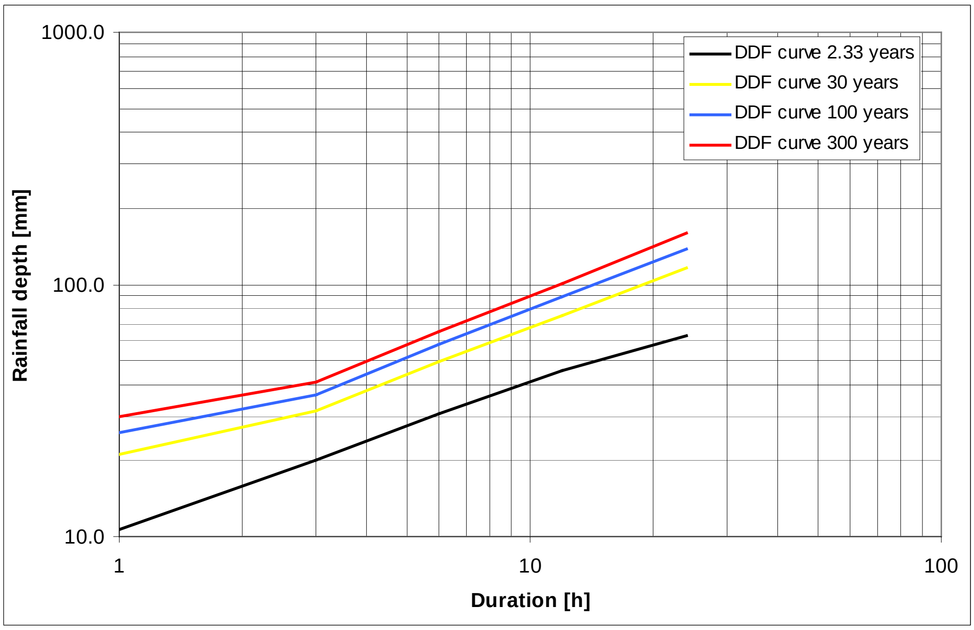

Figure 16. Depth-Duration-Frequency curve for Montana

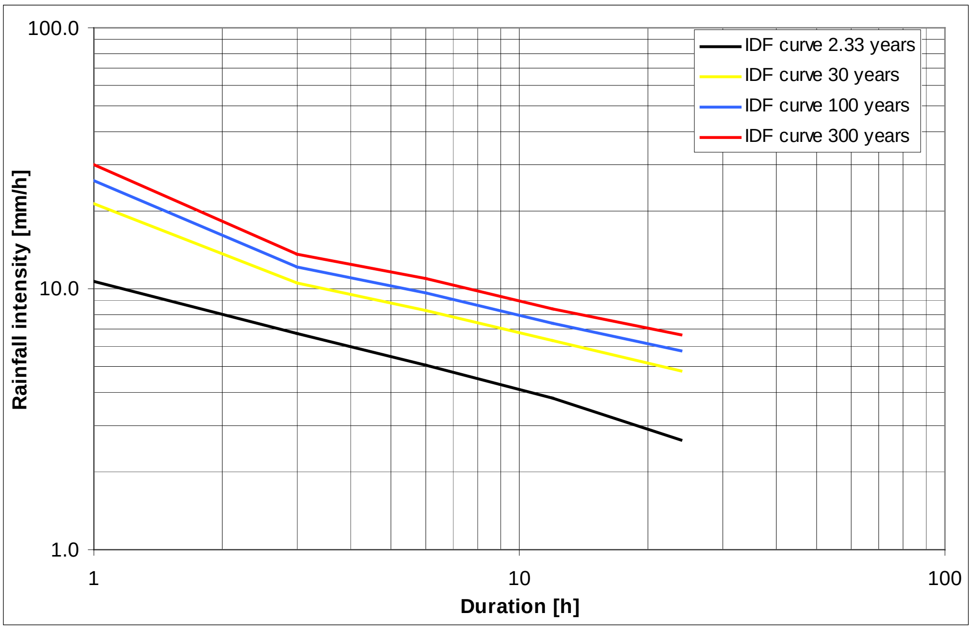

Figure 17. Intensity-Duration-Frequency curve for Montana

2.4.4 ANETZ station : Evolène/Villa

Visual inspection for 10-, 20-, 30min., 1h, 3h, 6h, 12h and 24h shows not too bad adjustments for all the timesteps considered. The Kolmogorov-Smirnov test was applied and the results showed that the Gumbel distribution fits all the time intervals considered, except for 30min., where the test at 10% confidence interval had to be rejected. We chose to use another GEV distribution function: the Fréchet (EVII) or log-Gumbel distribution function. The confidence interval was kept the same and after testing the data, the null hypothesis was not rejected.

To build the DDF and IDF curves, the 10- and 20min. intervals were included whereas the 30min. was rejected because of misleading results (i.e. fitted with another distribution function). One has to notice that the 20min. interval gives values close to the 1h interval; these values have to be taken with caution.
The total dataset could be used to build the DDF and IDF curves. Results are shown in Figure 18 and Figure 19, whose tables are listed in Appendix 11.

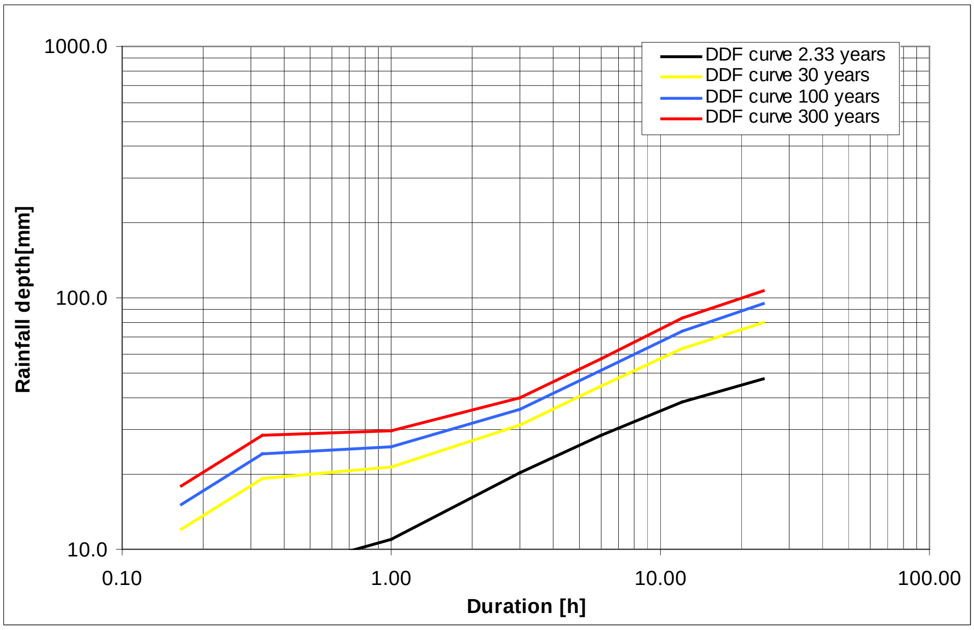

Figure 18. Depth-Duration-Frequency curve for Evolène

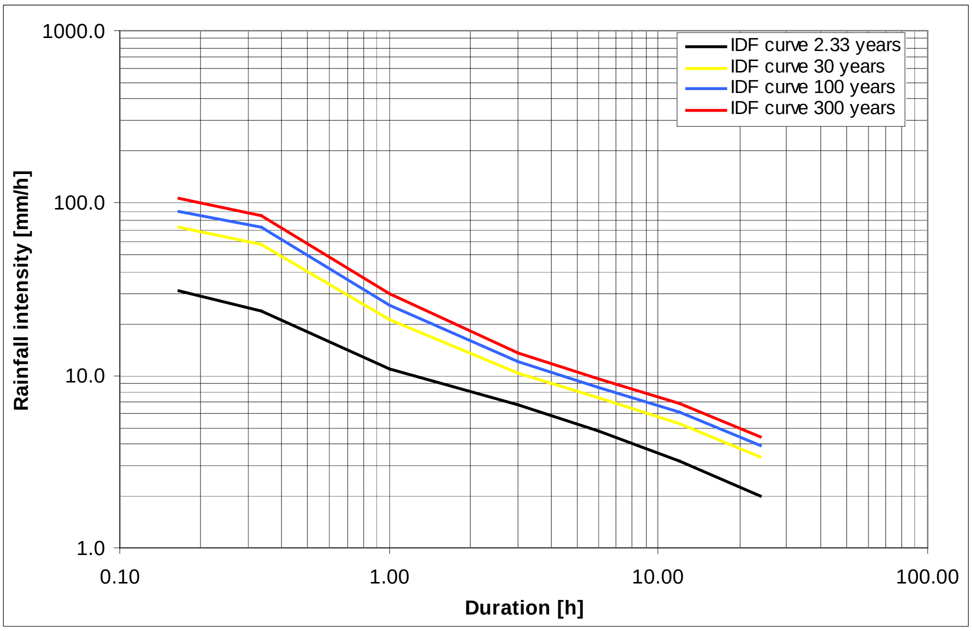

Figure 19. Evolene's Intensity-Duration-Frequency curve for Evolène

2.4.5 ANETZ station : Zermatt

Graphs for each timestep are listed in Appendix 5. DDF and IDF curves and related tables are displayed in Appendix 12.

2.5 Comparison with IDF curves from WSL

The IDF curves created during this work for the stations Sion, Montana, Visp and Evolène were compared with the one established by the WSL [69]. We interpolated and extrapolated from the WSL curves the values for T=30, 300 and 1000 years.

2.5.1 Sion

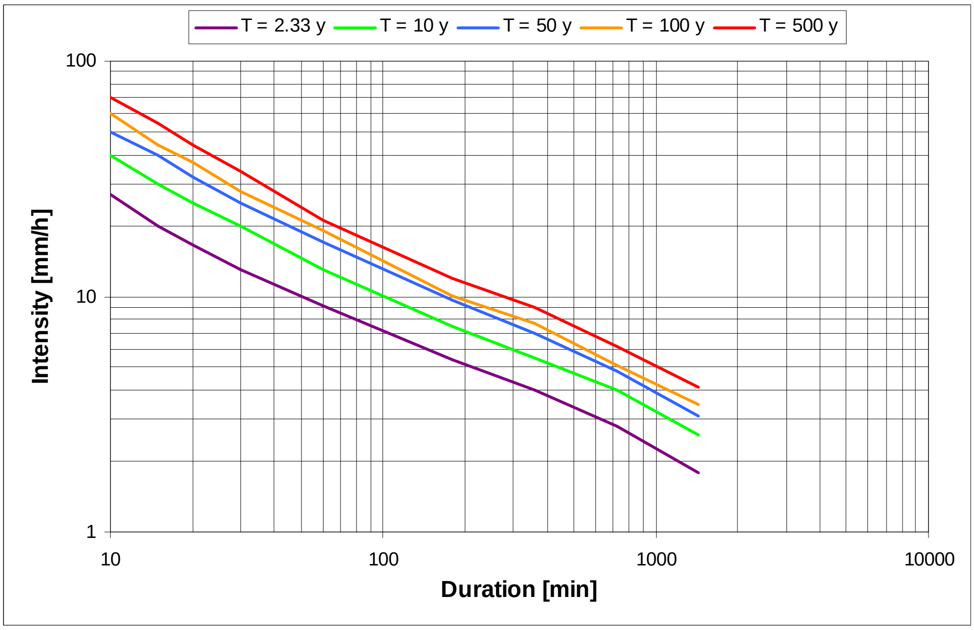

Figure 20. IDF curve for Sion [69]

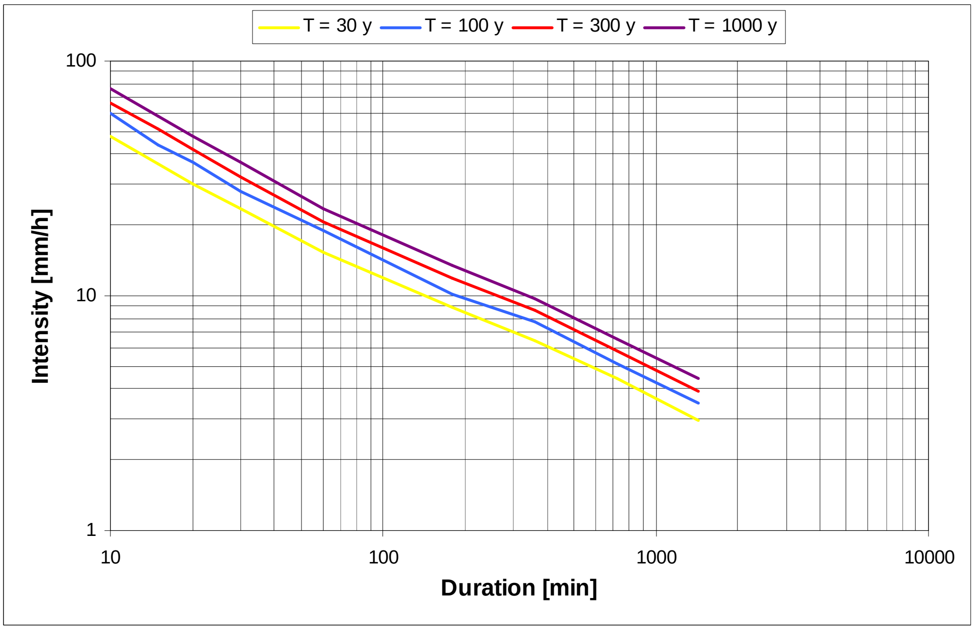

Figure 21. IDF curve for Sion (values interpolated and extrapolated from Figure 20)

Related tables and charts are listed in Appendix 13.

2.5.2 Visp

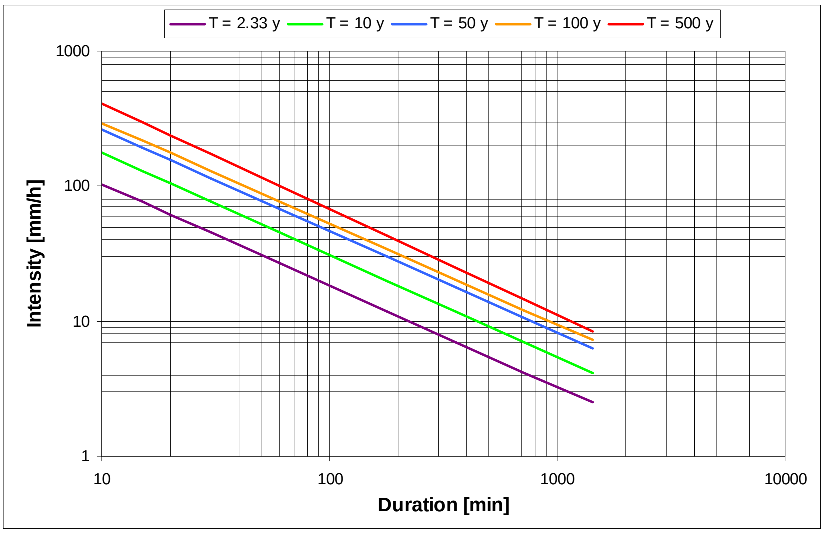

Figure 22. IDF curve for Visp [69]

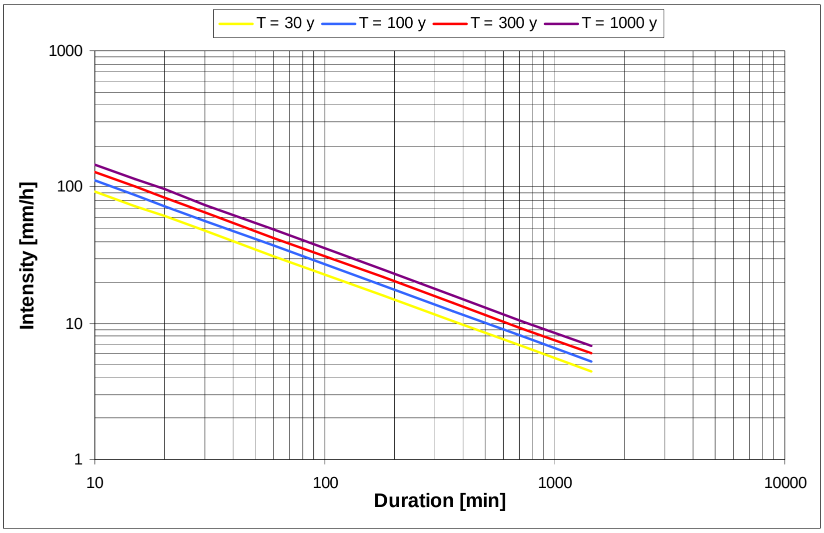

Figure 23. IDF curve for Visp (values interpolated and extrapolated from Figure 22)

Related tables and charts are listed in Appendix 14

2.5.3 Montana

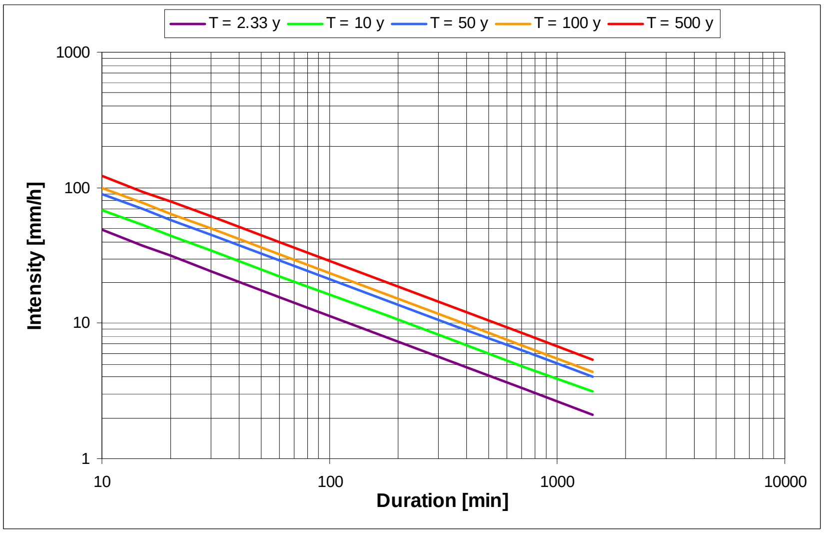

Figure 24. IDF curve for Montana [69]

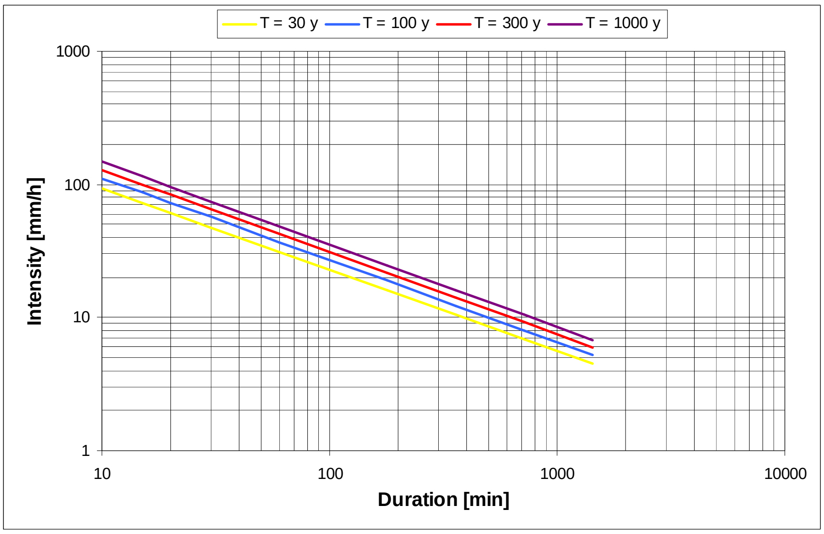

Figure 25. IDF curve for Montana (values interpolated and extrapolated from Figure 24)

Related tables and charts related are listed in Appendix 15.

2.5.4 Evolène

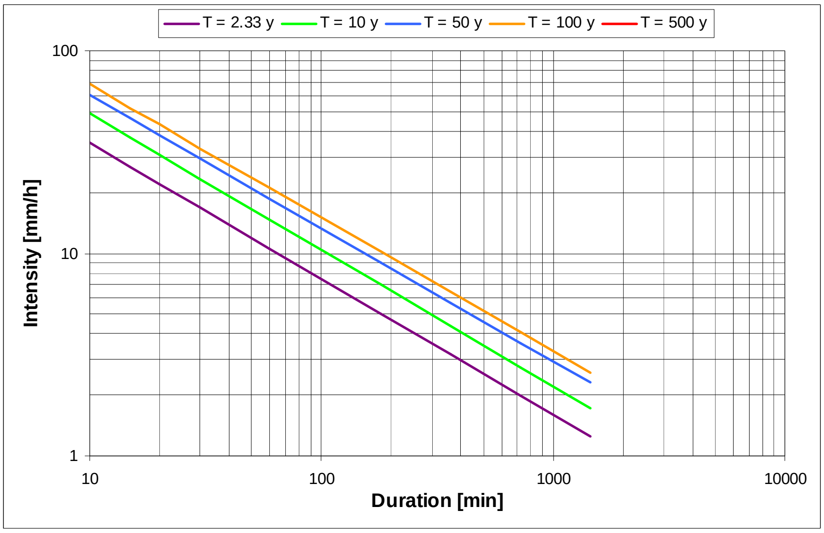

Figure 26. IDF curve for Evolène [69]

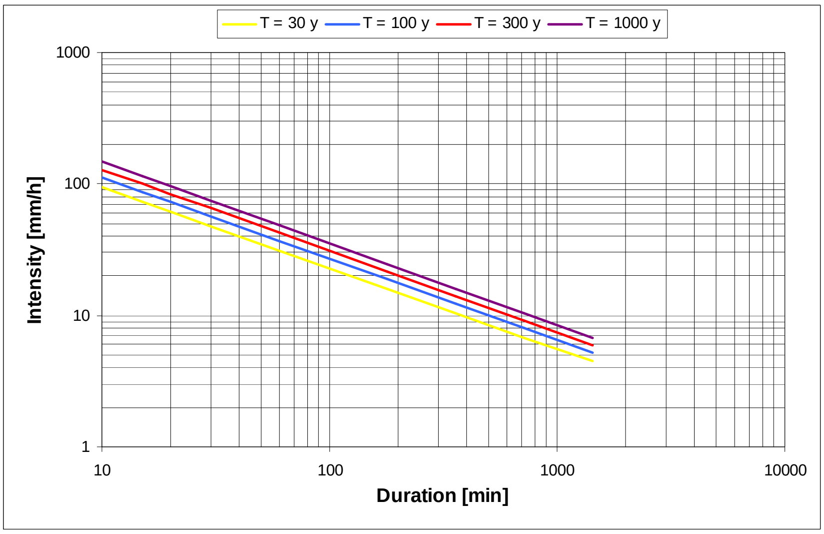

Figure 27. IDF curve for Evolène (values interpolated and extrapolated from Figure 26)

Related tables and charts are listed in Appendix 16.

A comparison have been done to look whether a constant shift appears between the two IDF curves or not and if the meteorological regimes between the period 1901-1970 and 1980-2008 are significantly different. The results are displayed in Table 4 to Table 7.

This analysis has shown that it is very difficult to find a consistent trend between the two series of data. This could be due to several factors and we made the following assumptions/comments:

- the data used in [69] are daily whereas from 1980 up to now, the timestep is 10min.; the interpolations done from a daily basis to finer timesteps leads inevitably to rash results.
- the precipitation distributions could have changed quite significantly in one century.

- measurement errors are in general diminished with ANETZ stations.
- the station of Sion operates since 1954; 23 years of data were used to build the IDF [69].
- the station of Evolène operated only for 11 years and was set 600m higher than the ANETZ one. The frequency analysis done in [69] is to take with caution.

Table 4. Comparison between the IDF curves obtained in this study (ANETZ data) and the WSL study (data ranging from 1954-1977) for the station Sion

Station	SION			
Return period [y]	T=2.33	T=30	T=100	T=300
Duration	Δ this study-WSL	Δ this study-WSL	Δ this study-WSL	Δ this study-WSL
[h]	[%]	[%]	[%]	[%]
1	13.2	32.8	31.0	39.8
3	8.0	0.7	2.6	-2.3
6	7.1	-3.5	-7.7	-8.7
12	3.3	0.9	1.8	-0.1
24	5.6	13.4	13.4	15.8

Table 5. Comparison between the IDF curves from these study (ANETZ data) and the WSL study (data ranging from 1913-1978) for the station Visp

Station	VISP			
Return period [y]	T=2.33	T=30	T=100	T=300
Duration	Δ this study-WSL	Δ this study-WSL	Δ this study-WSL	Δ this study-WSL
[h]	[%]	[%]	[%]	[%]
0.17	-76.7	-77.2	-76.9	-78.4
0.33	-71.1	-71.7	-71.6	-73.0
0.5	-69.5	-71.9	-72.3	-73.6
1	-66.6	-73.5	-74.8	-76.1
3	-47.2	-61.5	-64.7	-66.1
6	-30.0	-48.2	-52.7	-54.0
12	-10.2	-30.8	-36.9	-37.4
24	-0.8	-18.7	-25.7	-24.7

Table 6. Comparison between the IDF curves from these study (ANETZ data) and the WSL study (data ranging from 1929-1978) for the station Montana

Station	MONTANA			
Return period [y]	T=2.33	T=30	T=100	T=300
Duration	Δ this study-WSL	Δ this study-WSL	Δ this study-WSL	Δ this study-WSL
[h]	[%]	[%]	[%]	[%]
1	-31.8	-21.3	-19.6	-19.4
3	-14.6	-22.7	-24.6	-27.1
6	0.2	-6.5	-7.9	-10.5
12	15.5	10.5	9.7	6.9
24	24.1	30.5	32.5	30.6

Table 7. Comparison between the IDF curves from these study (ANETZ data) and the WSL study (data ranging from 1968-1979) for the station Evolène

Station	EVOLENE/VILLA			
Return period [y]	T=2.33	T=30	T=100	T=300
Duration	Δ this study-WSL	Δ this study-WSL	Δ this study-WSL	Δ this study-WSL
[h]	[%]	[%]	[%]	[%]
0.17	-11.1	26.4	32.6	38.4
0.33	7.6	58.3	66.7	74.3
1	3.5	21.4	22.8	25.2
3	33.1	23.0	18.2	16.6
6	50.3	38.7	33.0	31.1
12	61.3	56.0	51.0	49.9
24	59.6	57.0	52.5	51.8

As no clear relations were found within the dataset, we chose to use the IDF curves elaborated in the frame of this thesis, because the new available data from the ANETZ network provides more accurate rainfall depths than previously and hence representative results for timestep 1h, 3h, 6h, 12h and 24h.

2.6 Effects of altitude on rainfall distribution

Another aspect we looked into is the influence of the altitude on the precipitations. First of all, we would like to point out that in view of the distances and elevation differences between the stations, and in view of the micro-/macroclimates regimes that affect the canton of Wallis, the results shown below are to take with some care.

The Wallis is generally affected by three meteorological regimes: the continental, the oceanic and the mediterranean regimes [3] . These are responsibles for several microclimates and hence for the variability of the precipitations encountered in this canton as shown in Figure 28.

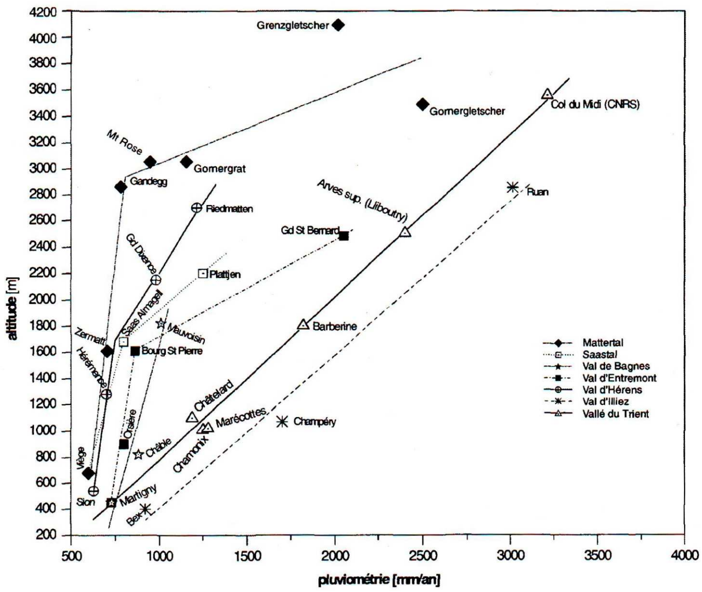

Figure 28. Precipitation gradients (function of altitude) through Penninic Alps and Mt-Blanc massif (Bezinge, 1974)

The basis for this analysis were the monthly and annual rainfall depth means (2001 to 2007) for the stations Sion, Visp, Montana, Evolène and Illgraben. The raingauge P1 in Illgraben (2210 m.a.s.l.) was used in this work because it is the most reliable of the three installed in the catchment.

After checking the data of Zermatt and after a few discussions about the meteorological regimes in Wallis, we decided to remove Zermatt from the further hydrological analysis: on one hand because Zermatt is affected by the southern precipitation that do not really influence Illgraben meteorological regime, and on the other hand because of its location (i.e. the furthest ANETZ of the five selected).

When plotting monthly rainfall depths vs. elevation (for all stations), many errors were observed on the graphs. Removing the winter and early spring values considerably enhanced the results. The reason for doing so is that during the winter months, only snow is falling at high altitudes and snowfalls are not recorded by raingauges (Appendix 19). Many other plots have been done for annual values, annual extrema for given duration (Appendices 17 and 18) but finally the monthly data have been used because we get the monthly rainfall depths for Illgraben and thus, we had an accurate comparison basis.

The effect of the precipitation gradient in Illgraben has been studied by Nydegger [45]. She focused on the precipitation data recorded by the three raingauges and analysed more than 20 storm events (only those showing a trend in precipitation increasing with altitude). She demonstrated that there exists a relative increase of precipitation amount linked to the differences of elevation between two points in the catchment. To ensure a link between the study of Nydegger and our, we applied the same methodology but based on the monthly precipitations instead of event ones. The results are shown in Figure 29 and Figure 30.

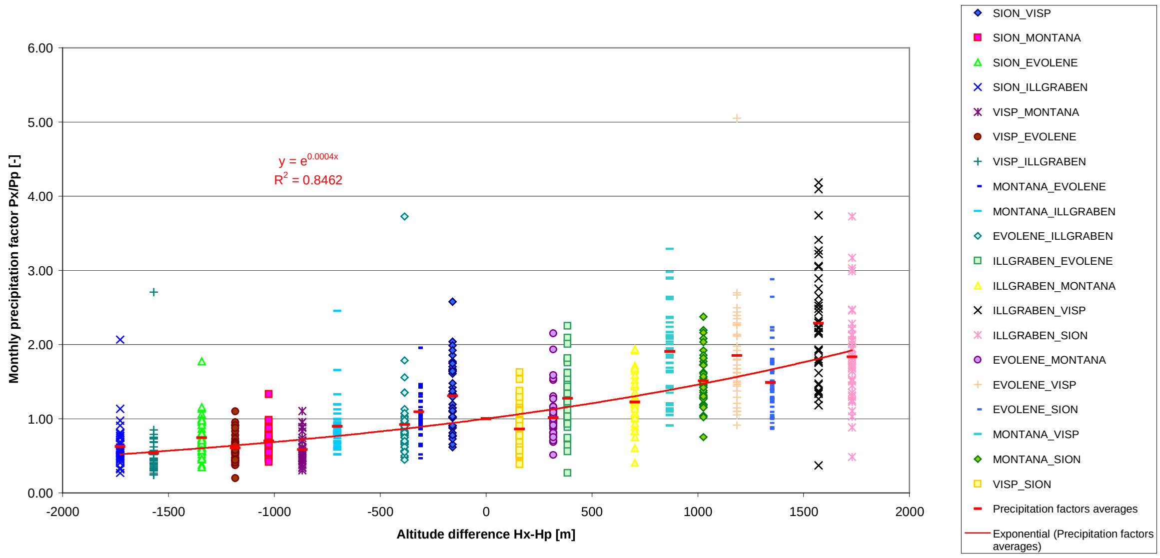

Figure 29. Monthly precipitation factor vs. altitude difference for stations Sion, Visp, Montana, Evolène and Illgraben – exponential ajustement

After computing the data and taking the mean of each serie of altitude difference (H_x-H_p), we obtained the following relations, for both linear and exponential regression functions:

***Linear regression*:**

$$P_x = P_p \cdot 0.0004 \cdot (H_x - H_p) + P_p \qquad \text{Eq.17}$$

Exponential regression

$$P_x = P_p \cdot e^{0.0004 \cdot (H_x - H_p)} \qquad \text{Eq.18}$$

where: P_x = precipitation at any point x in the catchment

P_p = precipitation at station P

H_x = elevation at any point x in the catchment

H_p = elevation at station P

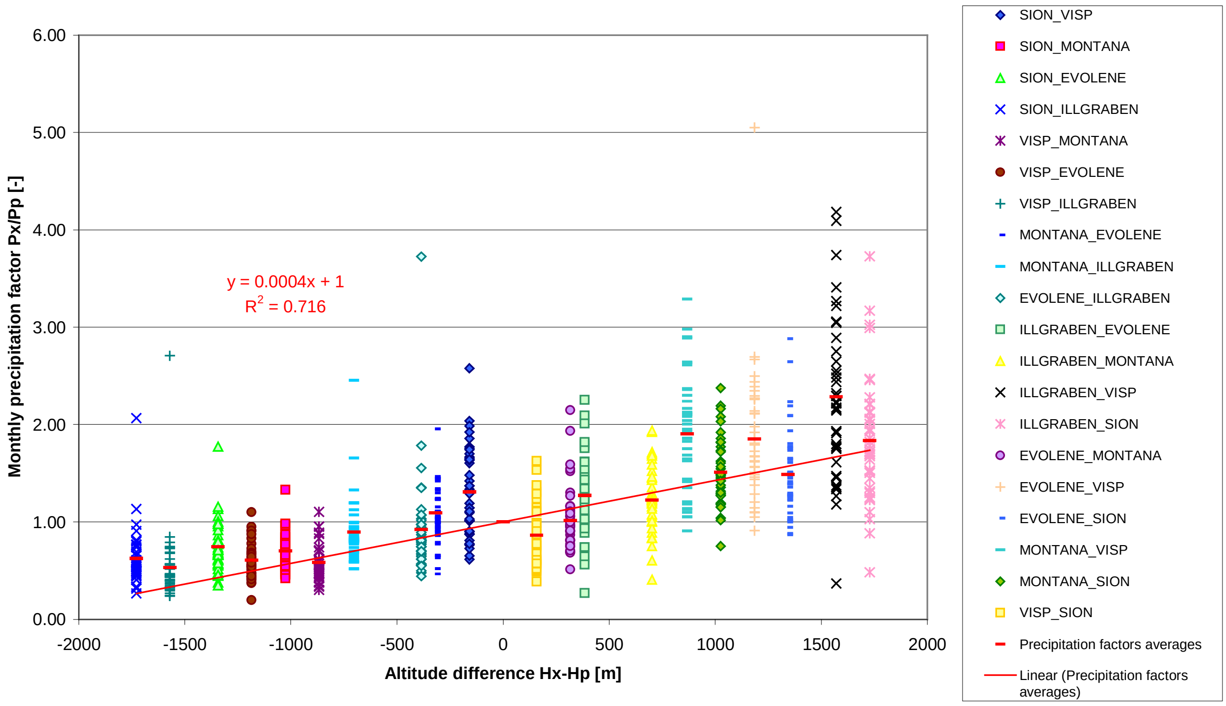

Figure 30. Monthly precipitation factor vs. altitude difference for stations Sion, Visp, Montana, Evolène and Illgraben – linear ajustement

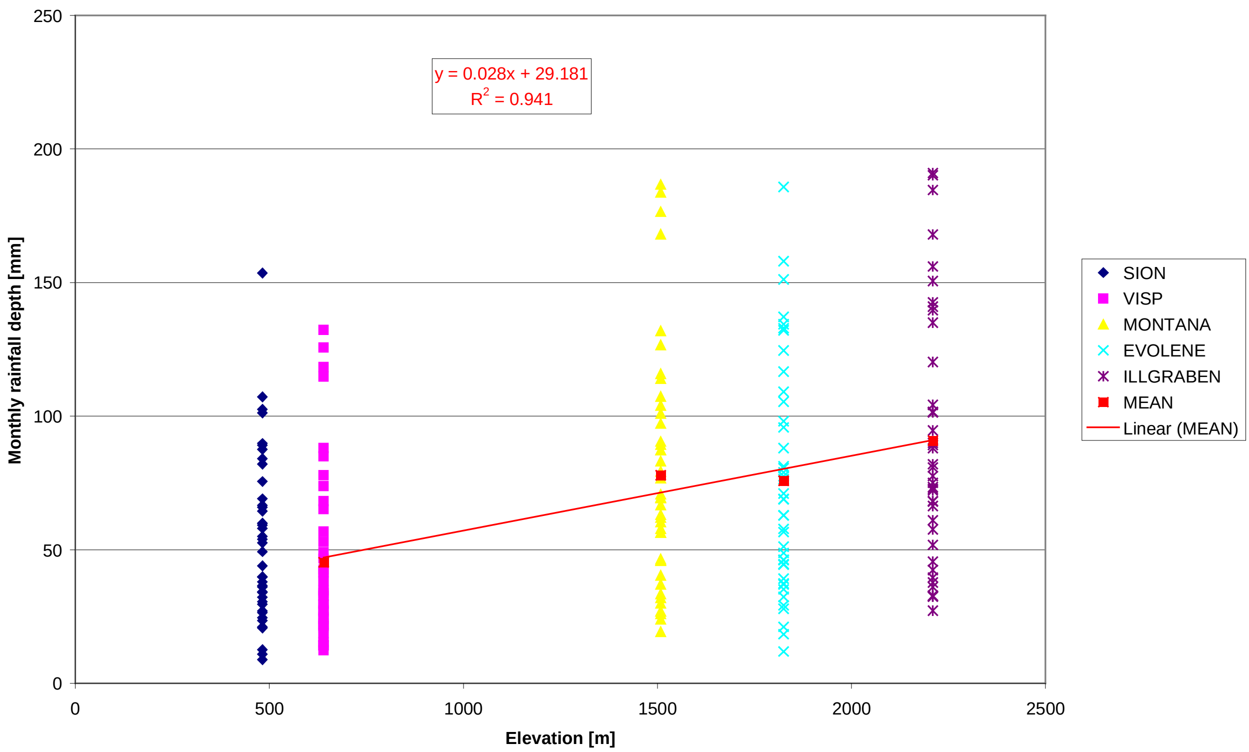

Figure 31. Monthly rainfall depth vs. elevation for the stations Sion, Visp, Montana, Evolène and Illgraben

A linear trend was chosen by Nydegger [45] to fit the data, choice that is discussed below. The reason for both linear and exponential function trials is based on the assumption that there is neither reason nor evidence that precipitations increase linearly with altitude; this assumption is partly verified based on the

correlation coefficient R^2 that shows a better correlation with the exponential function than the linear one. Figure 31 corroborates these assumptions; thus taking into account an altitude gradient for further analysis is rightful. But due to the high scatter amongst the data, one has to take this results cautiously.
Eq.18 has then been used to determine the different rainfall depths for each ANETZ; H_p is the elevation of the station and H_x was taken as the elevation equal to the centroid of Illgraben area (i.e. 1744 m.a.s.l.); this was done to bring back the precipitations of each stations to a value equal to the mean elevation of Illgraben (this is useful for calculations in §2.7.1.2)

2.7 Rainfall depth interpolation

At this stage, we have rainfall depths according to four different sources (for each ANETZ) :

- HADES plate 2.4
- HADES plate 2.4.2
- IDF curves for the ANETZ stations
- Modified rainfall depth (altitude effect) for the ANETZ stations

The two first methods [59] allow to read directly the values on a map. The two last one were obtained by interpolation. These methods are described below.

2.7.1 GIS methods for interpolating

The main functions used to interpolate precipitation values distributed in space with a GIS are:

- Kriging
- Thiessen polygons
- Inverse Distance Weighting (IDW)

The kriging method is precise when many data are available (which is not our case) and the two other methods are quite simple to make use of. The higher the ANETZ network density is, the more precise the interpolation is; but for this work, we based on the only accurate data available.

2.7.1.1 Thiessen polygons

Thiessen (or Voronoi) polygons define individual areas of influence around each set of points. Thiessen polygons are polygons whose boundaries define the area that is closest to each point relative to all other points. They are mathematically defined by the perpendicular bisectors of all the lines between all points. The Thiessen formula is of the form:

$$\overline{P}=\frac{P_1\cdot A_1+P_2\cdot A_2+\ldots+P_n\cdot A_n}{A_1+A_2+\ldots+A_n}=\frac{\sum_{i=1}^{n}P_iS_i}{\sum_{i=1}^{n}S_i}=\sum\alpha_iP_i \qquad \alpha_i=\frac{S_i}{\sum_{i=1}^{n}S_i} \qquad \text{Eq.19}$$

where
$\overline{P}$ = mean rainfall on the subcatchment
A_1 = relative surface of the first Thiessen (Volonoi) polygon
P_1 = rainfall data of the first Thiessen polygon's raingauge
n = number of raingauge stations
S = area of each subcatchment influenced by each raingauge
α = weight of each raingauge station polygon on each subcatchment Thiessen formula

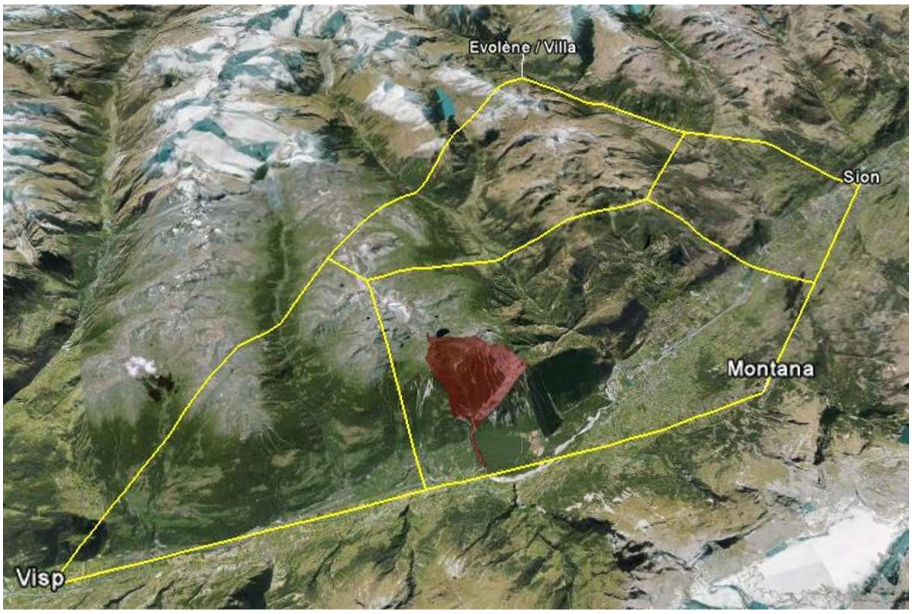

Figure 32. 3D-view of the influence of each station on Illgraben (in red) by the Thiessen polygons method (Google Earth™)

The Thiessen polygons method, as displayed in Figure 32, is not suitable for the context because of the important distances between the stations. The Illgraben catchment is included only within Montana's polygon, which is a rather rough assessment of the reality. This method will not be used further in this thesis.

2.7.1.2 IDW

The principle of IDW is the following: it is stated that the further is a point/value from the area of interest, the minor is its influence; example: the precipitations calculated in Evolène have a minor influence on the rainfall pattern in Illgraben than those of Montana. This method allows a better representation of the reality. Because the IDW function interpolates only according to distances, the altitude effect on the precipitations has been taken into account (see §2.6) before using IDW. Then we calculated from the values of all stations (for a given return period and duration), the corresponding value in Illgraben.

One aim was to compare values obtained from IDW with the one picked up in HADES [59]. Consequently, the interpolations were performed with the several parameters:

- Rainfall depths both with and without altitude effect
- Return periods of 2.33 and 100 years
- Rainfall duration of 1h and 24h

An example of IDW is shown in Figure 33.

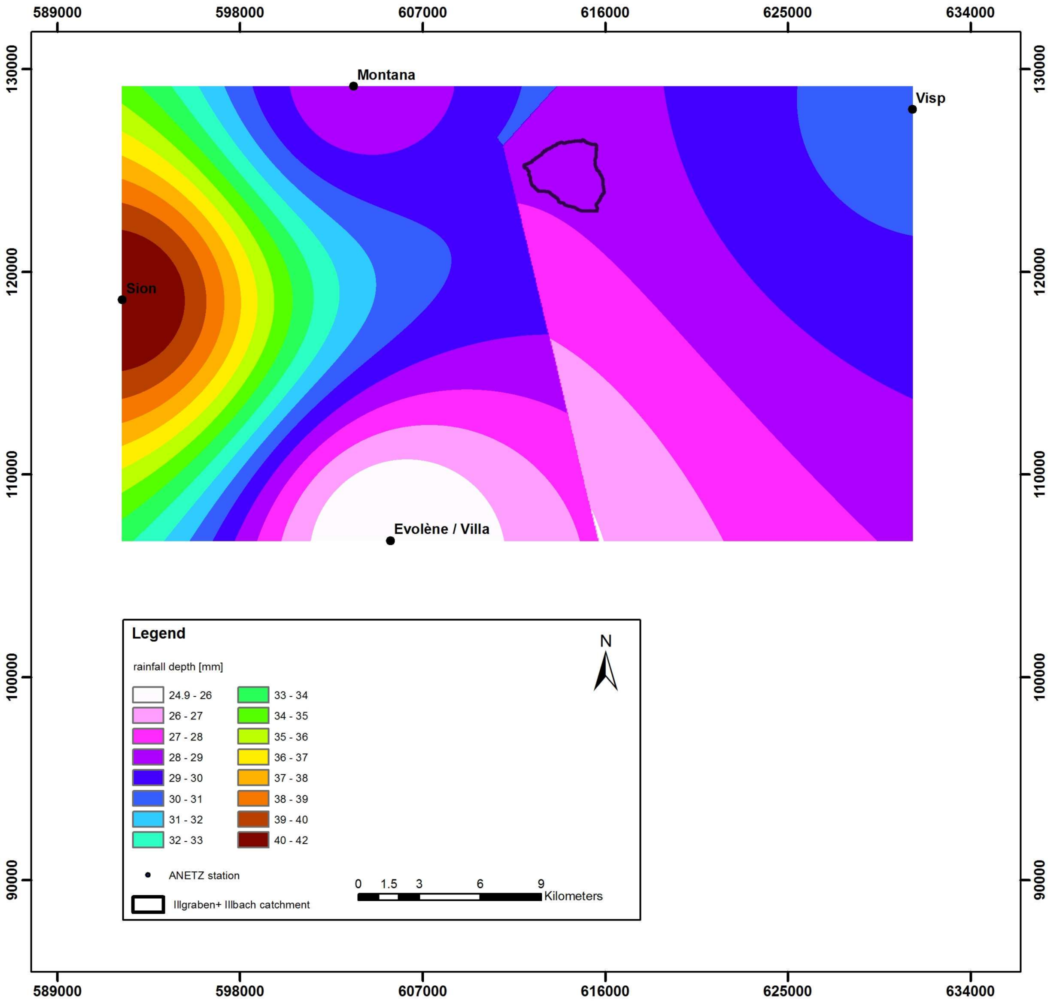

Figure 33. IDW technique applied with: altitude effect, return period=100 years and rainfall duration=1h

We can see that the rainfall distribution varies quite much close to the stations and this effect is smoothed as the distance from the station increases. We can also see an artefact created during the IDW interpolation, which is present in all calculations. The reason for this is unknown, but it has no or very few influence on the results as the values on each side of the ‘line’ have a difference of 1-2mm, which is part of the uncertainties inherent to such a methodology. As Illgraben is quite far from each station, the variation of precipitation amount within Illgraben catchment is rather small (1% to 5% between min. and max. values, which is accurate enough at the scale we are working). Figure 34 shows the tiny variations obtained through the catchment with IDW method.

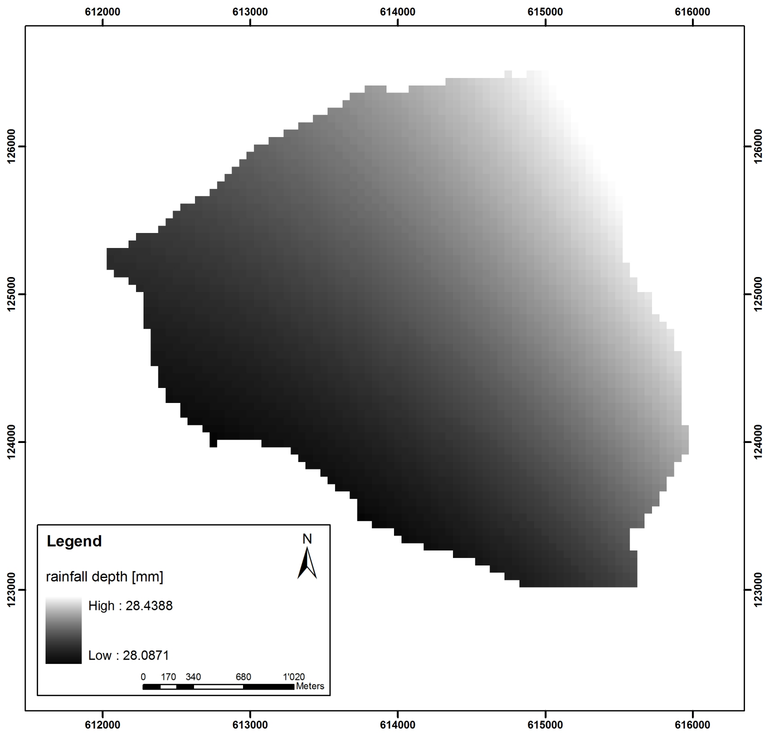

Figure 34. IDW- Zoom on Illgraben + Illbach catchments. Computed with: altitude effect, return period=100 years and rainfall duration=1h

2.7.2 HADES vs. IDW

Table 8 is a summary of rainfall depths obtained with the methods mentionned above. Important deviations in the results are noticed, depending on the method used. Comparisons have been made among these data to find whether a consistant relation exist or not.

Table 8. Summary of the rainfall depths obtained with different methods

		Duration [h]	HADES 2.4	HADES 2.4.2	IDW without altitute effect	IDW with altitude effect
			Rainfall depth [mm]			
Return period [year]	2.33	1	18	16	10.4	12.1
		24	42	42	24.3	28.3
	100	1	40	35	59.2	70.9
		24	90	90	128	154

The comparison between the two IDW calculations (with and without effect of altitude) shows that in the latter, the values increase between 17% and 20% (according to the return period and the rainfall duration chosen).

Differences with HADES are much more emphasized. However a constant trend was found: for 1h duration, the values with IDW are systematically lower than in HADES and for 24h duration, systematically higher: the reasons for such differences could be interpreted by two factors:

- a difference in the measurement technique (i.e. in HADES, records are daily, thus interpolation to 1h is rather uncertain: in our case, it led to an overestimation of the precipitation amounts whereas the 24h records led to an underestimation).

- the precipitation regimes due to climate changes, the interpolation techniques (point kriging for HADES and IDW for this study) and also the accuracy of measurements are among other parameters that influence the results.

Table 9. Rainfall depth differences between IDW and HADES

	Duration	
	1h	24h
ratio IDW with altitude gradient / HADES plate 2.4	-30%	+70%
ratio IDW with altitude gradient / HADES plate 2.4.2	-25%	+103%
ratio IDW without altitude gradient / HADES plate 2.4	-40%	+40%
ratio IDW without altitude gradient / HADES plate 2.4.2	-35%	+70%

Before starting the calculation of the peak discharges, one has to choose design rainfall depths from the many sources summarized in Table 8. Taking into consideration previous comments, HADES values were removed. Therefore, we kept the results stemmed from IDW analysis.

2.7.3 IDF curves Illgraben

The IDF curves for Illgraben were built following this approach: as the IDW were calculated for 2.33-, 100 years, 1h and 24h, we had to find the other values necessary to build the IDF with another approach; we determined the ratio ANETZ/Illgraben (i.e. data for Illgraben obtained from procedure in §2.7.1.2) whose results are displayed in Table 10 and Table 11, and we looked for the ANETZ/Illgraben ratio that keep constant (or nearly constant) for the different return period and duration contemplated. The only ANETZ which shows nearly constant ratio with Illgraben is Montana, while the other fluctuate by more than 20%.

We could have used the IDW technique to get the values to build IDF for Illgraben, but it was time-consuming and might not give better results.

Table 10. Ratio ANETZ station / Illgraben rainfall depth (from IDW without altitude gradient) for 1h-, 24h duration and 2.33-, 100y return period (T)

Station	Sion		Visp		Montana		Evolène	
Duration [h]	T=2.33 [y]	T=100 [y]	T=2.33 [y]	T=100 [y]	T=2.33 [y]	T=100 [y]	T=2.33 [y]	T=100 [y]
1	0.99	1.03	0.87	0.80	1.03	1.07	1.05	1.06
24	0.77	0.74	1.00	1.01	1.06	1.09	0.81	0.74

Table 11. Ratio ANETZ station / Illgraben rainfall depth (from IDW with altitude gradient) for 1h-, 24h duration and 2.33-, 100y return period (T)

Station	Sion		Visp		Montana		Evolène	
Duration [h]	T=2.33 [y]	T=100 [y]	T=2.33 [y]	T=100 [y]	T=2.33 [y]	T=100 [y]	T=2.33 [y]	T=100 [y]
1	0.85	0.88	0.74	0.69	0.88	0.92	0.90	0.91
24	0.64	0.62	0.83	0.84	0.89	0.90	0.67	0.61

The IDF curves of Illgraben are shown in Figure 35 and Figure 36. To built them, the values found with IDW were multiplied by the factor found in Table 10 and Table 11 for Montana. Raw data are listed in Appendix 21.

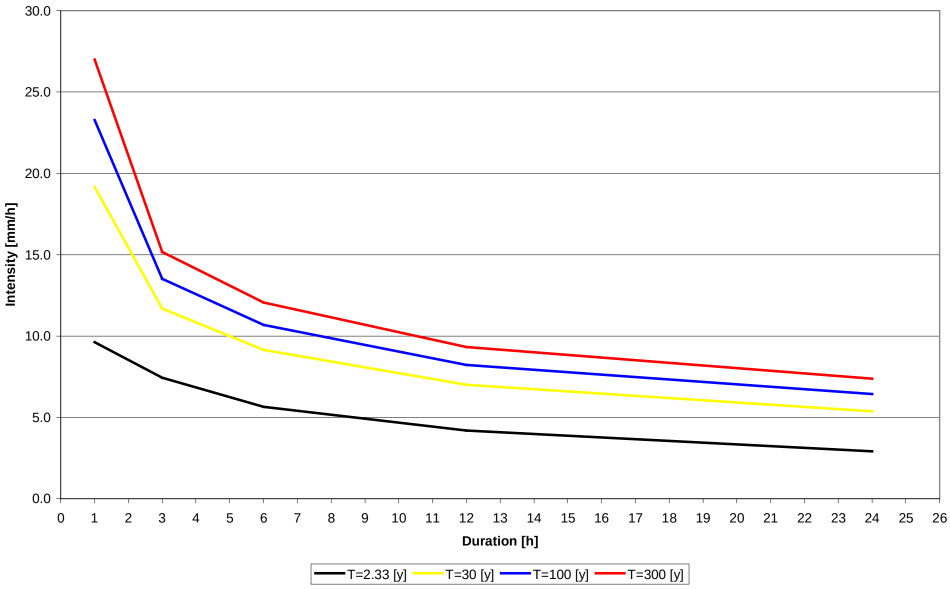

Figure 35. IDF curve for Illgraben (without altitude effect)

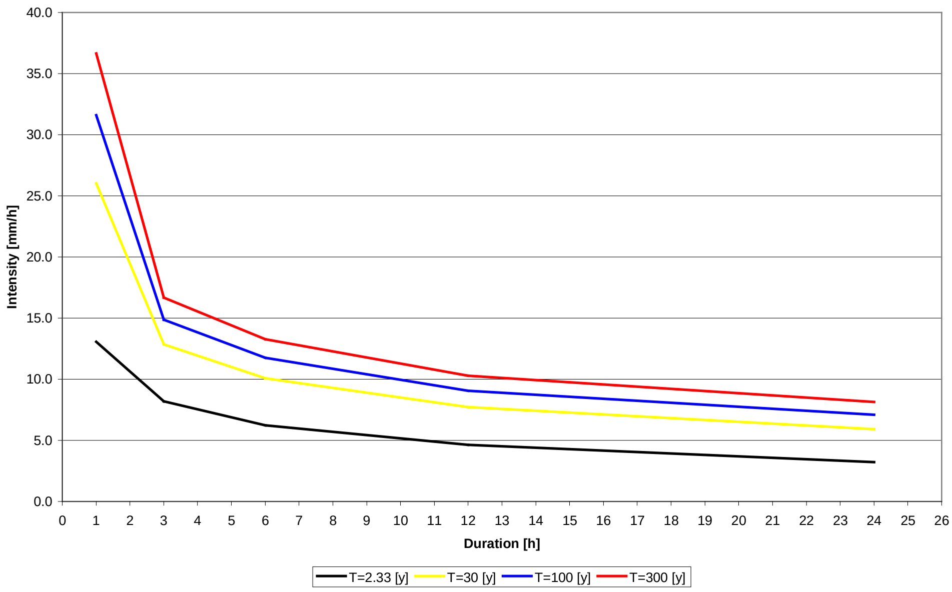

Figure 36. IDF curve for Illgraben (with altitude effect)

A last point was analysed by comparing the DDF curve Illgraben and the rainstorm events that triggered debris flows since 2001 (McArdell & Badoux, in review). Results are shown on Figure 37 and Appendix 21, Figure 3.

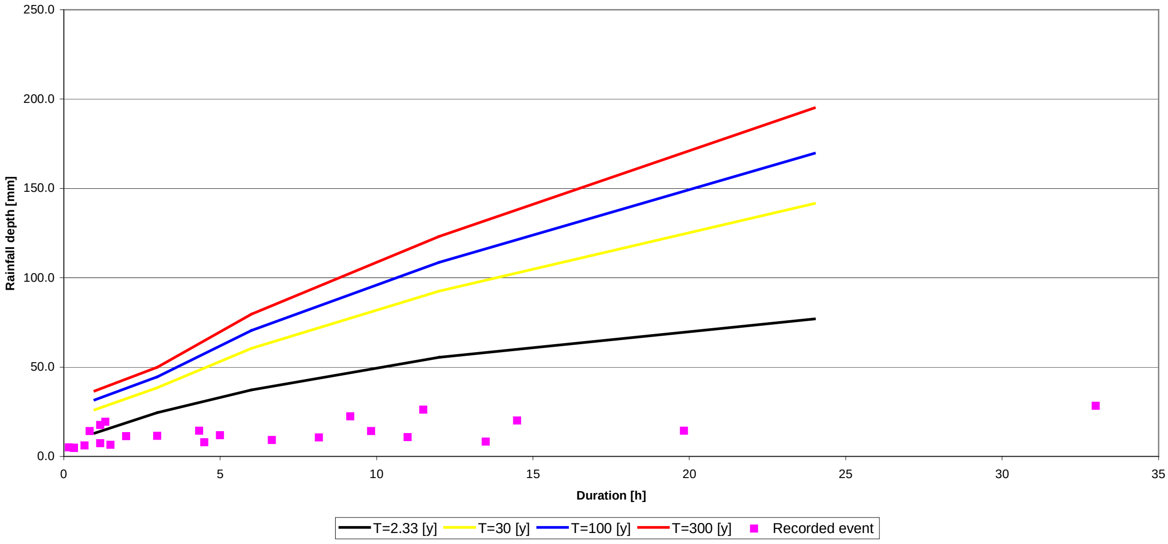

Figure 37. DDF curve of Illgraben area (with elevation gradient) and comparison with recorded events (pink squares)

We can see that most of the storm events that trigger debris flows are of a quite high frequency (return period less than 2.33 years, except for three events (31.07.2002, 03.06.2005 and 18.07.2006), whose return period are comprised between 20 and 30 years. We might also make the assumption that if events occur when precipitations are very frequent (and debris flow are generally triggered when high amounts of water are available), then either available material for debris flows is very sensitive to small discharge or there is other water supply acting at the same time as overland flow in the triggering process, like hydrogeological processes.

The attempt to find if a correlation between the storm return period and the debris flow volume exists was vain because at the time of writing, old debris flow volumes were recalculated with a new technique. The only debris flow volume known was the one at the extreme right handside of Figure 37 (~60'000 m^3).

3 DESIGN DISCHARGE AND HYDROGRAM ASSESSMENT

As mentionned in §2.7.2, the design rainfall depths to estimate the peak discharge in Illgraben have been fixed.

Several methods are available to assess design discharges for small catchments in Switzerland; but the most often used are the software packages HQx_méso_CH and HAKESCH (as well as the Kölla method).

3.1 HQx_méso_CH

HQx_méso_CH uses 6 different methods for calculating Q20, Q100 and Qmax: GIUB 96, Müller-Zeller, Kölla meso, Kürsteiner, Bad7 and the moment methods.

The GIUB 96 method is a method of enveloppe-curve, which allows to calculate Q100 and Q_{max}. There are two options: the first one gives Q100 and Q_{max} from the catchment area and the second one needs the mean discharge value of the torrent. In both cases, the discharges are calculated from the two parameters a and b that depend on the geographic location of the catchment. The methods of Müller-Zeller and Kürsteiner are envelopped-curve methods too. They allow to calculate Q100 and Q_{max}. The Kölla method allows to calculate Q20 and Q100 whereas the moment method and Bad7 provide values for Qmax.

HQx_méso_CH runs automatically. One needs to enter the parameters of the catchment and the outlet. The parameters a and b have already been introduced in the software for the whole Switzerland.

The software HQx_méso_CH was developped for catchment >10 km^2 (mesoscale). Thus the calculation was made only for Illgraben and Illbach catchments because Illgraben only is too small. Results are displayed in Appendix 23 (in blue = Q_{max}; in red = Q100. We can see that the discharges are very low compared with the one obtained with HAKESCH (see below). One reason for that might be the regionalisation of the parameters and the use of a large scale map, which doesn't accurately reproduce the catchment.

3.2 HAKESCH

The software HAKESCH 1.0 (**H**ochwasser **A**bschätzung in **k**leinen **E**inzugsgebieten der **Sch**weiz) consists of a package of 5 models (Müller, Taubmann, Kölla, modified rational formula and Clark-WSL) which give a range of peak discharges (20 years and 100 years return period) for small catchments (<10km^2, but the range in which the best results were obtained is comprised between 1 and 5 km^2). A new version of HAKESCH (2.0) will be soon available, but because of many numerical instabilities a few weeks ago, we decided not to use the beta-version.

3.2.1 HAKESCH methods

3.2.1.1 Müller modified

$$HQ_{\max} = 43 \cdot \psi \cdot E^{2/3} \qquad \text{Eq. 20}$$

HQ_{max} = maximal probable flood in the catchment [m^3/s]
ψ = runoff coefficient, given by RICKLI & FORSTER (1997)
E = catchment area [km^2]

The Müller method is based on discharge observations (until mid-1940's). From these results, an enveloppe-curve was built and is given by the above relation. The runoff coefficient ψ is obtained from the mean slopes of the catchment as well as from the soil map. This method is efficient from catchments bigger than 1km^2.

3.2.1.2 Taubmann

$$HQ(t,T) = A \cdot X(t,T,\alpha) \cdot Y(t,T) \cdot Z(t) \qquad \text{Eq. 21}$$

HQ(T) = discharge of return period T [m^3/s]
A = catchment area [km^2]
X = runoff factor [dimensionless]
Y = climatic factor [dimensionless]
Z = amplitude reduction factor [dimensionless]
T = critical rainfall duration (=concentration time)
T = return period [years]
α = complex runoff coefficient

The runoff factor X corresponds to the rainfall necessary to produce runoff. It depends on the complex runoff coefficient α which is determined from the soil occupation map and the Curve Number from SCS. The climatic factor Y is defined as the ratio between the determining rainfall intensity of the studied area and the one of a test catchment (Urbana, in the USA).
The concentration time is factor of the channel length L [km], the mean slope of the main channel [-] and the estimated flow height [m]. The method is used for catchments with area between 0.5 and 300km^2.

3.2.1.3 Modified rational formula

$$HQ(x)=0.278 \cdot i(T_c,x) \cdot \psi_s \cdot E \ \ [\text{m}^3/\text{skm}^2] \qquad \text{Eq. 22}$$

HQ(x) = peak discharge of return period x [m^3/s]
i = critical rainfall intensity [mm/h]
ψ_s = peak discharge after Rickli [dimensionless]
E = catchment area [km^2]
T_c = concentration time [min]
X = return period [year]
Conversion factor 0.278 is due to the chosen units

The concentration time, which corresponds to the longest time a raindrop will need to flow from the furthest point in the catchment to the outlet is given by:

$$T_C = T_B + T_{FI} \qquad \text{Eq. 23}$$

T_B = necessary duration to saturate the soil layer [h]
T_{FI} = total flow time [h]

T_{FI} can be divided into an runoff time and a conveyance time.
T_B depends on the properties of the soil layers and is automatically calculated from HAKESCH with the saturation volume of Kölla.

$$T_{FI} = 0.0195 \cdot L^{0.77} \cdot J^{-0.385} [\text{min}] \qquad \text{Eq. 24}$$

L = flow distance (distance between the outlet and the furthest point in the catchment) [m]
J = mean slope between the outlet and the furthest point within the catchment [-]

In the modified rational formula, we make the assumption that the rainfall duration is equal to the concentration time. The rainfall intensities for several return periods are considered as constant during the storm event and are calculated from the rainfall durations.

3.2.1.4 Kölla

$$HQ(x) = [i(T_C, x) - f(T_C, x)] \cdot F_{Leff} \cdot k_G + Q_{GI} \text{ with } T_C = T_B + T_{FI} \qquad \text{Eq. 25}$$

$HQ(x)$ = flood discharge of return period x [m^3/s]
$i(T_c, x)$ = precipitation of return period x and duration T_c [mm/h]
$f(T_c, x)$ = loss in the underground [mm/h]
F_{Leff} = catchment area which contributes to the floods [km^2]
k_G = factor taking into account anplification effect of the floods due to antecedant soil moisture [-]
Q_{GI} = discharge coming from the glaciers [m^3/s]
T_C = concentration time [h]
T_B = necessary duration to saturate the soil layer [h]
T_{FI} = total flow time [h]

The Kölla method is based on the total flow time (as modified rational formula). In this method, assumption is made that the major contribution to peak flow is based on areas closed to the channel (i.e. connected area in Introduction, which means here not more than 100m from the channel). The determining rainfall duration (=concentration time) depends mainly on the rainfall quantity necessary for runoff production from the connected areas. This method implies to know the saturation volume of a soil, which is function of the soils features as well as the geology of the catchment [20]. This volume is given in mm of rainfall. The rainfall intensities are given following the method described in [59], plate 2.4. The discharge coming from glacier Q_{GI} was not included in the calculations because there is no visible glacier (even if there might be firns remaining until late in the season due to the debris covering their surface and protecting from melting).

3.2.1.5 Clark-WSL

This method is the most recent of the 5 methods. It allows to determine the flood discharge for several return period for small catchments (1-5km^2). It combines linear storage and linear translation. This method is based on the one formulated by Clark (i.e. a rainfall-runoff model which describes flow as a combination of linear storage and linear translation). The linear resevoir is described by a constant K and is located at the outlet of the catchment. This constant in time-related and has an important effect on the discharge repartition in time and thus on the magnitude of the peak discharge. Linear translation is taken into account by a diagram Time-Area. Flow formation is based on the division of the catchment in zones having the same hydrological behaviour (i.e. isozones). For the numerical calculation of discharge Q(t), Clark chose to use a discrete time-step method, using the Muskingum method.

3.2.2 Expected results

Usually the Müller formula gives the highest discharge (which could be considered as the extreme event), whereas the Taubmann formula gives generally the smallest one. To have a satisfying result, the three other should lie in between; the design discharge should be taken as the mean between the two of the three methods that give the higher results.

3.2.3 Data and methodology

Before getting more into details, we have to clarify one formal aspect: if up to now, the designation Illgraben or Illgraben catchment meant the whole Illgraben area (Illgraben, Illbach, fan) because specification wasn't necessary, from now, the distinction will be used. To simplify the text, Illgraben catchment will be written ILL and the abbreviation ILLBAF will be used for Illgraben+Illbach catchment+Upper fan.

Most of the formula used in HAKESCH are based on rainfall and morphometric characteristics. The design precipitation values are summarized in Table 8.

The morphometric features include: catchment size, min. and max. altitudes, drainage system length, local slope and longest flow path. They have been calculated and all the design discharge assessment process have been applied for both ILL (Table 12 and Figure 38) and ILLBAF (Table 13 and Figure 39).The underlying idea for this splitting is that we consider that debris flows in Illgraben are mostly initiated at the back of ILL, where sediment supply are unlimited (transport-limited system); but we can logically assume that the Illbach catchment (and upper fan area) could contribute to feed the debris flow with water, even if since the construction of the Illsee dam, the discharges in Illbach have dropped down. Nevertheless this input could lead to an increase of the volume of debris flow (i.e. the max. volumic concentration for debris flows is set around 0.63 [32], which explains why the volume of a debris flow, in a transport-limited system, cannot increase indefinitely; but if water is added in the system, then debris flow volume might increase again).

The area and drainage system differ significantly between ILL and ILLBAF; these features have a great influence on the results in HAKESCH. The choice of the drainage system (Figure 40 and Figure 41) is important (i.e. determining the concentration time); it has been generated in ArcView and checked on the base of orthophotos and the national database lk_25.

The results would have to be analysed carefully to confirm or invalidate our assumptions. The other features (elevation, slope, flow path) are not differing much because they are derived from ILL.

Table 12 : Morphometric features of ILL

Illgraben+Illbach catchment+upper fan	**[km^2]**	**9.26**
Elevation max.	[m]	2300
Elevation min.	[m]	853
Max.elevation difference	**[m]**	**1447**
Max. channel elevation	**[m]**	2000
Min. channel elevation	**[m]**	853
Channel elevation difference	**[m]**	**1147**
Drainage system lenght	**[m]**	**44732**
Longest flow path	**[m]**	**3925**
Slope at the downstream part of the contributive catchment	**[-]**	**0.11**
Distance between top of channel and top of contributive catchment	**[m]**	**270**

Table 13 : Morphometric features of ILLBAF

Illgraben catchment	**[km^2]**	**4.77**
Elevation max.	[m]	2300
Elevation min.	[m]	886
Max.elevation difference	**[m]**	**1414**
Max. channel elevation	**[m]**	2000
Min. channel elevation	**[m]**	886
Channel elevation difference	**[m]**	**1114**
Drainage system lenght	**[m]**	**27441**
Longest flow path	**[m]**	**3547**
Slope at the downstream part of the contributive catchment	**[-]**	**0.11**
Distance between top of channel and top of contributive catchment	**[m]**	**270**

Beside the precipitations and morphometric data, the landuse (Figure 42 and Figure 43) and soil-types are of importance because they fix the storage capacities and infiltration rates. Thus the runoff coefficient (ratio between the rainfall which flows at the surface and the raw precipitations) could be calculated. This coefficient is a critical point because it determines the part of the catchment which contributes to the flood peak. However this coefficient is hard to define and most of the time, one gives a weighted average over the whole catchment (depending on the landuse and soil-type). Another aspect which should be pointed out is the relation runoff coefficient – rainfall duration, which is most of the time not taken into account in the formulations. In this work, we based our assessment on the table from the Institution of Engineers, Australia (1987). They suggest to multiply by a correction factor of 1.05 (for a 20 year return period event) and 1.2 (for a 100 year return period event) the runoff coefficient obtained from the tables.

Figure 38 : 3D-View of ILL (Google EarthTM)

Figure 39 : 3D-View of ILLBAF (Google EarthTM)

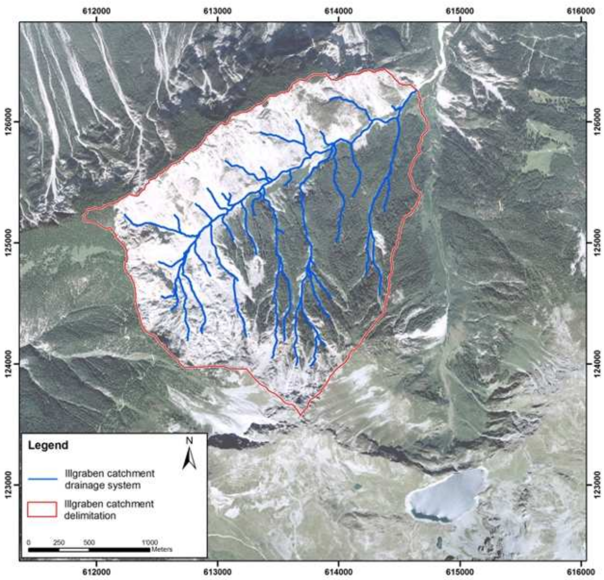

Figure 40 : ILL drainage system

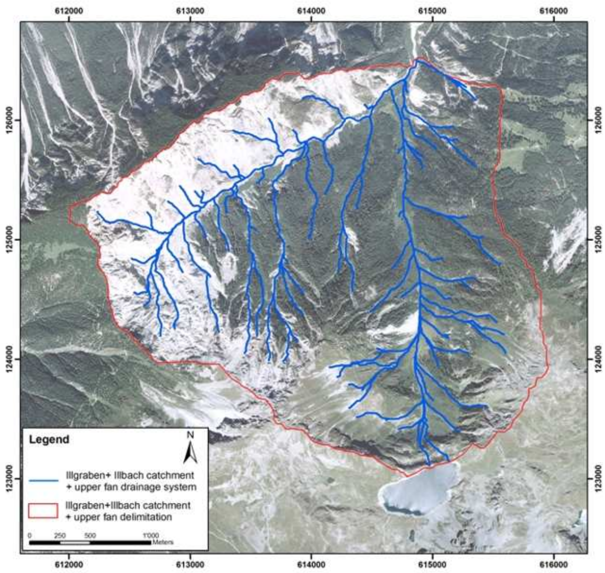

Figure 41 : ILLBAF drainage system

Some authors have proposed some methods to estimate the runoff coefficient (Rickli & Foster 1997; Müller & Melli), the Curve Number (Taubmann & Thiess 1984; Kuntner & Burlando 2003; Dobmann 2009) and for the Kölla method, the rainfall volume (Kölla, 1986). All detailed results are listed in Appendix 24.

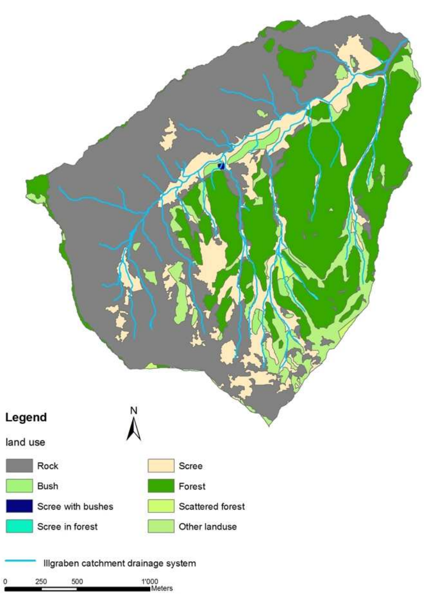

Figure 42 : Landuse in ILL

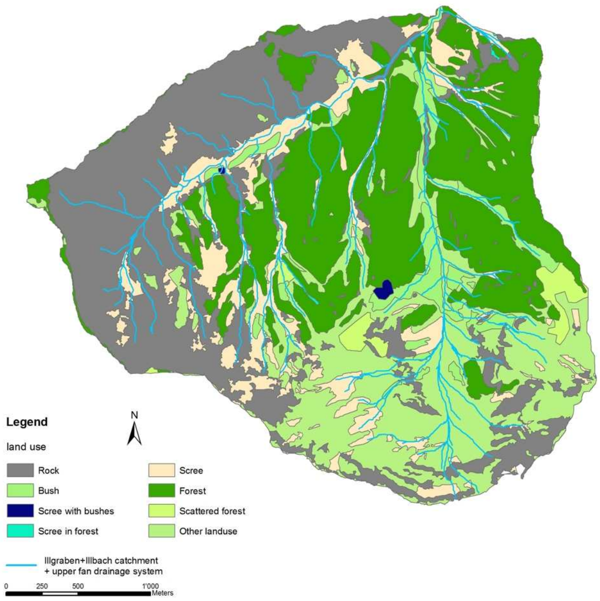

Figure 43 : Landuse in ILLBAF

The Clark-WSL method uses an approach, based not only on the morphometric features but also on the hydraulic properties of the catchment. The flow formation is based on the division of the catchment in zones that have a similar hydrological behaviour, that are called isozones (Figure 44 and Figure 45). These isozones were created by the mean of a GIS. After computing several geomorphic data (flow direction, flow accumulation), one has to define, on the basis of the drainage system network, which zones belong to channel and which not; this procedure allows to give different velocity rates depending on the zones (i.e. the water will normally flows faster in a channel that in open-land; the latter can be found in slope - landuse diagrams [2]). Then a tool permits to find the flow time in each cell and finally one might create the isozones. As we could see, the isozone process takes into account the morphology of the catchment (slope) as well as the flow velocity. The Clark-WSL method in HAKESCH uses isozones of 10min. interval.

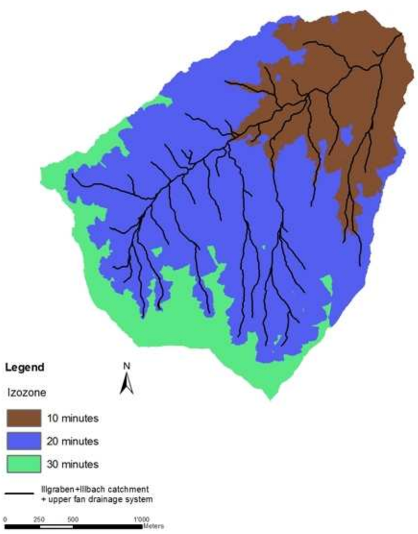

Figure 44 : Isozones in ILL

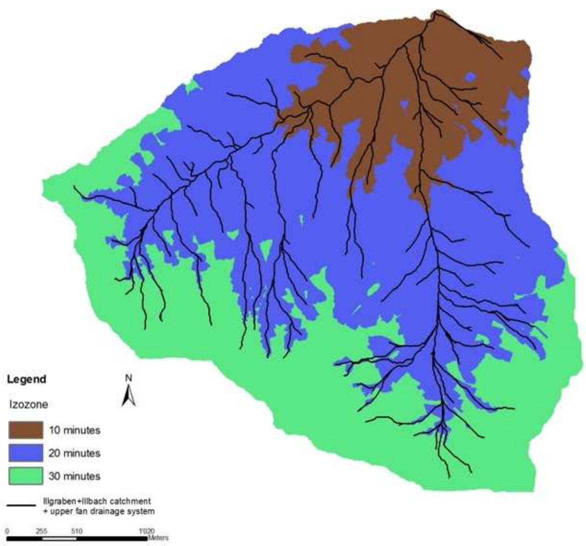

Figure 45 : Isozones in ILLBAF

3.2.4 HAKESCH results

The detailed results appear in Appendices 24 & 26.

The main results are listed in Table 14 and Table 15. As mentionned in §3.2.2, Müller method usually provides the maximum discharge, but this is not always valid in this study, whereas Taubmann method systematically gives the lowest results. As indicated in §3.2.2, the Kölla, Clark-WSL and modified rational formula methods will be used for the calculation of the hydrograms. For comparison with the results obtained in HAKESCH, we built the model described in [20] on MS-Excel (Appendix 25). We obtained the same results than in HAKESCH (difference of a few %).

As discussed previously, the differences between the two features (drainage system and catchment area) in ILL and ILLBAF respectively, led to huge gaps in the discharge results. The altitude influence also (see §2.6) induces a significant difference.

Table 14. Results of HAKESCH simulation for HQ_{20} and HQ_{100} – ILL

Catchment	Data source	HQ_x [m^3/s]	Method					HQ_x [m_3/s]
			Taubmann	Modified rational formula	Kölla	Clark-WSL	Müller	Proposition
ILLGRABEN	Rainfall without elevation effect	HQ20	14.5	16.8	16.7	24.7	48.7	22.2
		HQ100	26.5	40.7	31.6	43.7	48.7	42.2
	Rainfall with elevation effect	HQ20	20.4	29.1	26.6	38.3	48.7	27.8
		HQ100	38	66.5	49.5	66.5	48.7	49.5

Table 15. Results of HAKESCH simulation for HQ_{20} and HQ_{100} – ILLBAF

Catchment	Data source	HQ_x [m^3/s]	Method					HQ_x [m_3/s]
			Taubmann	Modified rational formula	Kölla	Clark-WSL	Müller	Proposition
ILLGRABEN + ILLBACH + UPPER FAN	Rainfall without elevation effect	HQ20	23.2	34.8	29.5	48.4	58.8	32.1
		HQ100	45.4	85.1	55.7	86.6	70.2	55.7
	Rainfall with elevation effect	HQ20	27.7	48.5	40.3	62.7	58.8	40.3
		HQ100	54.2	111.7	74.6	109.8	70.2	74.6

The area between ILL and ILLBAF changes almost from simple to double. As discussed in the introduction of this chapter, HAKESCH is well-calibrated for catchments whose sizes lie between 1 and 5km^2 . The choice of a design discharge could be made on the assumption that to assess a major event, one has to consider the worst case.

Floods were not really studied in Illgraben because debris flows are of greater interest; consequently accurate records are scarce; in these conditions, it would be hypothetic to give a exact value of the peak discharge for a given return period. Approached discharges are found within ILL. Moreover, as said previously, HAKESCH was calibrated on catchments whose sizes were 5 km^2 on the average; ILL, with 4.8 km^2 is in the order of magnitude.

Knowing the peak discharge, the peak time (assumed to be equal to the concentration time) and the runoff coefficient, we will try to build flood hydrograms and determine the related volumes for storm events of given duration and return period.

3.3 Flood hydrogram

3.3.1 Methodology

The Illgraben doesn't have a gauging station, as many other small catchment in Switzerland. The force plate under the cantonal road bridge is able to measure debris flows and mudflow/hyperconcentrated flow activity, but not water floods.

Nevertheless, there exists a method developped by Hager [24] which allows, with the determination of three independant parameters, to reconstruct the flood hydrogram of a given event. This method suggests an hydrograph in the form of an asymmetrical bell, that corresponds to the statistical distribution of Maxwell (Eq.26, often called 'Maxwell equation'). The relation is defined by three independent parameters and is given by [17]:

$$Q(t) = Q_{base} + Q_{peak}\left(\frac{t}{t_p} \cdot e^{1-\frac{t}{t_p}}\right)^n \qquad \text{Eq. 26}$$

where
$Q_{(t)}$ = flow at time(t) [m^3/s]
Q_{base} = baseflow [m^3/s]
Q_{peak} = peak flow [m^3/s]
T_p = time to peak or raising time [min]; it was calculated here with the relation: $T_p = 3/8\ T_c$
T_c = concentration time [min]
n = shape factor [-]

Usually, these parameters are determined from field measurements or by calibration with recorded events (especially parameter 'n'). In Illgraben, no flood hydrogram from past event is available for the calibration of the parameters. It led to the following assumptions :

- the baseflow is considered as unsignificant compared to the flood discharge.
- the catchment is rather small and very steep: the runoff reaction following a rainfall event is quick and the hydrograph should have a shape with a leptokurtic kurtosis and a strong positive skewness.
- the shape factor 'n' isn't known a priori, contrary to the runoff coefficients (see 3.2.3). One way to bypass this issue is to calculate the total volume of precipitations (1), use an initial value for 'n' (2), calculate with Eq.25 the different discharges at time (t) (3), calculate the total volume of the flood (4) and then divide (4) by (1). This operation gives a runoff coefficient that has to be ajusted to the right coefficient (i.e. the true runoff coefficients are known, see Appendix 24). To solve this issue we use a target value function, we find the shape factor 'n' and at the end we get the design hydrograms.
- the method described above and displayed in Table 16 has the advantage to take into account the physical features of the catchment (but one has to remind that the runoff coefficients have a range of uncertainty).
- this method is maybe less efficient than if we could fit our parameters on recorded hydrograms, but is a nice approach when no records are available.

Table 16 : Methodology used to determine the Q100 flood hydrogram – ILL (precipitations with elevation gradient)

	Return period	100 years	
	Flood type		
	modified rational formula	Kölla	Clark-WSL
Q_{peak} [m^3/s]	67	50	67
Shape factor n [-]	1.4	5.3	1.1
Concentration time [min]	36	132	30
Peak time t_p [min]	14	50	11
Rainfall intensity [mm/h]	104	38	120
Catchment area [ha]	477	477	477
Rainfall intensity[m/s]	2.9E-05	1.1E-05	3.3E-05
Raw rainfall volume [m^3]	297648	398772	286200
Runoff coefficient [-]	0.41	0.41	0.41

hypothesis : t_c is constant for the several return period, because it doesn't change significantly

Time [min]	Discharge			Volume		
	modified rational formula	**Kölla**	**Clark-WSL**	**modified rational formula**	**Kölla**	**Clark-WSL**
0	0	0	0	0	0	0
1	6.443705713	8.40408E-06	13.06402276	193.311	0.000	391.921
2	15.29666827	0.000305196	25.13838621	845.522	0.010	1537.993
3	24.29863797	0.002386356	35.42125508	2033.382	0.090	3354.782
4	32.74408611	0.009950259	43.93210085	3744.663	0.461	5735.383
5	40.32198477	0.029397735	50.8088334	5936.645	1.641	8577.611
6	46.9021585	0.069848281	56.22023225	8553.370	4.618	11788.483
7	52.45156204	0.14278711	60.33838161	11533.981	10.997	15285.241
8	56.99262332	0.261469223	63.32785441	14817.307	23.125	18995.228
9	60.57977564	0.440192583	65.34124588	18344.479	44.175	22855.301
10	63.28525719	0.693530758	66.5175336	22060.430	78.187	26811.065

3.3.2 Results

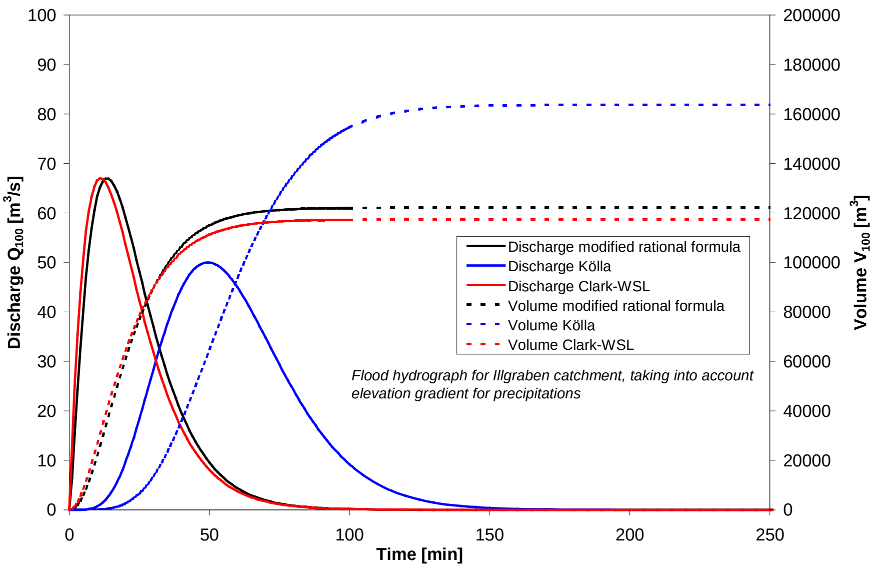

Figure 46. Flood hydrogram for Q_{100} – ILL (precipitations with elevation gradient)

The range of volumes found for the several flood types (Table 17) is wide, going for Q_{100} from 97'000 m^3 to 350'000 m^3. All hydrograms and raw data can be found in Appendix 27.

Up to this point, all scenarii were taken into account (ILL and ILLBAF, with or without altitude influence on precipitations).

The different flood hydrograms were analysed and some comments can be formulated:

- the Kölla method gives hydrographs with moderate positive skewness and mesokurtic kurtosis, compared to the Clark-WSL and modified rational formula (which solve the assumption formulated above).

- the volumes obtained with Kölla are always (and by far) the highest (see Table 17). This could be explained by the concentration times, that are much longer for this method (i.e. dependant on the catchment drainage length) than for the two others.

We also tried to look at the way we could use the previous results with the debris flows analysis.

- one important feature to know when working with debris flows is the magnitude of an event. Hampel (1977), cited in [27], suggested to use the flood volume to obtain debris flow volumes. The flood analysis done in this thesis was used to assess the debris flow volume (and thus return period, but this is quite hazardous). To switch from flood volume to debris flow volume, we based on an assessment that the average percentage of water and solid in the mixture, should be around 50% for water phase and 50% for solid phase (pers. communication McArdell); air phase is neglected.
- correlating the flood volume with debris flow volume could be quite hazardous; in Illgraben, the delay between the storm event and the trigger of a debris flow is often rather small; on the same reasoning, a flood happens when all the holes, depressions and infiltration capacities are exceeded, thus corresponding also to a delay between the storm event and the trigger of the flood. As debris flows in Illgraben are mostly trigger by loose sediment fluidization, the relation infiltration capacity exceedance – event trigger, and thus establishing a relation flood volume – debris flow volume could be seen as a possible way of hazard assessment.

Table 17. Summary of the results of volume calculation for ILL and ILLBAF

Catchment	Rainfall type	Volume [m^3]	modified rational formula	Kölla	Clark-WSL
ILL	rainfall without altitude effect	V2.33	10'878	15'839	26'386
		V10	38'540	55'520	37'210
		V30	66'980	94'860	64'300
		V100	101'850	142'280	97'630
		V300	151'910	219'140	145'550
	rainfall with altitude effect	V2.33	10'665	22'043	9'663
		V10	46'380	61'460	44'380
		V30	80'340	105'650	77'240
		V100	122'070	163'700	117'360
		V300	183'180	241'870	175'060
ILLBAF	rainfall without altitude effect	V2.33	21'616	31'868	20'039
		V10	76'680	106'720	65'020
		V30	120'750	168'760	104'190
		V100	193'380	267'100	166'700
		V300	302'750	428'200	254'050
	rainfall with altitude effect	V2.33	24'323	35'891	23'410
		V10	86'850	106'400	77'980
		V30	137'320	173'810	125'030
		V100	277'100	344'670	250'540
		V300	340'340	424'200	305'960

As conclusion, we can affirm that the most realistic design flood (and consequently volume) should be taken from ILL, with taking into account the altitude gradient of precipitations (realistic assumptions and security values because higher than those without elevation gradient) and using the modified rational formula or Clark-WSL method.

4 CHECK DAMS AS FLOOD-/DEBRIS FLOW MITIGATION MEASURE

4.1 Historic of the check dam concept

As already mentionned in the introduction, following the disastrous debris flow event of 1961, the canton of Wallis ordered a general safety concept which has resulted in the construction of a retention dam (check dam n°1, see Appendix 2) and 29 check dams built all the way along the Illbach torrent until the Rhône river (Appendix 1 and 2).

The aim of this chapter is to provide a general overview of the check dam concept as protection measure as well as their function in a steep headwater catchment like Illgraben.

The first appearance of check dams in Wallis dates back to the beginning of the 19th century: the goal was to 'break' the torrent rather than dyking it up. The check dams (called weirs at these times) were built with trunks set perpendicular to the torrent; they formed a caisson which was filled with stones. These structures were anchored both in the channel bed that in the banks. But soon, masonry structures replaced the wooden ones because of their relative fragility. At the origin of the check dam concept, there was a will to reduce bank erosion by giving the channel a lower gradient [14]. In the seventies, the reinforced concrete check dams did their appearance in numerous torrents where debris flows were a recurrent phenomenon (Illgraben, Merdenson, Mauvoisin,…)

Figure 47. Serie of check dams for channel stabilization [15]

4.2 Definition of torrent check dams

A check dam is a small sediment storage dam built in steep gullies to stabilize the channel bed. A common use for these structures is to control channelized debris flow frequency and volume. Check dams are expensive to construct and are therefore usually built only where important installations lie downslope (*Chatwin et. al*).

From this definition, we see that the check dams are used as storage and stabilizing structures (see Figure 48). However, the storage capacity in Illgraben is not the main reason for the choice of these structures because debris flows frequently occur and sediment transport is important; the difficult access to most of the check dams prevents to remove the accumulated sediments after each important event. Before going further on, we would like to clarify one point: in the following chapters, there will be the terms 'Illgraben' and

'Illbach channel' mentionned; the first one refers to the whole area (Illgraben+Illbach+fan) whereas the second one will be used to name the channel on the fan.

The real need for check dams in Illgraben was their stabilizing effect: indeed, due to its frequent debris flow activity, the Illbach channel and banks, especially on the fan, are made of sediments accumulated from previous debris flows. Even if the steep banks indicate some stability, this material would be destabilized as the bed is moving quite fast in Illgraben. Moreover, the deep incisions in the channel bed observed where check dams are missing indicate that debris flow will erode it quite easily: this process leads to debris flow feeding and subsequently to an increase in volume as well as a rise in sediment transport rate.

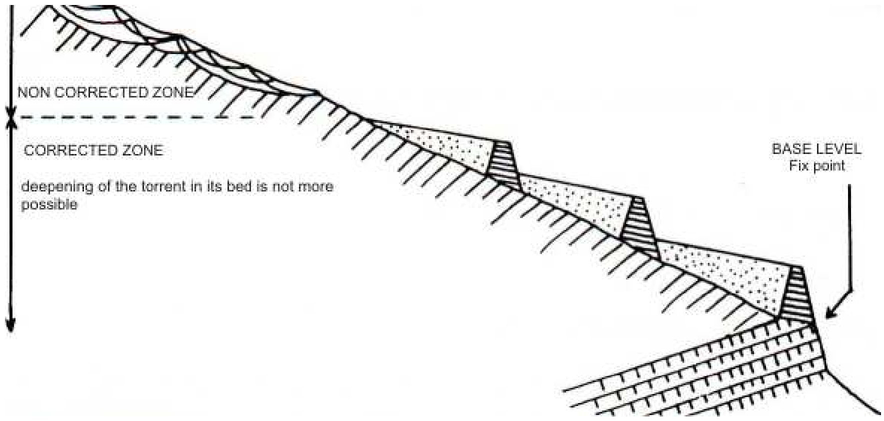

Figure 48. Check dam effects: retention and length profile fixation [42].

In classical hydraulics, the check dams (or weirs) induce important energy dissipations: in concrete terms, to be efficient, the height of the fall should be at least the height of the flow. For debris flows, energy dissipations are important when falling from a check dam only if the fall height is important compared to the flow height [15]. In practice, the order of magnitude of debris-flow height is around 1m; this means that to be efficient, the drop should be around 10m. In inverse, a typical debris-flow has the tendancy to ajust its flow channel in order to minimize the brutal energy losses. Thus, when a debris flow falls from a small drop, the area behind the check dam will rapidly fill with material that will more or less stagnate (because the strains in this zone are smaller than in other zones). In some cases, the strain rate could even not be reached, forming a dead zone (Figure 49). Thus the debris flow fill the holes at toe of the check dam and creates an intermediate slope between the top and the bottom of the check dam (Figure 49).

By placing a serie of small check dams close one from each other, a debris flow can 'see' them and ajust its flow before and after the check dam, which in definitive results in the same slope as the original one! The debris flow in this case considers that the check dam is a roughness a bit more pronounced that usual. But in the case of a important drop, energy dissipation really has an effect on the reduction of flow velocity [15].

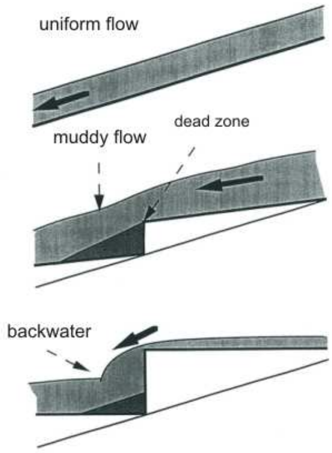

Figure 49. Effect of check dam on debris flow dynamic [15]

When designing a check dam, the engineer has to take care the check dam follows as much as possible the shape of the cross-section, in order the wings doesn't have to suffer important dynamic impacts.

During a debris flow, generally not much scour should appear at the foot on the check dam due to the dead zone previously defined.

4.3 Check dam purposes

Check dams are generally built in series (Figure 47, Figure 48 and Figure 50) and this for several reasons:

- to reduce the channel slope; this leads to a reduction of sediment transport and all gravity-driven processes in general, in which slope is a major feature; formula to assess debris flow motion and runout, are mostly based on geomorphic features. Slope has the major influence on debris flow stopping (Figure 50). This slope reduction has to be compensated with abrupt elevation transition (drop structure).

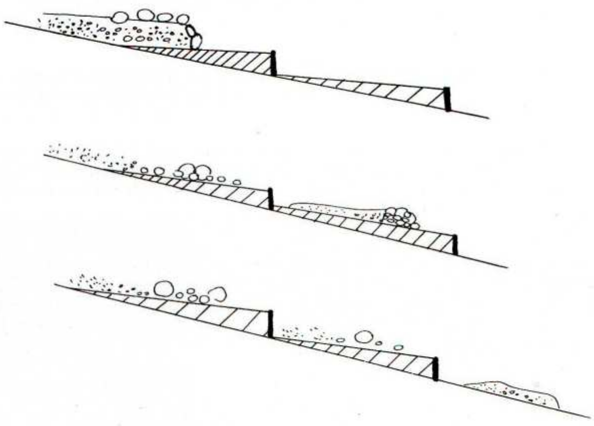

Figure 50. Effect of a serie of check dams on debris flow dynamic [42].

- where the flow has the tendancy and the space to evolve freely, bank undermining is to take into account, and this might lead to damages to infrastrutures placed on or near the bank of the channel. Check dams have the advantage to force the flow to follow a given direction (i.e. between the wings) and so prevent strong bank scour (Figure 51); also by decreasing the channel slope, they favour sediment deposition and thus enlargement of the channel width: this might lead the flow not to reach bank toe and run in between.

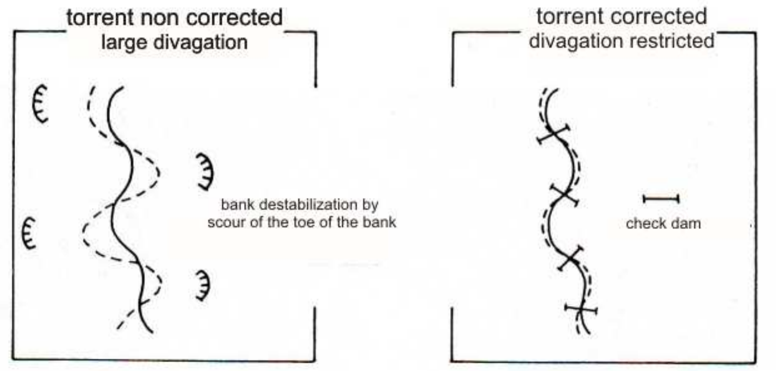

Figure 51. Influence of check dam on lateral erosion [42].

- check dams, as said above, have two main purposes: retention and stabilization. Retention is of limited use in Illgraben (i.e. continuous sediment supply), but the volume stored behind a dam could stabilize unstable sideslopes, as displayed on Figure 52. Depending on the height of the check dam, this volume might be consequent; depending on the channel morphology, it could have an influence quite far upstream.

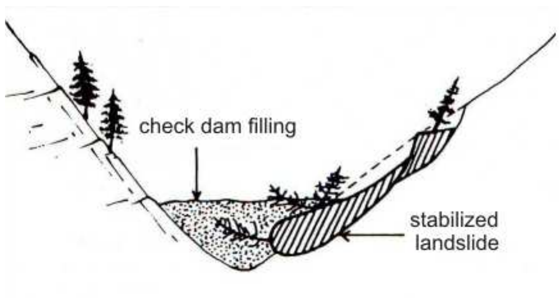

Figure 52. Stabilization of unstable slope [42].

- a check dam concept could be useful to prevent big damages due to bed fluidization; this process occurs in the channel itself [32]. The main issue with this phenomenon is the debris flow amplification concept [60]. In a certain range of slopes, a bed layer of substantial depth may be subject to fluidization by a small debris flow or even clear surface flow. A small debris flow initiated by short and intensive rainfall could trigger such a potential. Figure 53 shows the effect of amplification as a function of the bed slope. This graph was determined for a clear water input and a stony bed (Illbach channel bed is actually rather composed of medium size elements, but this could evolve in time). For slopes less than about 15%, amplification is negligeable (this is the case for all the section controlled by check dams). Between 15 and 35%, amplification increases almost linearly; in [72], it is reported that from 900 to 1200m a.s.l., the main channel slope lies around 20%. Between 40 and 45%, the amplification increases asymptotically, and over 45% it is out of the formula application (this correspond to the minimum condition for the occurrence of a landslide of a saturated mass of loose material) [32].

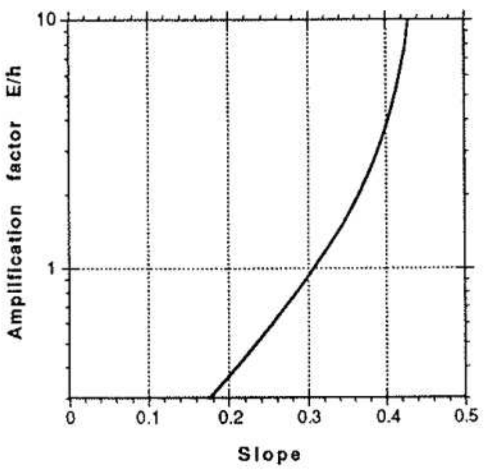

Figure 53. Ratio of bed fluidization to surface flow depth, according to [60]

Figure 54 demonstrates how a single debris flow pulse acts on the channel bed.

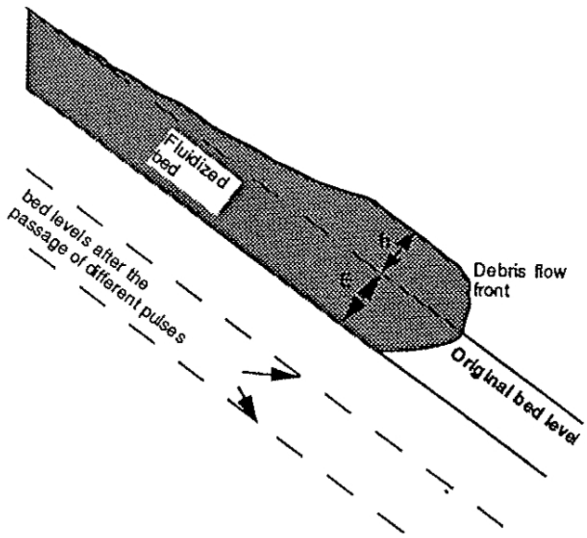

Figure 54. Bed fluidization by a debris flow. Successive erosion by following pulses occur [32].

The addition of water and sediment from the bed will increase the debris flow depth. According to Figure 53, the amplification should continously increase, but after Takahashi [60], a maximum volume concentration of 0.63 prevents an indefinite growth of a debris flow. The bed has usually a higher concentration of solids than the flow; it can be fluidized only if there is a supply of excess water. Because of the compensating effect of increased flow depth and limiting concentration, it's understandable why often erosion (which rather should be regarded as bed fluidization) by a debris flow is constant along a given channel reach.

The reduction of slope due to check dam may result in an important reduction of the amplification factor. Thus bed fluidization is reduced or even prevented. Only if the backfilling of the check dam is such that more or less the original valley slope is reached again by the deposition ('critical maximum slope', discussed later), then a partial fluidization of these deposits seems possible again.

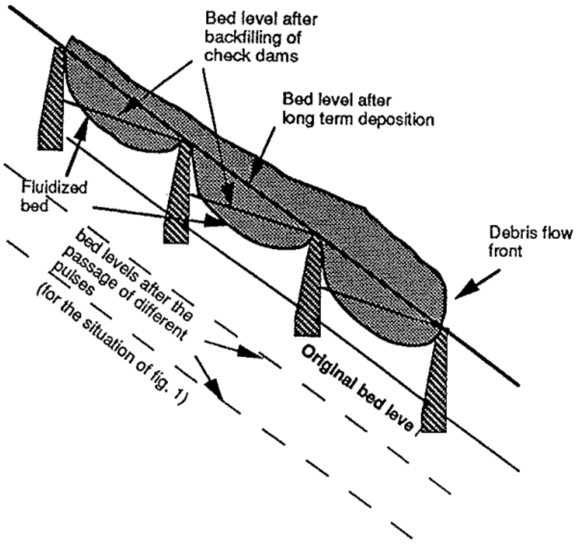

Figure 55. Schematic view of a debris flow process on a torrent secured by check dams [32].

Massive concrete check dams are expected to have a stabilizing effect even when huge rainfall events saturate the bed of the main channel. The first debris flow surge will mobilize the movable, fluidized bed, but after this surge, the bed will be rearranged by the flow in order to present a reduced slope, and further fluidization is not possible again.

Even if the collapse of one or several dams would not increase substantially the volume of sediment involved, the situation, locally, would be equal, but not worse, than in a natural situation, since the driving parameters are about the same [32].

- although check dams have been widely adopted in practice, these systems may not always help to control debris flow of an anticipated size as they might have previously been filled up with sediment transported by a number of small-scale debris flow in the torrent. Frequent removal of deposited sediment from check dams is not feasible for financial and technical reasons. Effective planning techniques should be promoted so that better control can be achieved even if check dams are filled up with sediment prior to a destructive event. An estimation of the sediment volume trapped by each check dam could be carried out, based on the potential storage volume (V_p) of each dam, which can be defined by equilibrium and initial bed deposition slopes. V_p can be calculated by [47]:

$$V_p = \frac{(H_d \cos\theta)^2 \cdot B}{2}\left\{\frac{1}{\tan(\theta-\theta_e)} - \frac{1}{\tan(\theta-\theta_0)}\right\} \qquad \textbf{Eq. 27}$$

where
H_d = height of the dam [m]
B = flow width [m]
Θ = slope of the original torrent bed [-]
θ_0 = initial bed slope of the storage area before debris flow [-]
θ_e = equilibrium bed slope corresponding to the sediment concentration of the debris flow [-]

The equilibrium bed slope is found by:

$$\tan\theta_e = \frac{(\frac{\sigma}{\rho-1})\cdot\bar{c}}{(\frac{\sigma}{\rho-1})\cdot\bar{c}+1}\tan\phi_s \qquad \text{Eq. 28}$$

where : σ = mass density of sediment particles [kg/m^3]
ρ = mass density of water including fine sediment [kg/m^3]
θ_e = equilibrium bed-slope corresponding to sediment concentration $\bar{c}$ of debris flow [-]
ϕ_s = inter-particle friction angle [°]

V_p of each check dam can be occupied fully only when an uniform supply of debris flow exists for an infinitely long time, which seldom happens in nature. Therefore, only part of V_p can be considered to be occupied during any debris flow. In order to be on the safe side, 20-30% of V_p could be assumed as estimated trapped volume, based on experimental results under different supply conditions [47].

4.4 General design features

A check dam is a cross structure along the channel. In Illgraben, due to frequent debris flows and important force impacts on the structures, reinforced concrete check dams have been set up, whose general shape is shown in Figure 47, Figure 56 and Appendix 2.

These structures, for Illgraben (and probably for many other torrents), were designed according to the following points:

- morphological characteristics of the channel and the banks (due to bed divagation, the design for numerous check dams has changed many times)
- federal guidelines for static calculations [57]
- no dynamic calculations were performed at that time, because it was not in use and the knowledge about debris flow processes was quite poor (pers. communication Missbauer).

There exists several types of check dams, depending on the need, the location, the geomorphological features, the budget, etc.

In Illgraben, the choice felt on gravity check dams. These dams are quite ‘easy’ to design compare to others (‘autostable’, ‘autostable with back-stabilizer’,…); they should have a height comprised between 2 and 4m to be economically suitable and are very sensitive to phenomena such as scouring, settlement and fundation resistance [18].

These dams are composed of a central body, an overflow section, lateral wings which are set up quite deep into the banks and barbicans to avoid water pressure behind the dam (Figure 56). As said in §4.2, one objective of check dams on debris flows is to guide their path. The wing walls have the same function as concrete lining of debris flow canals [32].

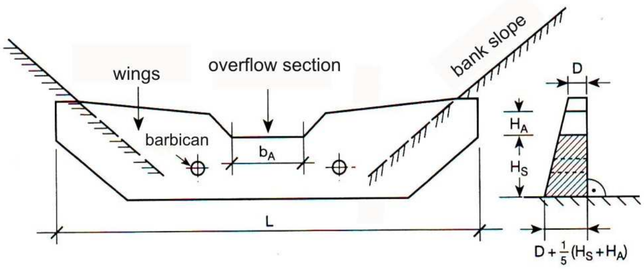

Figure 56. General sketch of a concrete gravity check-dam [7]

The main forces acting on a gravity check dam are the weight of the dam (i.e.'gravity dam'), the static pressure behind the dam as well as dynamic pressures from debris flows. The static pressure can be calculated by the hydrostatic pressure/force (Figure 57) and is described by:

$p_{(z)} = \rho g z$ (hydrostatic pressure) Eq. 29

$F = \frac{1}{2} \rho_w g H^2$ (hydrostatic force per unit width) Eq. 30

where
ρ_w = water density [kg/m^3]
z and H = height of the check dam [m]
g = gravitational acceleration [m/s^2] = 9.81

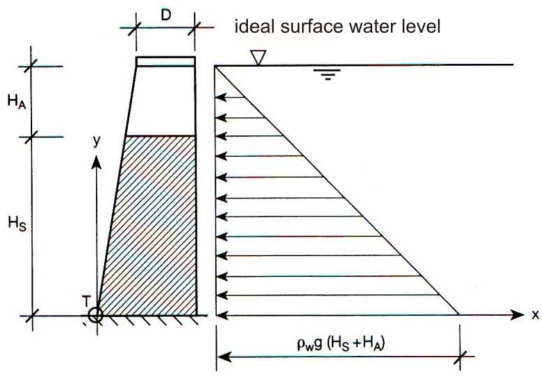

Figure 57. Hydrostatic pressure distribution behind a check dam [7]

The dynamic impact pressure of a debris flow on torrent control works is several time bigger than the water hydrostatic pressure, up to 13 times, but in general for design, the engineer has to take into account a pressure 6-7 times bigger [35].

The other main usual calculations in dam design (same as for retaining wall) are the earth thrust, tipping resistance, internal static calculation. The design of these structures relies mostly on observation and professionnal experience. The check dam design concept in torrents is quite often derived from the river engineering concept [31].

Osti & al. [47] developped a formulation to estimate the minimum spacing (L) required between two consecutive check dams:

$$L > \frac{H_d}{\tan(\bar{\theta} - \theta_e)}$$ Eq. 31

where
$\bar{\theta}$ = average bed-slope between the two check dams [-]
H_d = height of the dam [m]
θ_e = equilibrium bed slope corresponding to the sediment concentration of the debris flow [-]

This relation was tested by taking mean values from §4.6.2 and §4.6.2.1. θ_e was set to 0.03, $\bar{\theta}$ was set to 0.08 and H_d to 5m. We obtained a value of 102.24m; the condition L>102.24m is fullfilled in Illgraben. This relation could be used as a method for a first approximation on the minimum spacing needed for an efficient effect of check dams.

4.5 Weaknesses of check dams – issues overview

As mentionned previously, check dams have numerous advantages; but gravity check dam, in spite of their quite easy design, are very sensitive to scour and ground settlement.

Since the 1970's (period of construction of the check dams), tens of debris flows and floods occurred, flowing through these structures without damaging them too much compared to the high frequency of occurrence of the events. Nevertheless, on the 29 check dams built in the 1970's, 8 collapsed or are buried and at least 3 had to be maintained (n°20 (Figure 58), n°25 (repaired with flexible net) and n°29). The mechanisms leading to the collapse or severe damages to the check dams were (for the ones whose we know something):

- undermining
- lateral erosion: check dam n°19 almost broke up due to lateral overflow of a debris flow and subsequent incision in the banks; check dam n°20 right wing was destroyed following the intense storms of summer 1986 (Figure 58 and Figure 59) [52]; check dam n°25 right wing was also scoured and two flexible ring nets have to be set up to protect further lateral erosion and collapse of the dam (Figure 60).
- deficit in sediment supply: the collapse of check dams n°12 to n°15 is probably due to a deficit in sediment supply: this reach lies at the confluence between Illgraben and Illbach; until 1927, Illbach was a wild mountain stream, but in this year, Illsee dam was completed (and further heightened in 1943). The dam completely changed the hydrodynamic conditions of Illbach catchment by catching most of the water of the upper catchment. This led to a decrease in Illwasser (torrent draining the Illbach catchment) discharges as well as sediment transport. During the construction of the check dams, the channel bed was maybe in a non-equilibrium phase, with degradation dominating. This feature probably further led to the collapse of the dams.
- impacts of big boulders: especially in the upper part of the catchment, some check dam crests are seriously damaged (Appendix 28: figures 3 to 7).

If an appropriate civil engineering design is of major importance, flow dynamics and geomorphological features of Illgraben catchment cannot be neglected; not taking into account these parameters could lead to severe damages or even collapse of the concrete structures.

Figure 58. Lateral scour and destabilistation of check dam n°20 [52]

Figure 59. Overview of scour at check dam n°20 [52]

Figure 60. Lateral erosion and flexible ring net barrier at check dam n°25 [67]

The objectives concerning these issues are to get an overview of the geomorphological processes in Illgraben (from check dam n°9 to the Rhône river), with a closer look upstream and downstream of the check dams; the aim is to get an idea of the flow behaviour around these structures and to assess the actual state of the check dams according to channel morphological features and theoretical concepts (equilibrium and critical slopes, potential scour depths, sediment transport).

4.6 Geomorphological analysis

4.6.1 Field data

Illgraben channel morphology is mainly affected by debris flow and bedload dynamics. These two flow types interact strongly, creating a complex sediment transfert process (see Figure 77). A recent study (Berger, in prep.) tends to show there exists a relation between the 'flood-years' type and the 'debris flow-years' type on the channel bed level: floods (i.e. small, very frequent floods) seem to deposit material while debris flows and severe floods seem to remove this material.

A field campaign was conducted and consisted in measurements of length profiles as well as cross sections, the latter especially close to check dams. The measurements were done using the Leica DISTO A8™ laser device (for short distances and slopes/banks angles measurements) and the Leica Laser Locator™ binoculars for long distances and also for angle measurements (especially for the channel length profile). Three types of cross sections have been measured:

- the 'flood channel', incising into the debris flow deposits and being of most interest for the scour and sediment transport analysis (see Appendix 28: figure 2).
- the 'debris flow channel', which could be considered as what is called generally the minor bed.
- the top-bank cross sections, measured from the top of the 'debris flow' channel banks.

The scatter of the data is not equally distributed along the channel; the measurements density is greater at the vicinity of the check dams. Anyway the data gathered give a good view of the morphology of the channel along the fan and its evolution close to the structures.

4.6.2 Length profile and slopes

The data collected are summarized in Figure 61. We can observe that at the fan apex (i.e. check dam n°15), the slope mean is around 9.5% while near the Illgraben mouth, slopes lie around 7%. After Zimmermann & al. [72], mean fan slope is 10.1%, divided into an upper part with a mean of 11.1% and a lower part with 8.4%. A calculation of the original slope (without taking into account check dams) between check dam n°15 and check dam n°29 gives a slope of 9.2%. On all reaches between two consecutive check dams, the mean actual slope doesn't exceed this value (see Table 19); the reduction of slope is the most important benefit from check dam construction. However, even if the mean slope doesn't exceed the original bed slope, the slopes at the fan apex are close to this value and decrease from upstream to downstream (Figure 61).

This weird feature, at least for the section between check dam n°16 and n°19, could be explained by a huge rockfall which occurred on the left handside of the Illbach channel; the torrent is incising this mass, increasing the bed slope. Moreover, between the Bhutan bridge and check dam n°19, a debris flow overflowed on the left bank, creating a new channel and bypassing the previous one until check dam n°19. This shortening had to be compensated by an increase of the slope. But the explanation for the entire fan has to be found elsewhere.

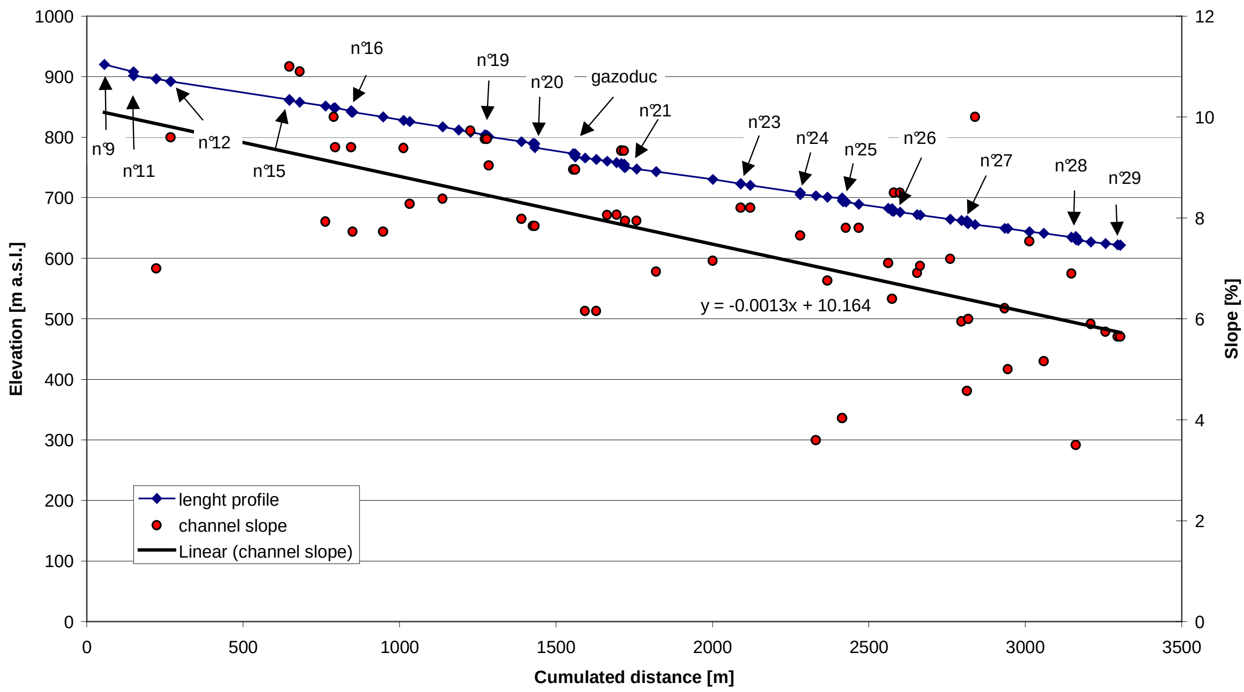

Figure 61. Illgraben length profile and slopes (November 2008 data). Location of check dams are given as indication.

We went further in the topic to find whether there exists any consistency between the slopes measured in the channel and the one found on the fan.To do that, we draw two cross profiles at ~45° across the fan on the W and on the E of the Illbach channel (Figure 62). Results are displayed on Figure 63, Figure 64 and Appendix 32. On Figure 63, we are able to see a decrease of the slopes when going downstream across the fan (the representation of the channel slope is bad, as the cell size used is 40m: thus the slopes are influenced by the steep slopes of the banks and are not representative).

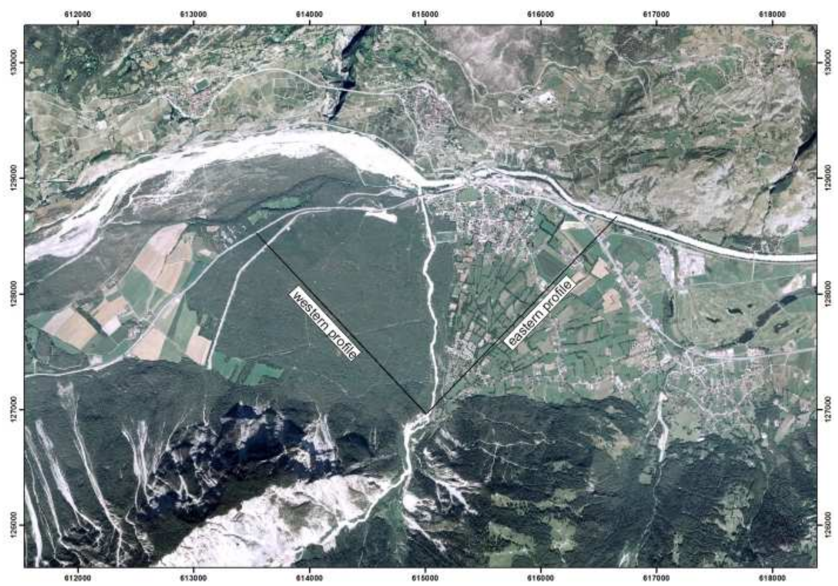

Figure 62. Location of the slope profiles along the Illbach fan

The general trend is:

- slope of more that 10% for the upper part of the fan

- slope between 8-9 % at the middle of the fan
- slope around 7% for the distal parts

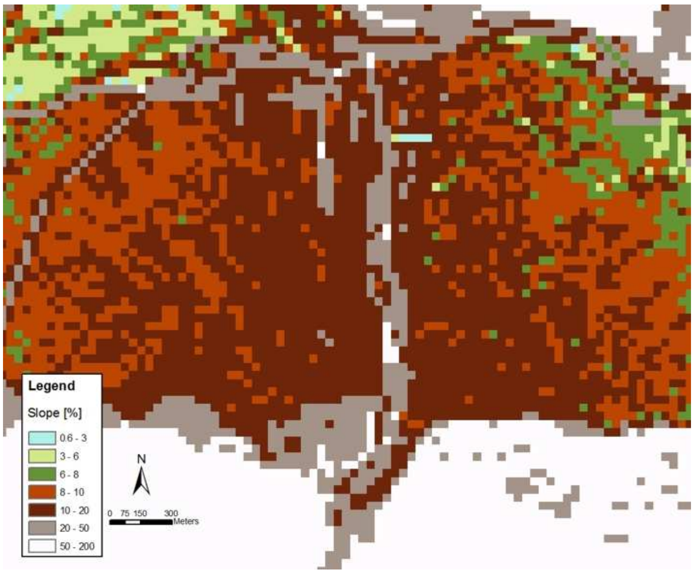

Figure 63. Slopes on the Illbach fan; cell size = 40m

Figure 64 shows much more into details the spatial distribution of slopes for the three profiles analysed. We have the confirmation of a general decrease of slopes with distance from fan apex, even if there is no clear break between slopes. This general trend is quite uniformly widespread. One explanation for this feature, on a large scale, would be related to the deposition pattern of debris flow across the fan. Slope is a major factor for debris flow dynamics and flatter slopes lead to deposition.

The successive debris flows have stopped depending on their rheology, their volumes, the bed slopes, etc. and these slope patterns could be used as a marker of deposition over time: small and frequent debris flows are less prone to reach the Illbach mouth than big and rare ones. The former would deposit much material or even stop close to the fan apex and the latter would flow further down. Deposition is enhanced as the debris flow flows out of the channel. These successive depositions could actually explain quite well the fan slope gradation.

Being aware of such processes might be important to roughly evaluate the area prone to erosion and deposition (depending on the sediment-transport process). Debris flows would rather deposit in the upstream part of the fan and provide less sediment for the downstream reaches, whereas floods would remove these deposits (because on steeper slope) and deposit further downstream (where slopes are more gentle).

Moreover, a comparison was performed between all available length profiles from 1998 to 2008, and it seems to exist a constant increase in slopes with time (Appendix 29). These observations are limited between check dam n°15 and check dam n°20 and could be explained by several geomorphological changes that occurred during this period:

- a bypass (explained above)
- numerous observations made at check dam n°15 and n°16 (Figure 65) show that the channel bed is moving vers fast and could lead to local slopes which are completely different from the bulk one.

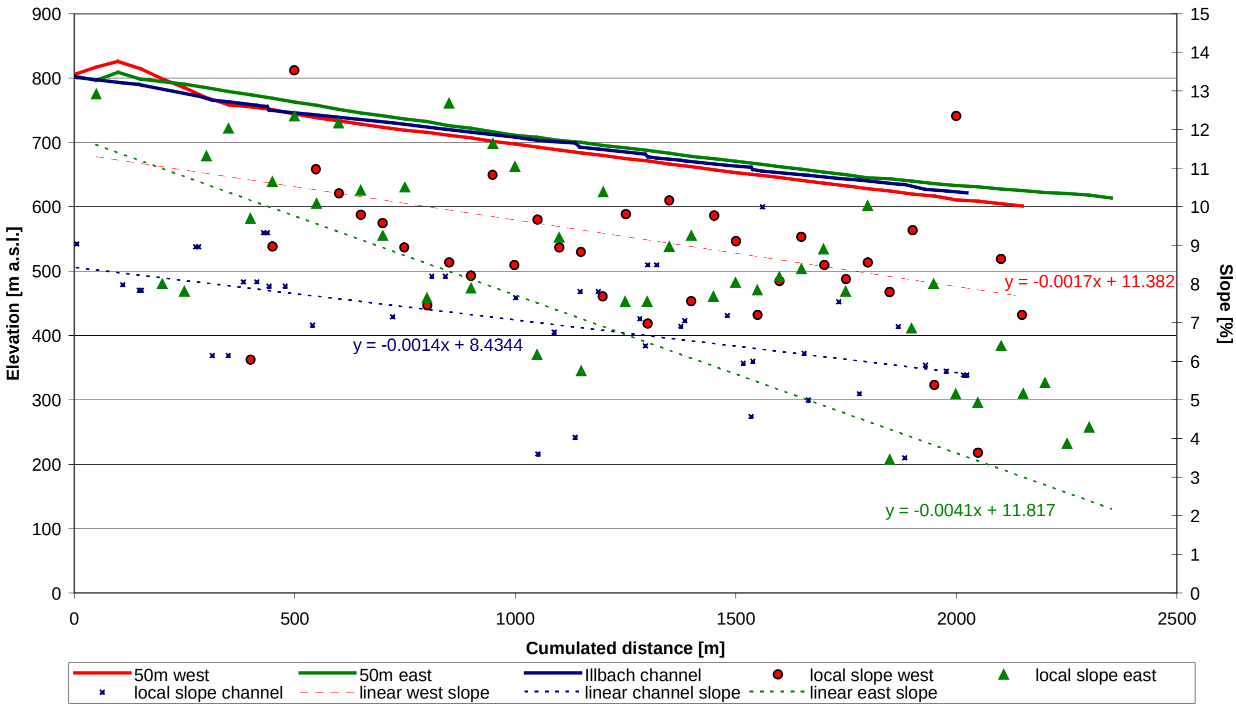

Figure 64. Synthesis of slopes on the eastern, channel and western part of Illbach fan.
Most upstream point is check dam n°19

Caution should be taken to the scale at which data are analysed: working on an event time scale / local spatial scale is completely different than working on the year or decade time scale / fan spatial scale. Making a direct link between local observations and fan observation could lead to wrong interpretations.

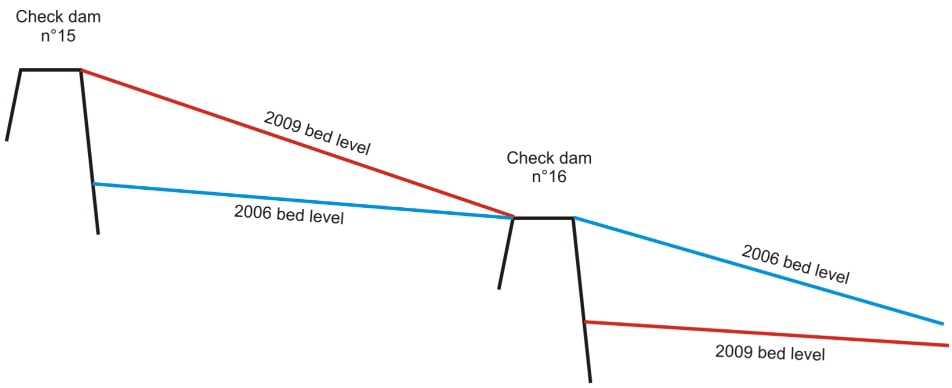

Figure 65. Bed elevation between check dams n°15 and n°16 between 2006 and 2009 (observations made by Bardou)

4.6.2.1 Equilibrium slope

After computing and comparing the slopes over time in Illgraben, we had a look more into details on the differences between the initial bed slope of Illbach channel, the actual slope influenced by the check dams and the concept of equilibrium slope.

The equilibrium slope is mentionned in many papers [7],[36],[47],[68] and is described as the equilibrium state to which each channel tends to reach. High-gradient streams often exhibit a naturally formed step-pool architecture, which likely represents self-ajustment of stream towards higher bed stability (Lenzi, 2001).

Lenzi and Comiti have done many researches on the topic of natural step-pool morphology and tried to demonstrate that the river creates by itself such drop structures in order to minimize its energy. The same reasoning might apply for torrent check dam building that is a reduction of the destructive energy of floods and debris flows. Equilibrium slope could be defined as the slope below which channel bed will not move; it is a balance between erosion and deposition of sediments [7]. Figure 66 shows the effect of check dams on the equilibrium slope: as this ideal case is seldom reached, check dams allow to diminish the potential eroded volumes compared to the one which would occur without these concrete structures.

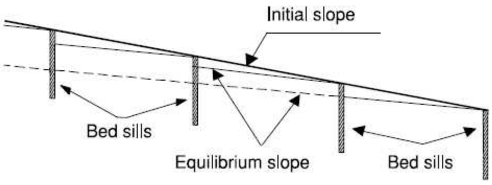

Figure 66. Effect on check dam on the eroded volume to reach the equilibrium slope [39].

Equilibrium slope J_E (see Figure 67) is related to shear stress (which could be seen as a function of intrinsic bed properties (like grain size), as defined by Meyer-Peter); once the latter is exceeded, sediment transport, and thus erosion, can start. Two granulometric profiles have been realized under the Bhutan bridge and between check dams n°26 and n°27, in the flood channel, by Minoia [44]. The raw values as well as granulometric curve are listed in Appendix 30.

If during a flood or concentrated flow, the bed slope is greater than $J_{E,}$ then bed erosion will occur and if this equilibrium hasn't been considered when designing the check dams, the stability of the upstream check dam is threaten. This is the reason why, at least, the check dam at the most downstream part of the channel should lie on a fix point, to prevent a total collapse of the system. As a general rule, the critical gradient should not be assumed to be more than 4% (pers. communication Böll).

J_E could be calculated, using the following relation [7]:

$$J_E \cong \frac{0.4 \cdot d_{90}^{9/7}}{q_{\max}^{6/7}} \qquad \text{Eq. 32}$$

where

d_{90} = grain size whose diameter is represented by the 90th-percentile from the grain distribution curve [m]

q_{max} = maximal specific discharge per meter channel width [m³/s/m]

Eq.32 is used for rectangular channel. For trapezoidal channel, we use:

$$q_{\max} \cong \frac{Q_{\max}}{b_m} \quad \text{where} \quad \frac{b_m}{y} > 8 \qquad \text{Eq. 33}$$

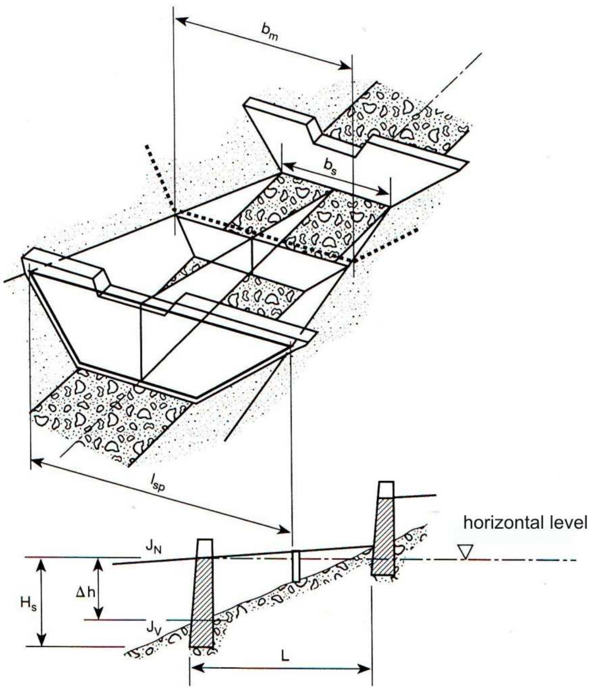

Figure 67. 3D-sketch of a serie of check dams and equilibrium slope concept [7]

From Eq.32, we calculated the equilibrium slope for each reach lying between 2 successive check dams. Results are displayed on Table 18. We can see that no reach, following the method in [7], is in equilibrium and thus all reaches are prone to erosion.

Table 18. Theoretical equilibrium slopes calculated for Illgraben from check dam n°11 to n°29. Flood discharge is taken from hydrological analysis (return period: 2.33 years; method:modified rational formula, with elevation effect on precipitations)

			Illgraben reaches											
			11 to 15	*15 to 16*	*16 to 19*	*19 to 20*	*20 to gazoduc*	*gazoduc to 21*	*21 to 24*	*24 to 25*	*25 to 26*	*26 to 27*	*27 to 28*	*28 to 29*
equilibrium slope	**J_E**	**[-]**	**0.03**	**0.03**	**0.03**	**0.03**	**0.03**	**0.03**	**0.03**	**0.03**	**0.02**	**0.03**	**0.03**	**0.02**
grain size d_{90}	d_{90}	[m]	0.21	0.21	0.21	0.21	0.21	0.21	0.21	0.21	0.21	0.21	0.21	0.21
max specific discharge	q_{max}	[m^3/s/m]	2.0	1.7	2.0	2.3	2.1	2.3	2.1	2.3	2.5	2.0	2.0	3.5
minor channel width	B	[m]	8.7	10.1	8.7	7.3	8.0	7.5	8.1	7.3	6.8	8.6	8.4	4.9
max discharge	Q_{max}	[m^3/s]	17	17	17	17	17	17	17	17	17	17	17	17

flood return period = 2.33 years
maximum discharge taken from the modified rational formula for Illgraben, with altitude effect on precipitations

If we now compare these values with the ones obtained by calculating what we have called the ‘critical minimum slope’ (Figure 68) (that is the mean slope between the foundation of the upstream check dam to the crest of the next downstream check dam; it represents the mean slope below which scour could occur at the toe of a check dam; see details in Appendix 34), we observe that the critical minimum slopes are, except for 2-3 locations, above J_E. When looking at the critical maximum slope (Figure 68), one can see that 3 reaches reach the maximum slope: this means that these reaches are a kind of ‘maximum slope possible’ and are prone to erosion (in fact, on the 3 reaches concerned, 2 are located where check dams have been destroyed). The equilibrium slope is probably never reached in Illgraben, but by building check dams, one allows to approach it and to reduce the potential amount of bed erosion. This equilibrium concept provide a limit for stable bed to flow erosion; however, even if the critical slopes are often exceeded, one has be aware that the chosen flood here has a quite high discharge and doesn’t correspond to very frequent events; by taking a 5

m^3/s flood, the critical slope values raise to 5 to 9%, which correspond to the mean slope between the check dams.

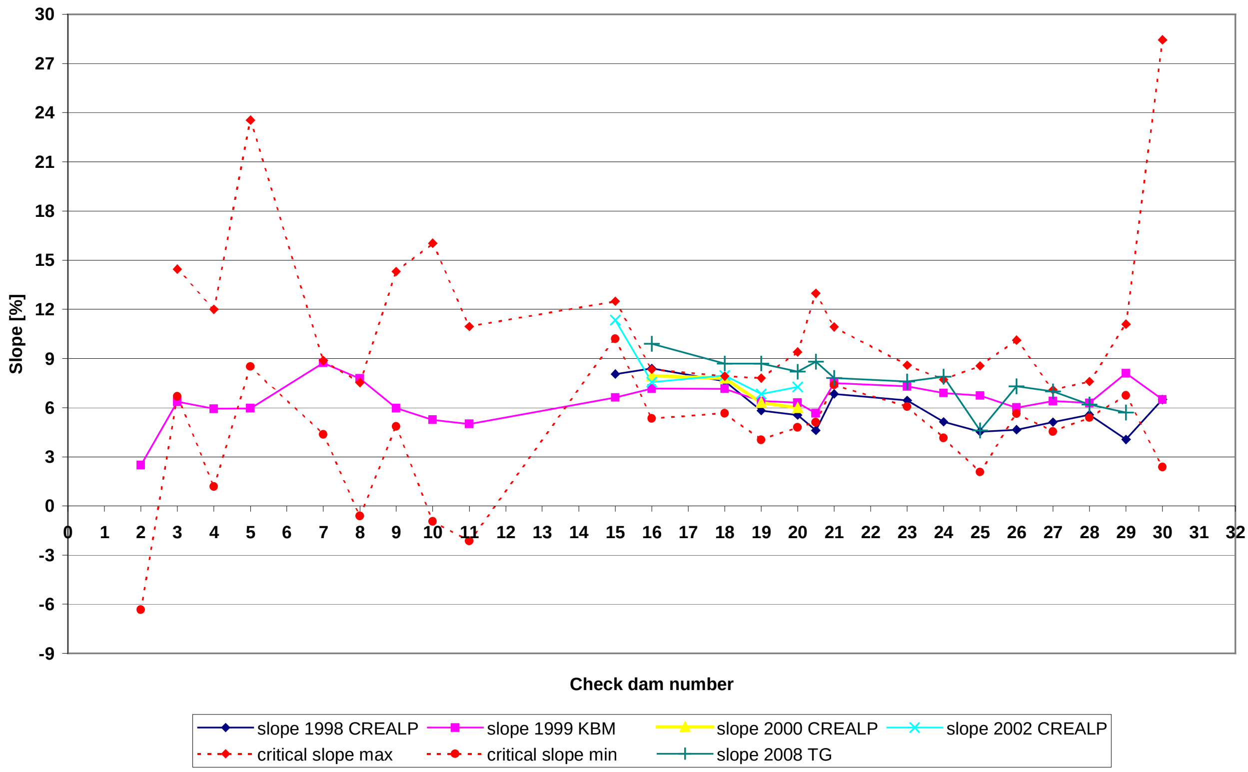

Figure 68. Comparison between measured slopes and critical minimum and maximum slopes

4.6.2.2 *Scour problematics*

Scour is a major issue for gravity check dams and has to be considered cautiously. From the field dataset, some features specific to check dams could be detected. From the raw cross-section data, we tried to enhance the results by representing the channel morphology not with the real width, but with a ratio: measured channel width / mean channel width. To do that, we divided the dataset into two parts: the ‘flood channel’ width and the ‘debris flow channel’ width; the top-bank width hasn’t been used for this analysis.

Then we calculated the mean channel width for both classes (after removing the outliers) and we divide all the measured cross-sections by these values to obtain the ratio of a given channel width to the main values (which could be assess as a kind of equilibrium width). The aim of this representation was to have a visual representation of the zones which are enlarged or narrowed compared to a reference width. The result is shown on Figure 69 and Figure 70. One can see that by looking at the ‘flood channel’, there is an almost systematic enlargment just downstream of check dams and sometimes upstream too. This feature is interesting because it shows that something happens around these structures; enlargement of the channel at the right of a check dam is not a positive aspect because it means that scour happens.

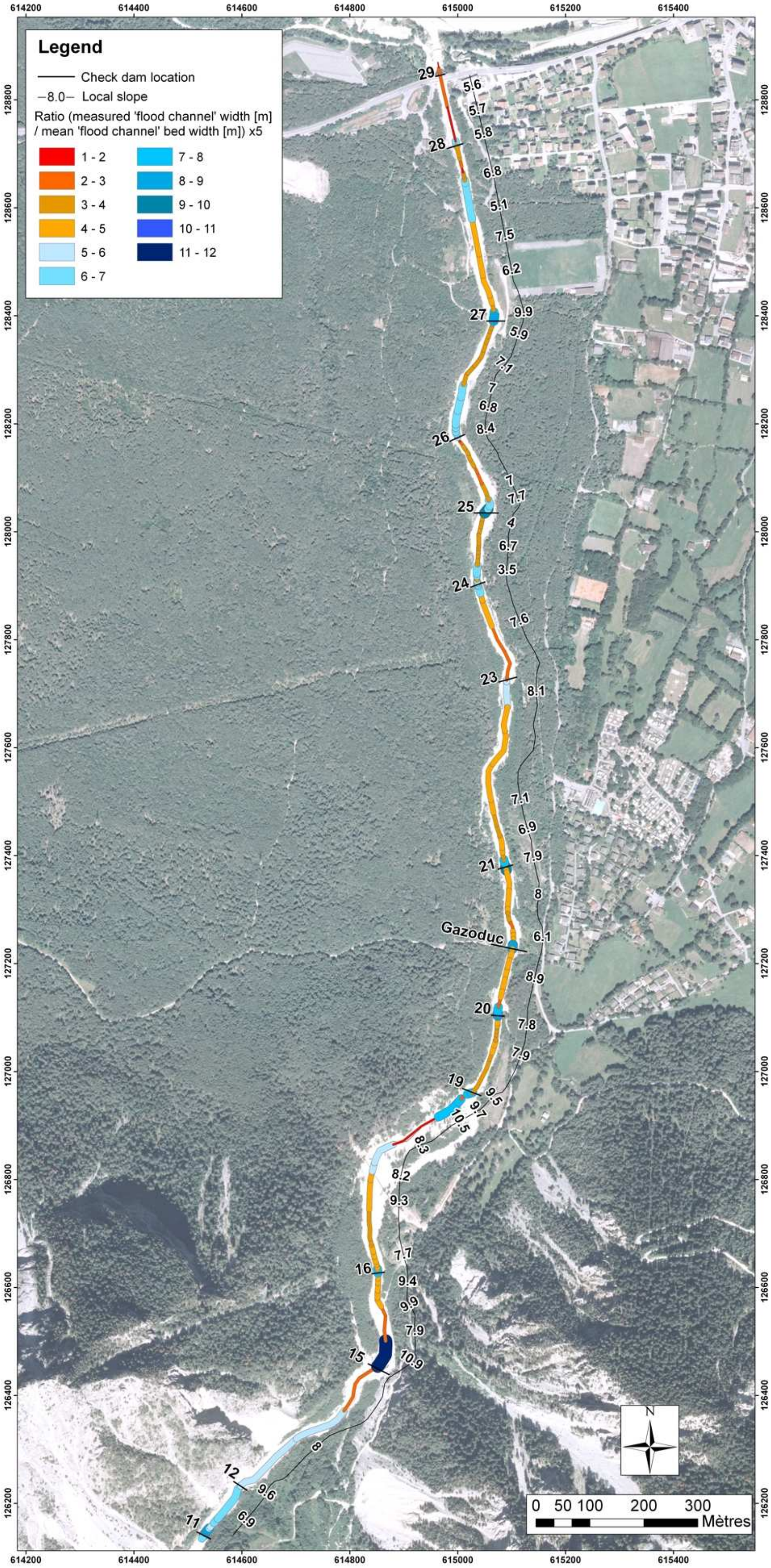

Figure 69. View of Illgraben fan. Represented is the ratio: measured flood channel width/main flood channel width from check dam n°11 to Rhône river; local slopes are indicated beside

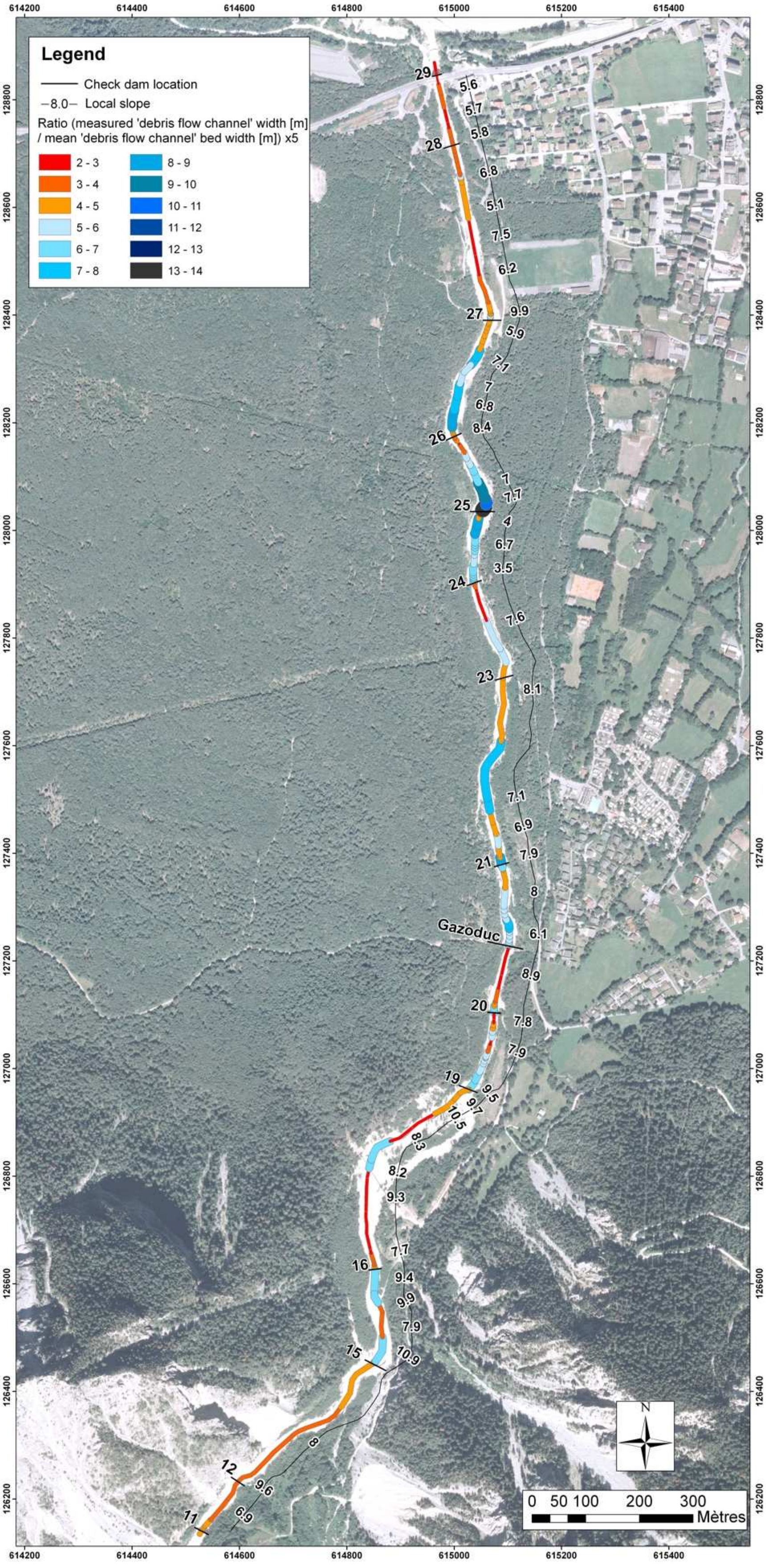

Figure 70. View of Illgraben fan. Represented is the ratio measured debris flow channel width/main debris flow channel width from check dam n°11 to Rhône river. Local slopes are indicated beside.

From Figure 69 and Figure 70, we tried to see if a link was possible between these enlargements and the local slopes; no systematic trend could be observed.

Scour is a process which can occur in both vertical and lateral directions. The check dams, by straightening the slope up, have to compensate this flattening by an abrupt transition to the next reach. This vertical drop (Figure 71) induces an increase in velocities and when reaching the channel bed, the accelerated flow has to dissipate the extra kinetic energy gained by turbulent processes. These processes provoke erosion of the ground layer before the flow reaches a normal regime again. These energy dissipation at the toe of a check dam creates most of the time a scour hole, whose length and depth depend on many factors like discharge, slope, drop height, etc.

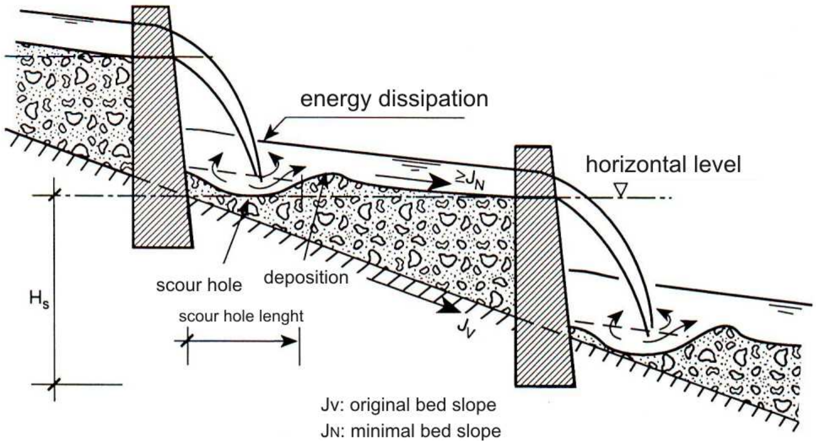

Figure 71. Minimum(=equilibrium) slope and energy dissipation due to check dam implantation [7].

Although strong scour holes in Illgraben have been reported in many reports and could be observed partially on one or two check dams, the trend during the measurement campaign was more on partial deposition and partial scouring at the toe of check dams, as shown on Figure 72 and Appendix 29. This figure is very interesting and shows quite well the problematics. We can see on the left bank at the toe of the structure a small landslide; the middle part of the channel is filled with ~1m of gravel and sand deposition while on the right bank, we see the scour under the check dam as well as a small lateral landslide. Figure 73 shows well the lateral incision from water into the toe of the right bank, generating bank destabilization.

The deposition downstream of check dam are made of gravels, sand and are quite uniformly distributed. There are probably due to bedload transport, which, due to energy losses, hasn’t enough strenght to move the sediment further downstream; this deposition will be washed away at the following important flood or debris flow. However, this sediment amounts force the flow to move lateraly as it cannot continue straight in the channel; these lateral derivations seem to induce the observed lateral erosion.

Depending on the flow process dominating (debris flow, flood, baseflow), the morphology of the channel and thus the state of check dams will continously change.

Long period of baseflow will tend to fill the channel, major floods would tend to erode (depending on the transport capacity, discussed below) and debris flow would include both processes: the front will tend to erode as the tail could be associated to hyperconcentrated flows and will tend to deposit depending to its transport capacity. In Illgraben, balance budget seems to show that debris flow is more an erosion process than a deposition one, but this topic is still subject to discussion.

Figure 72. Deposition and scour at check dam n°11

Figure 73. View from the brink of check dam n°11 on lateral erosion

An analysis of maximal potential scour depth has been performed based on empirical formulations. They give a maximum potential scour depth given a flood discharge. The first method is described in [37]. Results are displayed in Appendix 34. The maximum potential scour depth for a 2.33 years flood lies between 9m and 46m; these values are overestimating the reality; the reason which could explain such extremes values is in the equation: the sill spacing has to be introduced. As spacing between check dams are very important in Illgraben, this led to inadequate results.

Another method, described in [7], was approached but one needs to know among other parameters the velocity and flow height downstream of the check dam. As we have no information about these parameters, we just made a simple calculation, with average parameters (that are representative of Illgraben check dams) and a 2.33 years flood. The result T_G is given as scour depth measured from the energy line to the deepest point of the scour depth (see Figure 74). This method has the advantage to take into account solid transport (if present). A value of 3.25m was found, from which kinetic energy and flow depth has to be removed. These values are much more realistic and it might be interesting for further studies, to look at the potential scour depth which could result from a given flood.

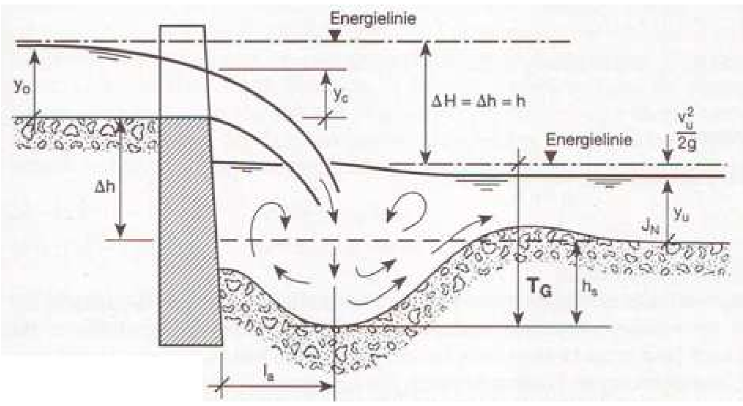

Figure 74. Schematic view for scour depth calculation with [7].

4.6.2.3 Sediment transport capacities

As sediment transfer for frequent to very frequent events seems more related to flood than debris flows, it was interesting to have a look at the flood transport capacity of the Illbach, to more or less visualize which reaches (based on 2008 survey) are prone to erosion and which one to deposition. We based our calculations on the concept of maximum transport capacity of a given flood. Meyer-Peter developped a method for flat river while Rickenmann and the SOGREAH extend the formulations to mountain torrent (with limiting slope at 20%). We used this two methods to assess the maximal sediment transport capacity for each reach, whose main features are given in Table 19. We made the assumption that Illbach river is a transport-limited river (at least for the upper part) and that the paving layer in Illbach river is inexistant (due to the high frequency of debris flow events which are eroding this layer at each surge).

Table 19. Main features of channel morphology in Illgraben

reach	mean slope	mean 'debris flow channel' width	mean 'flood channel' width	distance between check dam
[-]	*[%]*	*[m]*	*[m]*	*[m]*
11 to 15	8	10.8	8.7	498
15 to 16	9.15	16.1	10.1	202
16 to 19	8.83	10.2	8.7	434
19 to 20	7.98	13.6	7.3	152
20 to gazoduc	8.96	9.5	8.0	129
gazoduc to 21	7.43	17.9	7.5	156
21 to 24	7.55	20.7	8.1	562
24 to 25	4.62	14.3	7.3	134
25 to 26	7.19	22	6.8	160
26 to 27	6	14.1	8.6	239
27 to 28	6.6	14	8.4	348
28 to 29	5.45	12.7	4.9	141

The flood hydrogram for a $Q_{2.33}$ flood event was obtained in the hydrological analysis and is given is Figure 75. The solid transport starts not long after the beginning of the flood and solid hydrogram shows peak values comprised between 2 and 3 m^3/s.

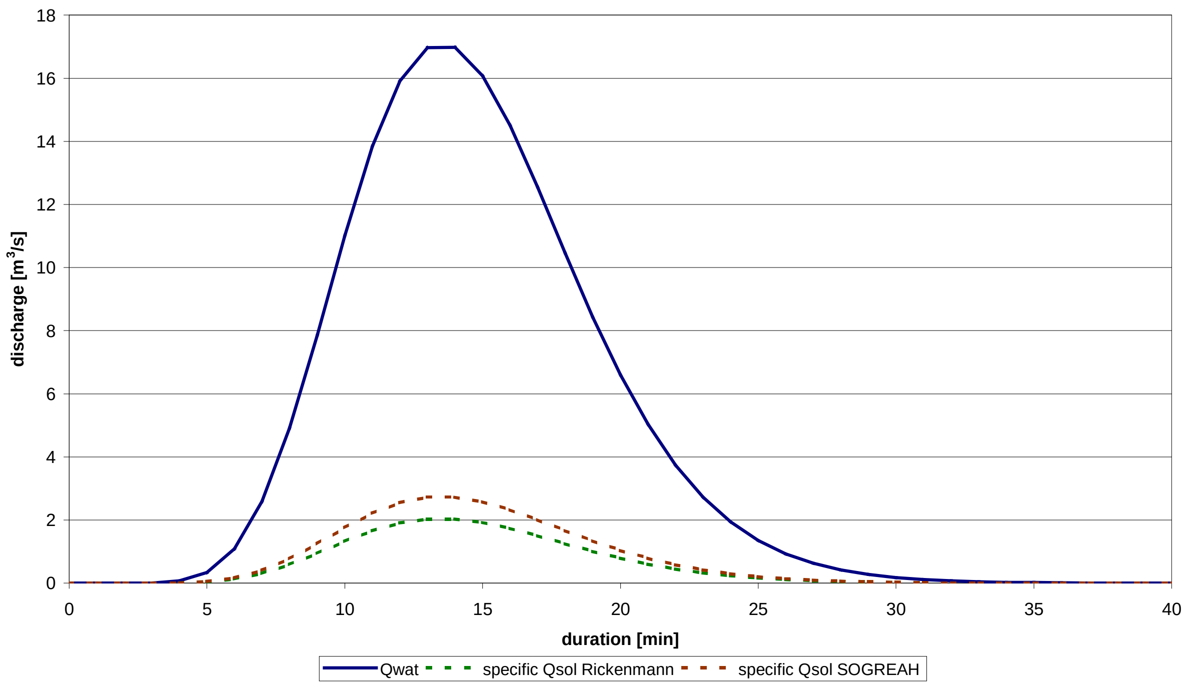

Figure 75. Hydrogram and solidogram for a $Q_{2.33}$ flood, using the modified rational formula (with altitude-rainfall effect)

The total maximum sediment volumes that can be transported by the flood are displayed on Figure 76. Calculations have been performed for all reaches and total volumes which could transit within a reach are given as the sediment balance between two consecutive reaches; if the maximum transport volume on the downstream reach is higher than on the upstream one, erosion will occur (unless J_E is reached); if not deposition will take place. Results are given in Table 20.

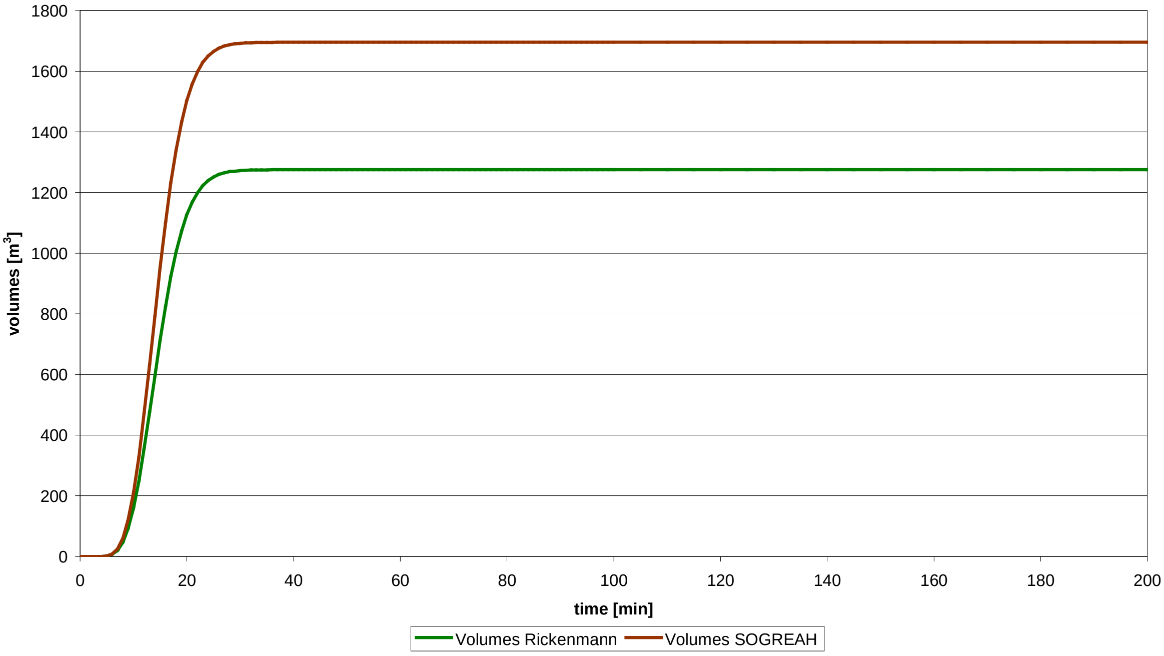

Figure 76. Solid volumes for a $Q_{2.33}$ flood, calculated from hydrogram given in Figure 75.

Table 20. Maximum sediment transport capacity calculated for each reach from check dam 11 to 29, considering a 2.33 years flood

reach	Sediment transfer in debris flow channel								Sediment transfer in flood channel							
	volume with Rickenmann formula		sediment balance	sediment process	volume with SOGREAH formula		sediment balance	sediment process	volume with Rickenmann formula		sediment balance	sediment process	volume with SOGREAH formula		sediment balance	sediment process
[-]	[m³/m]	[m³]	[m³]		[m³/m]	[m³]	[m³]		[m³/m]	[m³]	[m³]		[m³/m]	[m³]	[m³]	
11 to 15	2'748	29'682			3'051	32'951			2'748	23'911			3'051	26'544		
15 to 16	3'596	57'891	28'208	erosion	3'745	60'288	27'337	erosion	3'596	36'317	12'406	erosion	3'745	37'820	11'277	erosion
16 to 19	3'349	34'155	-23'736	deposition	3'547	36'178	-24'110	deposition	3'349	29'132	-7'185	deposition	3'547	30'857	-6'963	deposition
19 to 20	2'735	37'191	3'036	erosion	3'039	41'335	5'158	erosion	2'735	19'963	-9'169	deposition	3'039	22'187	-8'670	deposition
20 to gazoduc	3'448	36'823	-368	deposition	3'627	37'667	-3'668	deposition	3'448	27'583	7'620	erosion	3'627	29'014	6'827	erosion
gazoduc to 21	2'371	42'433	5'609	erosion	2'725	48'782	11'115	erosion	2'371	17'779	-9'804	deposition	2'725	20'439	-8'574	deposition
21 to 24	2'448	50'669	8'236	erosion	2'793	57'811	9'029	erosion	2'448	19'827	2'048	erosion	2'793	22'622	2'182	erosion
24 to 25	916	13'099	-37'569	deposition	1'314	18'796	-39'015	deposition	916	6'687	-13'140	deposition	1'314	9'595	-13'027	deposition
25 to 26	2'220	48'836	35'736	erosion	2'592	57'021	38'225	erosion	2'220	15'095	8'408	erosion	2'592	17'625	8'030	erosion
26 to 27	1'546	21'792	-27'044	deposition	1'965	27'701	-29'320	deposition	1'546	13'292	-1'803	deposition	1'965	16'896	-729	deposition
27 to 28	1'870	26'184	4'392	erosion	2'274	31'830	4'129	erosion	1'870	15'710	2'419	erosion	2'274	19'098	2'202	erosion
28 to 29	1'275	16'193	-9'991	deposition	1'695	21'527	-10'303	deposition	1'275	6'248	-9'463	deposition	1'695	8'306	-10'793	deposition

Erosion / deposition processes are fluctuating quite constantly from one reach to the other one. But the main issue we can see are the volumes eroded or deposited within a same reach. If the volume coming to check dam n°11 could be justified because sediment supply upstream is quasi unlimited, we are in right to ask what is happening for the following reaches. The volumes eroded are really huge. To demonstrate it: if we take the reach 15 to 16, that is ~200m long, an eroded volume of ~28'000m^3 would mean around 140m^3/m. By taking a mean channel width of 14m and bank erosion, we would have a vertical erosion of 6-8m, which is, for a $Q_{2.33}$ flood, not reasonable at all.

In order to deal with empirical erosion values, we made the assumption, this time, of a Q_{100} flood and erosion was calculated using empirical formulations. They were developed to assess the potential maximum erosion depth for debris flow; the first one is taken from [20]; it stipulates that for debris flow, the incision of the bed could be estimated as 1/3 to 1/5 of the channel width (1/3 for material very sensitive to erosion). The other relation is taken from Kronfeller-Kraus (1984) and was developped following extreme debris flow events that occurred in Austria; it is given by:

$$e = 1.5 + 12.5 * J \qquad \text{Eq. 34}$$

where

e = maximum potential erosion [m]
J = slope [-]

The first estimation would give, for a mean channel width of 14m, a maximum erosion depth of 2.8m to 4.6m and Eq. 42 gives, for a mean channel slope of 8%, an maximum erosion depth of 2.5m.

As these formulas were developped for rare events, it is justified to make the calculations with a Q_{100} flood. The results are given in Table 21 and Table 22. Sediment balance have been calculated here as the maximum volume transported, but with taking account for erosion when the flow has enough strenght to erode. For the calculation of the erosion depth, we use the Eq. 34. The erosion depths were multiplied by the length and mean width of each reach to get the maximum erosion volume. We assumed that the transport capacity entering in the system (i.e. check dam n°11) is total. This gives huge volumes (~400'000m^3); afterwards, the erosion/deposition volumes have been calculated for each reach. If the erosion depth could be assumed as realistic, the maximum sediment transported reaching check dam n°11 corresponds to an extreme debris flow event volume! and for such discharges and transported volumes, debris flow are more prone to occur than floods.

Table 21. Maximum sediment transport and maximum erosion depth for Q100 for debris flow channel type (modified rational formula; with altitude effect)

reach	Sediment transfer in debris flow channel									
	volume with Rickenmann formula		maximum erosion volume	sediment balance	sediment process	volume with SOGREAH formula		maximum erosion volume	sediment balance	sediment process
[-]	[m^3/m]	[m^3]	[m^3]	[m^3]		[m^3/m]	[m^3]	[m^3]	[m^3]	
11 to 15	37'223	402'008				40'151	433'631			
15 to 16	41'174	662'901	8456	410464	erosion	43'338	697'742	8'456	442'087	erosion
16 to 19	38'344	391'109	11510	391109	deposition	41'063	418'843	11'510	418'843	deposition
19 to 20	31'316	425'898	5163	396272	erosion	35'224	479'046	5'163	424'005	erosion
20 to gazoduc	39'481	375'070	3211	375070	deposition	41'983	398'839	3'211	398'839	deposition
gazoduc to 21	27'147	485'931	6782	381852	erosion	31'608	565'783	6'782	405'621	erosion
21 to 24	28'032	580'262	28429	410281	erosion	32'386	670'390	28'429	434'050	erosion
24 to 25	10'494	150'064	3981	150064	deposition	15'344	219'419	3'981	219'419	deposition
25 to 26	25'422	559'284	8444	158508	erosion	30'072	661'584	8'444	227'863	erosion
26 to 27	17'702	249'598	7582	166090	erosion	22'845	322'115	7'582	235'445	deposition
27 to 28	21'420	299'880	11327	177417	erosion	26'406	369'684	11'327	246'772	erosion
28 to 29	14'605	185'484	3906	181323	erosion	19'736	250'647	3'906	250'678	deposition

Table 22. Maximum sediment transport and maximum erosion depth for Q100 for flood channel type (modified rational formula; with altitude effect)

reach	Sediment transfer in flood channel									
	volume with Rickenmann		maximum erosion volume	sediment balance	sediment process	volume with SOGREAH formula		maximum erosion volume	sediment balance	sediment process
[-]	[m3/m]	[m^3]	[m^3]	[m^3]		[m3/m]	[m^3]	[m^3]	[m^3]	
11 to 15	37'223	323'840				40'151	349'314			
15 to 16	41'174	415'857	5'636	329'476	erosion	43'338	437'714	5'636	354'950	erosion
16 to 19	38'344	333'593	9'770	333'593	erosion	41'063	357'248	9'770	357'248	erosion
19 to 20	31'316	228'607	2'677	228'607	deposition	35'224	257'135	2'677	257'135	deposition
20 to gazoduc	39'481	315'848	2'580	231'187	erosion	41'983	335'864	2'580	259'715	erosion
gazoduc to 21	27'147	203'603	2'852	203'603	deposition	31'608	237'060	2'852	237'060	deposition
21 to 24	28'032	227'059	11'437	215'040	erosion	32'386	262'327	11'437	248'497	erosion
24 to 25	10'494	76'606	2'360	76'606	deposition	15'344	112'011	2'360	112'011	deposition
25 to 26	25'422	172'870	2'557	79'163	erosion	30'072	204'490	2'557	114'568	erosion
26 to 27	17'702	152'237	5'293	84'456	erosion	22'845	196'467	5'293	119'861	erosion
27 to 28	21'420	179'928	7'454	91'910	erosion	26'406	221'810	7'454	127'315	erosion
28 to 29	14'605	71'565	1'460	71'565	deposition	19'736	96'706	1'460	96'706	deposition

Following the previous results, a last calculation have been made: this time, we took a $Q_{2.33}$ again, but assuming an erosion depth of 0.5m. The erosion volumes have been obtained with the same method as previously explained and the maximum transport capacity was assumed in the reach 11 and 15. A sediment balance have been done in order to see the maximum volume transported in each reach and if erosion or deposition occur. Results are displayed in Table 23 and Table 24. As we can see, for debris flow channel, the eroded volumes are not very important expect for the reach between 21 and 24 (where check dams are missing). All the upper part is in erosion process (except reach 20 to gazoduc where a tiny volume could deposit) whereas huge deposition volumes are expected between check dams 14 and 15. Downstream, erosion is the major process.

Table 23. Maximum sediment transport and maximum erosion depth for Q2.33 for debris flow channel type (modified rational formula; with altitude effect)

reach	Sediment transfer in debris flow channel									
	volume with Rickenmann formula		erosion	sediment balance	sediment process	volume with SOGREAH formula		erosion	sediment balance	sediment process
[-]	[m^3/m]	[m^3]	[m^3]	[m^3]		[m^3/m]	[m^3]	[m^3]	[m^3]	
11 to 15	2'748	29'682				3'051	32'951			
15 to 16	3'596	57'891	1626	31'309	erosion	3'745	60'288	1626	34'577	erosion
16 to 19	3'349	34'155	2213	33'522	erosion	3'547	36'178	2213	36'790	deposition
19 to 20	2'735	37'191	1034	34'556	erosion	3'039	41'335	1034	37'824	erosion
20 to gazoduc	3'448	36'823	613	35'168	erosion	3'627	37'667	613	37'667	deposition
gazoduc to 21	2'371	42'433	1396	36'565	erosion	2'725	48'782	1396	39'063	erosion
21 to 24	2'448	50'669	5817	42'381	erosion	2'793	57'811	5817	44'880	erosion
24 to 25	916	13'099	958	13'099	deposition	1'314	18'796	958	18'796	deposition
25 to 26	2'220	48'836	1760	14'859	erosion	2'592	57'021	1760	20'556	erosion
26 to 27	1'546	21'792	1685	16'544	erosion	1'965	27'701	1685	22'241	erosion
27 to 28	1'870	26'184	2436	18'980	erosion	2'274	31'830	2436	24'677	erosion
28 to 29	1'275	16'193	895	16'193	deposition	1'695	21'527	895	21'527	deposition

For the flood channel type, the erosion/deposition processes are more balanced. However, the volumes deposited in reach 19 to 20, 24 to 25 and 28 to 29 are important, of several meters.

Table 24. Maximum sediment transport and maximum erosion depth for Q2.33 for flood channel type (modified rational formula; with altitude effect)

reach	Sediment transfer in flood channel									
	volume with Rickenmann formula		erosion	sediment balance	sediment process	volume with SOGREAH formula		erosion	sediment balance	sediment process
[-]	[m³/m]	[m³]	[m³]	[m³]		[m³/m]	[m³]	[m³]	[m³]	
11 to 15	2'748	23'911				3'051	26'544			
15 to 16	3'596	36'317	1020	24'931	erosion	3'745	37'820	1020	27'564	erosion
16 to 19	3'349	29'132	1888	26'819	erosion	3'547	30'857	1888	29'452	erosion
19 to 20	2'735	19'963	555	19'963	deposition	3'039	22'187	555	22'187	deposition
20 to gazoduc	3'448	27'583	516	20'479	erosion	3'627	29'014	516	22'772	erosion
gazoduc to 21	2'371	17'779	585	17'779	deposition	2'725	20'439	585	20'439	deposition
21 to 24	2'448	19'827	2276	19'827	erosion	2'793	22'622	2276	22'622	erosion
24 to 25	916	6'687	489	6'687	deposition	1'314	9'595	489	9'595	deposition
25 to 26	2'220	15'095	544	7'231	erosion	2'592	17'625	544	10'623	erosion
26 to 27	1'546	13'292	1028	8'259	erosion	1'965	16'896	1028	12'084	erosion
27 to 28	1'870	15'710	1462	9'720	erosion	2'274	19'098	1462	12'430	erosion
28 to 29	1'275	6'248	345	6'248	deposition	1'695	8'306	345	8'306	deposition

4.6.3 Synthesis

The analysis done through this chapter allowed to have an overview of the sediment transport processes acting in the Illgraben and influencing the geomorphology of the channel. We have seen that check dams play a major role in these processes as they act on the channel slope distribution and allow for bulk reduction of erosion, by approaching or reaching the equilibrium slope. However these structures are sensitive to scouring and from the check dams analysis, we could observe that both deposition and erosion processes could occur at the same time, one increasing the other one sometimes. If debris flows are the processes that lead to major geomorphological changes, frequent floods and bedload transport seem to have an important role to play in Illgraben. The deposition and erosion around check dams were caused by such phenomenon and if no debris flow occur, this situation might worsten (increasing of lateral erosion and check dam toe scour) or get better (sediment deposition and filling of the bed). When a big debris flow occur, then strong erosion destabilizes the whole system; the 'normal' processes then start again on this new situation (Figure 77).

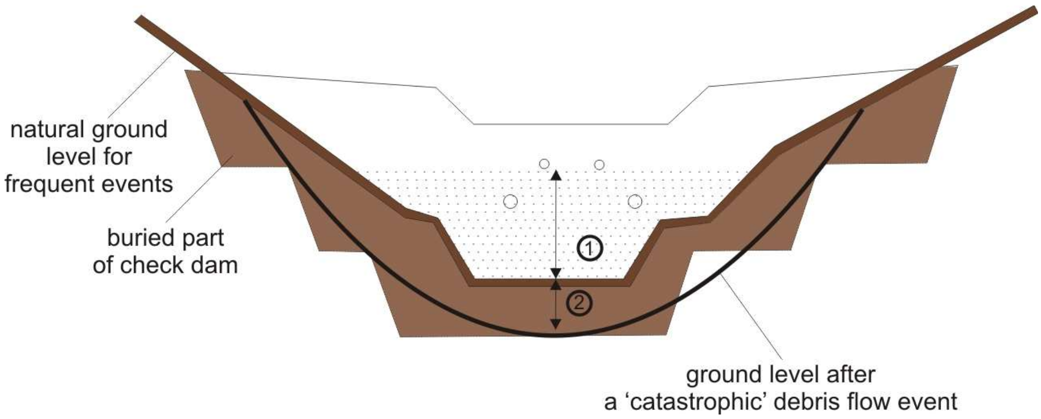

Figure 77. Evolution of the channel bed in time. 1) represents the evolution of the channel bed for frequent sediment transport events (bedload, small debris flow). 2) represents the bed degradation after a big debris flow event. Bed level evolution starts again from this new erosion level. (Bardou et al., in prep)

The sediment transport capacity calculated for mountain torrent are directly related to sediment size and slope; if slope is increasing, sediment transport will increase too, leading to bigger destabilisation of the channel (erosion/deposition pattern). We calculated the effect of a quite frequent flood, entering the system (in check dam 11) with a complete transport capacity and then we assumed a bed erosion of 0.5m. The results of this analysis (conducted for both debris flow channel type and flood channel type) were that:

- the erosion volumes along the reaches are comprised between 300 and 6000 m^3 (depending on the channel type and reach length)
- if the maximum transport capacity assumption upstream is fullfilled, then the deposited (and then bed aggradation) and eroded (bed deggradation) volumes are very important for both debris flow hazard (overflows possible) and check dam stability (scour due to erosion).
- the sediment volumes transported by bedload might be rather important and are generally not taken into account in the calculations of sediment balance in Illgraben (i.e. the force plate was set up to measure debris flow and not bedload transport).

The informations derived from these calculations might be useful to define which zones have to be looked cautiously after a important event and could be useful to define potential erosion area for debris flow in the numerical model RAMMS (discussed in §5.3).

5 DEBRIS FLOW MODELISATION

5.1 Debris flow generalities and modelisation

We have seen in the previous chapters that check dams have an important influence on flood and debris flow dynamics but they have their weaknesses. If the previous chapter was more focused on check dams themselves, geomorphological concepts as well as empirical considerations about sediment transport, we wanted to go further in the study of flow dynamics, and especially debris flow dynamics. The well-instrument Illgraben catchment provides accurate debris flow data, that have to be exploited intensely, as real time debris flow records are very scarce. We performed the debris flow simulations using the softwares AVAL-1D and RAMMS (2D model), both developped by the WSL.

5.1.1 Debris flow triggering mechanism

For the formation of debris flows, large amounts of sediment, water and steep slopes are required (Costa 1984). There exist different mechanisms for debris flow initiation (Costa 1984, Zimmermann 1990):

- Landslides (with liquefaction of a sliding mass)
- Firehouse effect (scree mass movements on steep slopes at the toe of rock faces)
- Liquefaction of channel bed (i.e. fluidization)
- Natural dam collapse (i.e. lake outburst)

Debris flow initiation by sudden surface runoff is characterized by a progressive destabilisation of the channel bed and a rapid transition from intense bed-load transport to hyperconcentrated flow and finally to mature debris flow. This rapid transition happens within a short distance from the onset point of the motion of particles.When the clear-water discharge reaches the erodible sediment layer, part of this water infiltrates, depending on the permeability of the sediment and the position of the water table. The rest remains surface runoff and initiates the motion [63].

5.1.2 Illgraben debris flows features

Debris flows can be seen as a flowing mixture composed of a matrix of water and fine sediments (forming the fluid part) and a granular part, with blocs that can reach several meters in diameter. They are often imbricated in each other and differentiation can be done on the percentage of each component: if matrix dominates, it is called matrix-supported debris flow and if blocs dominates, clast-supported debris flow. The classification of a slurry is thus done by the percentage of each phase (Figure 78). In opposition to water flows in which water and sediment phases are clearly separated, debris flows are generally considered as a single phase flow composed of a fluid and a solid part; the air phase is neglected (i.e. due to motion and strong internal pressures, air is expulsed of the mixture).

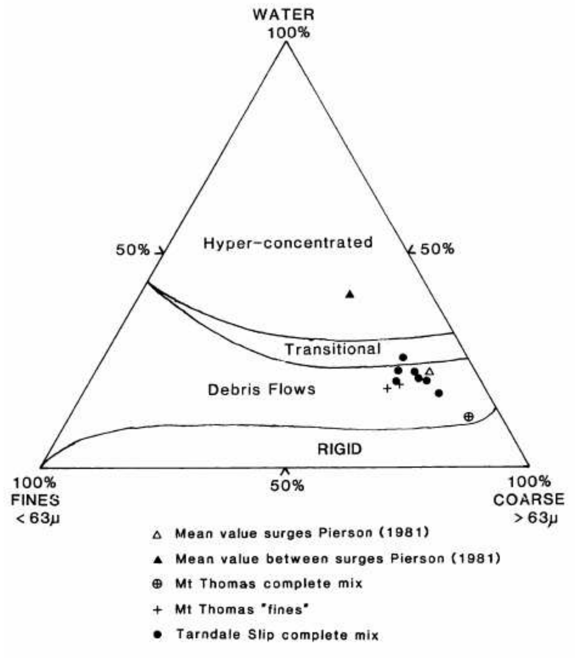

Figure 78. Three-phase diagram of debris flow materials (Philips and Davies, 1991)

Debris flow in Illgraben are most often related as muddy ones; they generally consist of muddy slurries (dolomites) with some boulders of quartzite or calcite [28]. Depending on the availability of upstream material, the proportion between these two parts could vary quite much. Video records show a large range of debris flow types occuring in Illgraben.

Since the force plate has been installed on check dam n°29 (see Introduction), measured bulk densities for debris flow are available: for the bulk flow, densities ranging from 2000 to 2250 kg/m^3 are calculated [40]. Based on rough estimates, a percentage of 50% water and 50% solids (pers. communication McArdell) could be assumed on the average in Illgraben.

These considerations allowed us to roughly get debris flow volumes based on flood volumes. The link between flood hydrograph and debris flow hydrograph was already mentionned by Takahashi (1980).

Debris flow volume is one of the essential input parameter needed in AVAL-1D and RAMMS.

5.2 AVAL-1D model

5.2.1 Theoretical concepts and litterature review

AVAL-1D is a one-dimensionnal model developped by the institute WSL mainly for avalanche calculations [4], [10], but has been subsequently successfully applied to debris flow modelling. The model is based on the Voellmy model (1955), modified by Salm (1966, 1972) in which an homogenous block-fluid motion is considered (Figure 79). AVAL-1D is based on a numerical solution of the shallow water equations (i.e. which describe the motion of the flowing mixture) which have been extended to granular flows. The flowing friction is based on the Voellmy equations, in which the basal shear stress (controlling the flow resistance and the depositional behaviour) consists of a turbulent Chezy-like friction term ξ (varying with the square of the velocity) and a dry Coulomb-like friction term μ and is given by [4]:

$$\tau_{z,r}(0)=\mu\sigma_2+\frac{\rho g}{\xi}U^2$$ Eq. 35

where
μ = dry friction coefficient [-]
ξ = turbulent friction coefficient [m/s^2]
U = mean velocity [m/s]
τ = shear stress at the base of the flow [kPa]
σ = normal stress at the base of the flow [kPa]
ρg = bulk unit weight

The total friction slope S_f is given by:

$$S_f=\mu\cos\psi+\frac{U^2}{\xi h}$$ Eq. 36

where
h = flow height [m]
ξh = dynamic resistance parameter covering turbulent effect in motion

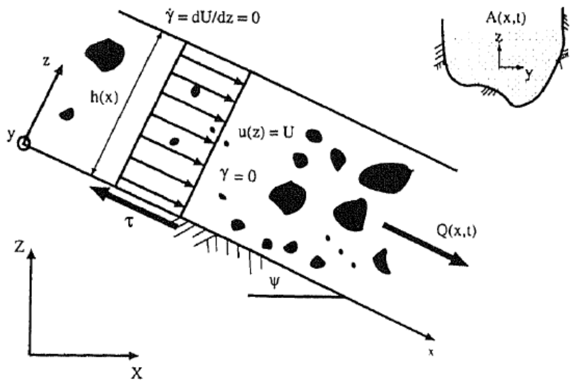

Figure 79. Voellmy fluid representation [4]

Apart from the total mixture volume, the two parameters μ and ξ mainly control flow depth and velocity. The more fluid-like behaviour (at higher velocities) is represented by ξ and the more solid-behaviour (at lower velocities) by the friction coefficient μ.

The dimensionless value of μ is the ratio of the force required to slide on the interface to the force perpendicular to it. It is a measure of the resistance to motion caused by molecular adhesion of one face to the other over the areas of true contact. The value of μ not only depends on the load (pressure or perpendicular force), but is also dependent on the contacting materials and the state of the interface (i.e. lubricated, dry, wet, contaminated, etc.) [8]. The rougher either is, the more friction there will be. In application of the semi-empirical techniques of the Voellmy rheology to rock avalanches, McLellan and Kaiser (1984) found that the travelling geometry is one of the major considerations in the choice of μ. The upper and lower bound limits of μ are given by the inclination of the line joining the top of the pre-failed block and the distal tip of the debris and the slope of the shallowest segment, respectively. The best prediction may be achieved by assuming that μ = tan α, where α is the average runout slope or slope of streaming the ramp (which separates the rupture surface and the main accumulation of debris).

An additional component to the Voellmy-Salm model allows active and passive earth-pressure effects to be accounted for [28]. The stress in the longitudinal direction is proportionnal to the hydrostatic pressure. This earth-pressure or 'geotechnical' parameter λ could be discriminated into an active (tensile) and passive (compressive) parameter depending on the velocity gradient in the longitudinal direction [4].

As previously mentionned, the basis for AVAL-1D is the analytical Voellmy-Salm model, but in comparison to the theoretical frame, real cases have shown that few changes happen in the reality, especially about the friction parameters. μ is a parameter that depends:

- on the material characteristics (density, water content, etc.)
- on the debris-flow pressure perpendicular to the ground
- slightly on velocity (μ decreases as velocity increases)

Little changes should be applied to this parameter.

For ξ, things are different. ξ is a parameter that depends on:

- the geometry of the acceleration zone (roughness, confinement, etc.)
- real topography (less uniform than in Voellmy-Salm model), which causes adding loss of energy that had to be compensated by higher ξ values (i.e. less turbulent friction).
- flow depth: in the analytical model, flow depths are considered higher than reality shows. Since the force of ξ is directly dependant on the flow depth, a higher ξ value has to be applied to compensate the smaller flow depth. The increase of ξ means higher velocities in the debris flow track and at the beginning of the runout zone.

The evaluations showed that, in comparison to the analytical Voellmy-Salm model, the increased variation of the slope in the runout distance slows down the avalanche stronger than using the analytical Voellmy-Salm model; in definitive, in most cases, the calculated runout distances of both models do not differ significantly.

An extensive sensitivity analysis has been done on two well documented debris flow in Switzerland [54]. These parametrizations allow to establish which parameter/feature has an influence on which flow feature:

- a higher ξ = to higher velocities and longer deposit zone
- a higher μ = to slighltly lower velocities and shorter deposition zones
- higher debris flow volumes = higher velocities and longer deposition zones
- higher fracture zone height = slighltly higher velocities and slightly longer depostion zones

5.2.2 Advantages/Disadvantages of 1D-model

First attempts for the calibration of the friction parameters μ and ξ have been done using the software RAMMS. But due to its greater complexity, parametrization was time-consuming. For this reason, our choice felt on AVAL-1D: it allows a much faster parametrization than RAMMS, but on the other side, the data resolution (cell size for RAMMS; accuracy and density of cross-sections for AVAL), the simplification could influence much the results; in any case, parametrization has to be performed again with RAMMS. But knowing the range of friction values saves a lot of time.

5.2.3 Description of AVAL-1D parametrization procedure

AVAL-1D allows to calculate, for a granular flow, the velocity, flow height as well as flow pressure at any given point along a reach. The input features needed are:

- a release block volume

- friction values μ and ξ (considered as constant along the channel, which is a simplification of the reality)
- cross-sections; X,Y,Z position, channel width, bank angles (i.e. for the calculation of lateral friction)
- flow density; this value is constant over a simulation and doesn't influence the results because this term disappears when the equations are solved.
- earth pressure coefficient λ: this coefficient represents the energy losses due to earth pressure on the flow. If usually set as 1 for water, for debris flow, this value was set at 2.5 (pers. communication McArdell; Hungr,1995)
- time step, total calculation time, element size (i.e. cell size)
- observed runout location as well as calculation point could be defined anywhere; they allow, if real data are available, for comparison of observed event with simulated ones. This is a very interesting feature because it becomes easy to visualize the effect of a parameter on the sensitivity analysis.

We calibrated our simulations on observed debris flow events extending from 2001 to 2008 (Appendix 4). As AVAL-1D needs cross-sections as input, the choice of debris flow events felt on years where accurate cross sections were available:

- 2005: the DTM-AV was made in 2005; the profiles were obtained with the software GEOMENSURA (description of the software by Minoia [44]).
- 2008: measured cross sections from this work

The events selected are listed in Table 25. The release zone for all events was fixed a few hundred meters upstream of check dam n°1, as the events were recorded by the geophone installed on check dam n°1.

Table 25. Main characteristics of debris flows for calibration with AVAL-1D (McArdell & Badoux, in review)

Source	Date	Time	Event volume [m^3]	Volume method	Q_{max} [m^3/s]	H_{max} [m]	V_{front} [m/s]
WSL	28th May 2005	16:00	86'000	?	147	2.37	9
WSL	3d June 2005	19:20	28'000	?	17	1.37	2.09
WSL	13th June 2005	09:10	23'000	?	40	1.13	6.13
WSL	16th June 2008	09:00	10'000	?	19.85	1.39	2.37
WSL	1st July 2008	19:23	59'896	Strickler integration	101.0	2.35	5.3

5.2.4 Results: sensitivity analysis

Tens of trials have been performed to observe the influence of the main parameters involved in the simulations. Graphic results of flow height and flow depth are displayed in Figure 80 and Figure 81.

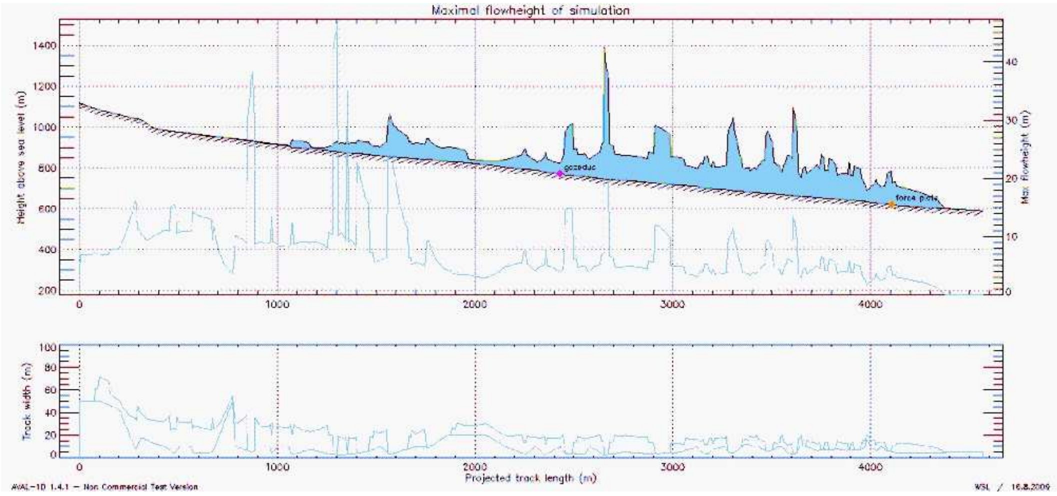

Figure 80. Maximum flow height distribution for the debris flow calibration of 28.05.2005 with AVAL-1D

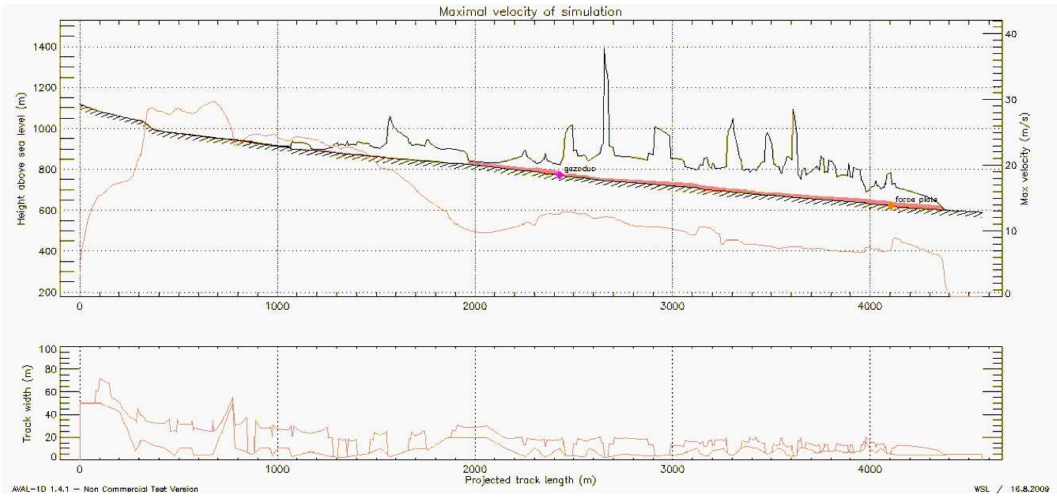

Figure 81. Maximum flow velocity distribution for the debris flow calibration of 28.05.2005 with AVAL-1D

In particular the two friction parameters, release volume, release height and location of the release zone in the channel have been analysed. It has to be said that in comparison with other studies where runout zones and corresponding flow heights are taken as the result people used for calibration, in Illgraben, flow velocities and heights are quite well-known in comparison to runout distance, which doesn’t exist (i.e. debris flow are washed away by the Rhône river).

- μ : this coefficient has a great influence on the runout distance and a minor one on velocities and flow height. As it is related to the topography (i.e. surface roughness), by increasing this value, we increase the roughness and the mass is slowed down. With μ values between 0.09-0.1, the debris flows are not able to reach the Rhône river, even by increasing ξ until more than 1000 m/s^2. Empirical trials have shown that μ has to be equal or lower to the slope of the river bed. By taking 0.1, we are over the mean slope values found in Chapter 4. For values of 0.08 and lower, debris flows reach the Rhône.

- ξ : the range of values for the turbulent parameter is important. It has a great influence on flow velocities and height (see Eq. 35) and is a sensitive parameter. The higher ξ , the higher velocities we observe.
- Release volume: the higher volume, the higher flow velocities and heights we get at the outlet.
- Release height: the release height has no influence on the results in our case, probably due to the fact that the release area is located far away from the force plate.
- Location of the release zone: one trial has been done by changing the location of the release area, and results are completely different. We haven't investigate further in this way because we knew that true release zones were situated upstream of check dam n°1.

The results obtained in this study confirmed most of the results found in previous studies and the one cited in § 5.2.1. As always, with two (or more) parameters to adjust, several set of adequate parameters are possible. Anyway, most of the time, μ was more ore less fixed first, then ξ was changed, because of its greater sensitivity.We plotted the two friction parameters against the debris flow volume, in order to look whether a trend exists in the data or not. Results are displayed in Figure 82 and Figure 83 (the 16th June 2008 event doesn't appear because the debris flow never reached the force plate even by changing all the parameters).

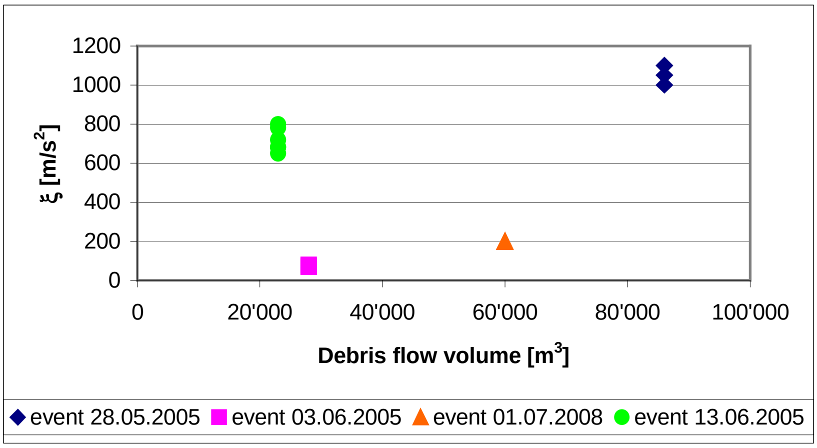

Figure 82. Relationships between turbulent friction parameter ξ and debris flow volume

Table 26. Values for ξ in relation to volume

28 mai 05, 16:00	86'000	1000
	86'000	1050
	86'000	1100
03 juin 05, 19:20	28'000	80
	28'000	70
	28'000	70
	28'000	75
13 juin 05, 09:10	23'000	650
	23'000	680
	23'000	680
	23'000	720
	23'000	780
	23'000	800
01 juil 08, 04:00	60'000	200
	60'000	200

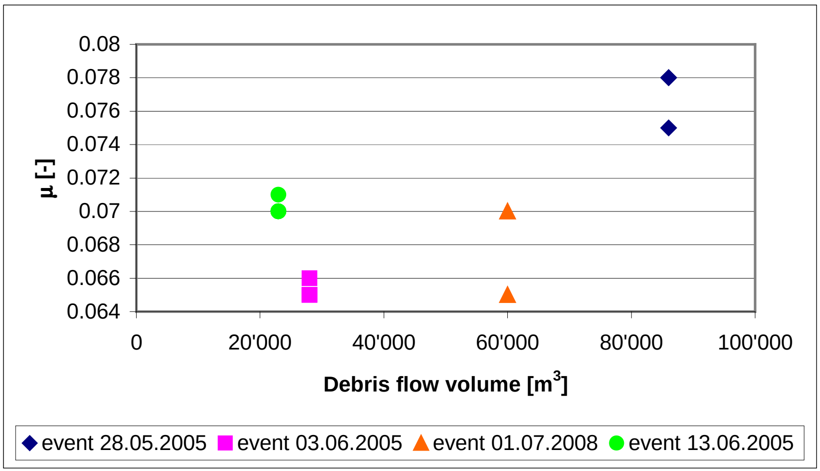

Figure 83. Relationships between basal friction parameter μ and debris flow volume

Table 27. Values for μ in relation to volume

28 mai 05, 16:00	86'000	0.075
	86'000	0.078
	86'000	0.078
03 juin 05, 19:20	28'000	0.065
	28'000	0.065
	28'000	0.065
	28'000	0.066
13 juin 05, 09:10	23'000	0.07
	23'000	0.07
	23'000	0.07
	23'000	0.07
	23'000	0.07
	23'000	0.071
01 juil 08, 04:00	60'000	0.065
	60'000	0.07

The following comments has to be taken with care because only four simulations could be performed, due to scarce topography data available:

- μ doesn't vary much (between 0.6 to 0.8) from on event to the other, but a very slight increase (except for the 13.06.2005 event) with the volume size is visible.
- ξ varies much more with event volume, ranging from 70 to 1100 (except again for the 13.06.2005 event). This feature could be interesting for further investigation: as ξ depends of the flow velocity and height, it is a justifiable approach to link it up with event size, because as volume increase, flow depth and velocities increase too.

The range of values found for μ and ξ is in accordance with results from other studies (Appendix 35) and with two relations developped in [71]. The latter consider that μ is independent of the volume (i.e. adequate with values displayed in Figure 83, as range of value is tiny) but related to the catchment area (i.e. the more water available, the more fluid the debris flow will be). The formula are given by [71]:

$$\mu = 0.13 \cdot S^{-0.35} \text{ (lower value)} \qquad \text{Eq. 37}$$

$$\mu = 0.18 \cdot S^{-0.3} \text{ (upper value)} \qquad \text{Eq. 38}$$

where
S = catchment area [km^2]

With an area of ~5 km^2, we found, for Illgraben, values comprised between 0.075 and 0.1. Moreover, the values for μ and ξ in Illgraben, published in [71], were fixed at 0.06 and 0.6 for a 20'000 m^3 event, which is almost the same that we found for the 03.06.2005 event (see Table 26 and Table 27).

5.2.5 Influence of check dam on the flow behaviour

The presence of check dams along the channel modifies quite much the flow behaviour. As for open channel hydraulics it is quite well documented, for debris flow, literature is scarce on the topic.

An attempt has been done using AVAL-1D to simulate a well-calibrated debris flow event and look close to check dams the reaction of the flow. This trial was done to understand how the model reacts in the presence of a drop structure and if any link could be made (especially based on energetic considerations) between debris flow behaviour and open channel hydraulics at this location. The shallow water equations are not accurate for vertical drop feature and AVAL-1D doesn't allow for such particularities (i.e. in the topography editor, when creating a vertical drop, all values are put to '0'); that the reason why we entered a very steep slope, representing an abrupt change in the channel morphology. According to Rickenmann & al. (2001), the 1D-model FEMTOOL, used to model debris flow scenarii in Illgraben, isn't able too to take into account this drop structures and so the topography was smoothed at these locations.

As AVAL-1D models the channel by the intermediate of cross-sections, and as water flow properties are changing very quickly at a drop structure (Figure 84), we add cross-sections close to the concrete structures.

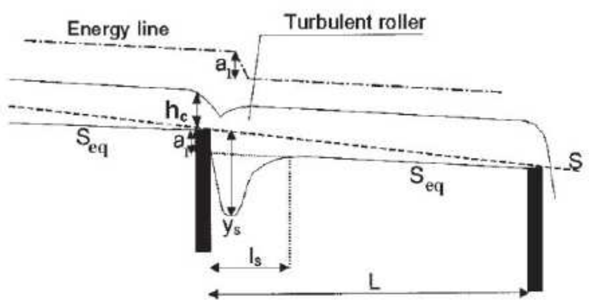

Figure 84. Water flow behaviour at the right of a check dam [39]

The first attempt was done by considering an 'ideal' channel of constant width, constant bank angles, an average drop height of 5m and a real debris flow input (i.e. 01.07.2008 event).

The results are given in Figure 85. We are able to see that the flow accelerates when approaching the check dam, with a peak at the brink of the check dam and at its toe. Then the flow decelerates as it flows on milder slopes. The model is hence able to reproduce a quick transition in topography.

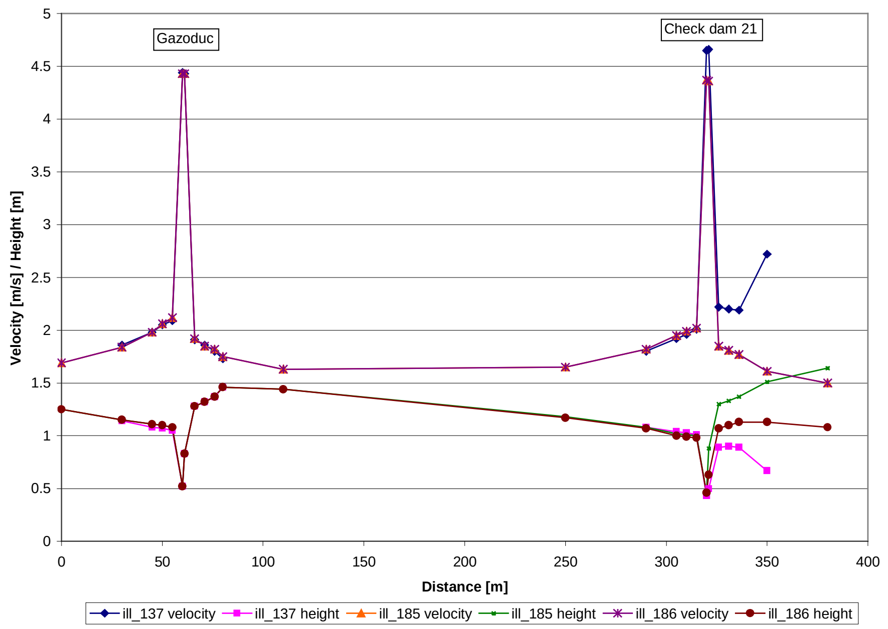

Figure 85. Debris flow behaviour at two successive check dam, considering an'ideal' channel

Then, we added cross-sections to get a dense network of measurements points (20m upstream-, 10m upstream, 2m upstream-, 1m upstream-, check dam crest, bottom of check dam, 5m downstream-, 10m downstream- and 20m downstream of check dams n°19, n°20, gazoduc, and n°21). The aim was to observe the evolution of the energy grade line . Results are displayed in Figure 86.

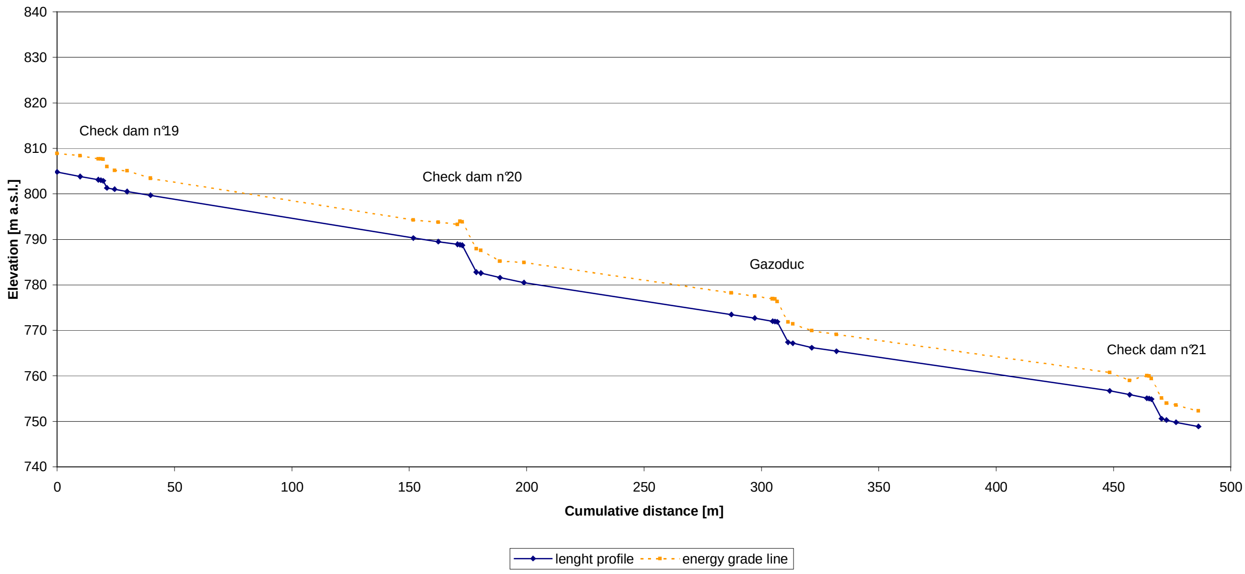

Figure 86. Illbach channel length profile and 01.07.2008 debris flow energy grade line between check dams n°19 and n°21

As velocities and depths are obtained at each selected point, we were able to draw the energy grade line by applying the Bernouilli equation for each point:

$$z_1+\frac{p}{\gamma}+\frac{v_1^2}{2g}=z_2+\frac{p}{\gamma}+\frac{v_2^2}{2g}+\Delta h \qquad \text{Eq. 39}$$

where
z_1 and z_2 = energy of position of the bed (i.e. elevation) [m]
p/γ = energy of pressure (i.e. here considered as the flow height) [m]
$v_1^2/2g$ and $v_2^2/2g$ = kinetic energy (i.e. related to flow velocity) [m]
Δh = head loss (i.e. mecanic energy loss by transformation from kinetic energy into heat) [m]

The Bernouilli relation takes into account the potential energy (given by the elevation of the bed at a given point), the pressure over specific weight, which means that the pressure is proportional to flow depth and is considered as hydrostatic, and the kinetic energy, which is related to the flow velocity.

If the general shape of the energy grade line is satisfying, some weird features appears at the brink of some check dams (n°20 and 21). There is a sudden peak of energy before falling down again. At the toe of the check dam, there is also a weird feature, as the energy grade line goes down and up a few meters further downstream.

The reasons for these features could be that some assumptions expressed in the Voellmy model are not completely fulfilled, especially the ratio p/γ: as the flow accelerates, then the pressure is not hydrostatic anymore but is transformed into a dynamic pressure; a coefficient might be necessary to take into account for this pressure change.

AVAL-1D, in its actual shape, 'see' the drop as a steep slope and the mass is accelerated after the check dam; this results in larger velocities and energy grade line goes up. Immediately afterwards, the mass decelerates, because of friction and energy decreases. AVAL-1D will always conserve energy (pers. communication Bartelt). The problem is that AVAL-1D doesn't take into account momentum/energy losses due to an impact (dam, drop structure,…). The energy losses due to friction are integrated in the equations (this is the reason why the energy grade line follows quite good the channel bed). There friction losses are the main energy losses to take into account. The intrinsec energy dissipation of a debris flow is taken into account with the 3 parameters μ, ξ and λ.

It would be worth looking at the effect of an extra energy dissipation (i.e. impact energy loss) on the energy grade line and if it would be valuable for the model to take it into account. In open channel hydraulic modelisation, as in HEC-RAS, this extra energy dissipation is modeled by adding an expansion or contraction coefficient loss to the Bernouilli equation. By comparing with flume data, one showed that it could adequately fits the reality. A drop structure will be considered as a contraction, because flow is accelerating. The coefficients are multiplied by the absolute difference in velocity heads between the current cross section and the next cross section downstream, which gives the energy loss caused by the transition. It is given by:

$$\Delta h_s = C \cdot \left| \frac{v_2^2}{2g} - \frac{v_1^2}{2g} \right| \qquad \text{Eq. 40}$$

where

Δh_s = energy loss due to impact [m]
C = contraction coefficient [-]
$v_1^2/2g$ and $v_2^2/2g$ = kinetic energy at upstream and downstream cross-section [m]

For abrupt transition, a contraction coefficient of 0.6 is recommended (HEC-RAS hydraulic manual).

A trial was made by using an additionnal energy loss (Eq.41) added to the values used to draw the energy grade line (Figure 86). Results are displayed in Figure 87. We can see that applying an extra energy loss as used in hydraulics doesn't modify much the energy grade line and sometimes create extra 'bumps at the brink of the check dam. The actual state is satisfying and shows that losses due to friction seem to be the main energy losses involved in the process.

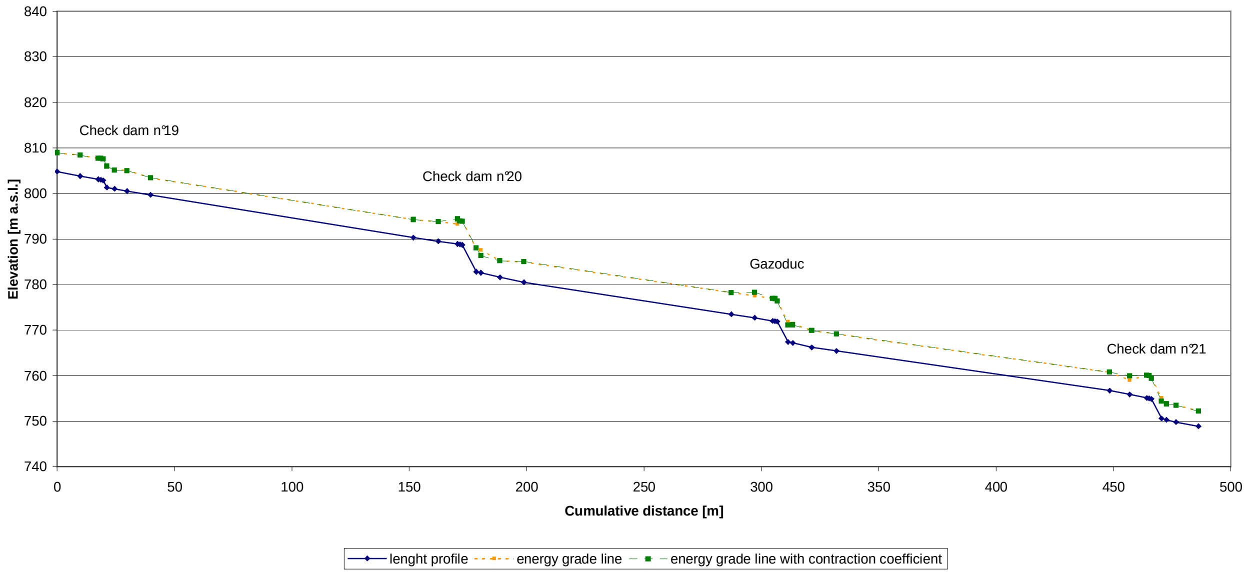

Figure 87. Illbach channel length profile; 01.07.2008 debris flow energy grade line (orange); energy grade line taking into account an extra dissipation due to impact (green) between check dams n°19 and n°21

5.3 RAMMS

RAMMS was used in this work to look at the flow pattern in two dimensions at the vicinity of check dams as well as to look if it reproduces the observations made with AVAL-1D. We also used a promising module that allows to calculate the erosion capacity of a debris flow, by defining (with the knowledge of few parameters) an erodibe layer. This tool was used here more in an experimental way, because for the moment, no comparison is possible with other studies. There is only one paper available on the subject that handle with rock and ice avalanches (Schneider & al., in prep).

5.3.1 Theory

RAMMS (RApid Mass MovementS) is a 2-D numerical model developped by the institute WSL (Switzerland). This physically based dynamic model basically solves the same flow equations as AVAL-1D , with the difference that it uses a finite volume scheme to solve the 2-D shallow water equations for granular flows (implying the horizontal extension of the flow is greater than their vertical thickness). It also uses a different numerical solver than AVAL-1D.

The frictional resistance S_{fx} in x-direction and S_{fy} in y-direction, which is acting against gravitationnal acceleration, is described by using a Voellmy approach which incorporates, same as for AVAL-1D, the friction parameters μ and ξ [4]. The simulated output can easily be integrated into a GIS environment [12]. The friction slope is given by:

$$S_{fx} = \left[gH\mu\cos\alpha + \frac{g\cos\alpha\left(U_x^2+U_y^2\right)}{\xi} \right] \frac{U_x}{\sqrt{U_x^2+U_y^2}} \qquad \text{Eq. 41}$$

$$S_{fx} = \left[gH\mu\cos\alpha + \frac{g\cos\alpha\left(U_x^2 + U_y^2\right)}{\xi} \right] \frac{U_y}{\sqrt{U_x^2 + U_y^2}} \quad \text{Eq. 42}$$

where
g = gravitational acceleration [m/s^2]
H = flow height [m]
α = slope angle [°]
U_x = velocity component in x-direction [m/s]
U_y = velocity component in y-direction [m/s]

5.3.2 GUI and parameters

To run simulations with RAMMS, one has first to get a DEM on ascii format and a topographical map or an orthophoto. As RAMMS is based on the Voellmy-Salm model, the release mass is drawn as a block (release area) but for that, one has to know the volume of the event. The calculation domain is then built. To reduce considerably the calculation time, the domain has to be drawn as close as possible to the limit of the studied area (it saves precious calculation hours!). Then μ, ξ ,λ, calculation time, dump step, density (same as in AVAL-1D) have to be set, as well as the cell size (here it is based on a DEM and not on cross-sections; the advantage is that a very fine resolution is possible; if resolution is coarse, then a 1-D model (if cross section measured precisely) could be of better use.

5.3.3 Entrainment of material

In RAMMS, there is now the possibility to observe erosion evolution. This module allows to check visually and on a log-file (for each time step required) the erosion mass, volume, entrainment rate, and this for several soil layers. To use this module correctly, one has to know the depth of the erodible layer, its density and an erodibility factor, which reflects the susceptibility of the material to be eroded by a debris flow or not.

Very scarce simulations on the topic are available; this factor has to be defined through a sensitivity analysis. To perform this analysis on a good way, one has to know to which kind of soil, water saturation, etc., this erodibility factor corresponds. There is also an erosion law to define. Three types are available:

- Velocity driven law
- Momentum driven law
- Velocity square driven law

For our simulations, we chose the two last one, because velocity driven law is a rather old formulation. Momentum driven law is explained below. Velocity square driven law is the most used and the most realistic one. It is based on the shear stress formulation (related to the velocity squared).

The total volume of a debris flow is often not constant along the debris-flow path, as deposition/erosion occurs during an event. When erodible layers are defined along a debris flow path and if the debris flow has enough drag force to entrain material, then this effect has to be taken into account. In [55], simulations had been done without using the entrainment algorithm, and that led to strong unconstitencies with observed events. Since recently, RAMMS includes such an algorithm to account for entrainment of a ground layer. The entrained mass is accelerated instantaneously to the debris flow velocity. Experimental studies have shown that the increase in mass depends mainly on the velocity of the flow U and on the availability of the material. The front of the debris flow is very erosive and generally the highest depths are measured at this location. Even if the tail could have high velocities, generally it has small heights. The entrainment rate is given by [55]:

$$\dot{Q} = \frac{\rho_e}{\rho_a} k_2 H U \qquad \text{Eq. 43}$$

Momentum is given by p = mU, where m = mass. p is explicitly given by the product of the flow depth H, the debris flow density ρ_e and the calculation cell area.

Factor k controls the rate at which the erodible layer is entrained into the flowing avalanche. Values for debris flow should range between 1 (muddy tail) to 10 (erosive front) (pers. communication McArdell)

5.3.4 Results

5.3.4.1 General inputs and outputs

The event used for the simulations is the one of 28.05.2005. The release area was drawn a few hundred meters upstream of check dam n°1, with a release height of 5m and a total volume of 86’000 m^3. The choice of 5m was based on the total volume of the event and on the channel width upstream of check dam n°1. This value is probably not realistic but as previously mentionned, the release height has no influence on the flow features if the control section is set far enough from the release area (which is the case for the force plate). The calculation domain was set first very close to the channel to save time, but this way of doing led to mistakes so we extended the domain to a wider zone.

Then we had to check if the set of parameters obtained with AVAL-1D was adequate; a check/recalibration is always necessary, but by knowing the range of parameters that fit, we saved a lot of time. A few simulations have been performed: parameters have been changed a little and have been fixed at μ=0.07 and ξ=1000.

As for AVAL-1D, the flow behaviour close to check dams evoluates very quickly, with mass accelerating at the brink of check dam and decelarating a few meters further. To represent as best the blocking effect of a check dam on debris flow, we modified the DTM-AV by adding 2-3 meters to the wings of check dams n°19 to n°21. The results of the previous comments are displayed in Figure 88 and Figure 89. The velocities jump from ~3-4 m/s to 9-10 m/s in a few meters.

5.3.4.2 Erosion inputs and ouputs

The erosion inputs are:

- the choice of a bed layer (top, middle, bottom; in our case only the top layer was considered)
- the layer depth: taken at 0.5m (rough trial estimation, but it might be more)
- the density of the bed layer (taken at 1800 m^3/kg)
- the erodibility factor (which was changed from 0.2 to 10)
- a potential erodible area; for this parameter, we had the choice between defining the entire calculation domain as affected by debris flow to be potentially eroded, or to specify erosion zones; the latter was chosen by taking only the channel bed from check dam n°2 to Rhône river and by

removing the check dams (they would have been considered as an additionnal amount of mass by RAMMS).

The eroded volumes displayed in the GUI are found by choosing the flow depth results, then eroded volumes. It is possible to check the eroded volume at each time step or for the total event.

Numerous simulations have been done; bugs appeared at the beginning because negative volumes increased with time; as deposition is not possible to take into account in RAMMS, this artefact was corrected by widening the calculation domain; in fact, the issue was that mass was flowing out of the domain, leading to volume inconsistencies (pers. communication Christen).

The main features which were changed were the density of the soil layer, the erodibility factor and the erosion law. General considerations can be formulated:

- The erosion law (momentum driven or velocity square) doesn't influence much the results (between 1 to 4% difference in the eroded volumes for the event considered).
- The density of the erodible layer seems to have a great importance on the erosion volume; by taking densities of 1800 kg/m^3 and 2200 kg/m^3, we obtained a difference of 17% less volume for the 1800 kg/m^3.
- The most influencing parameter seems to be the erodibility factor. If for erodibility factor ranging from 0.5 to 10, the whole 50cm-layer was eroded, by taking a value of 0.2, only half of the mass was eroded along the reach.

On Figure 88 and Figure 89, we can see the result of a simulation. For a 86'000 event, we have overflows at some places, that were not observed in the reality.

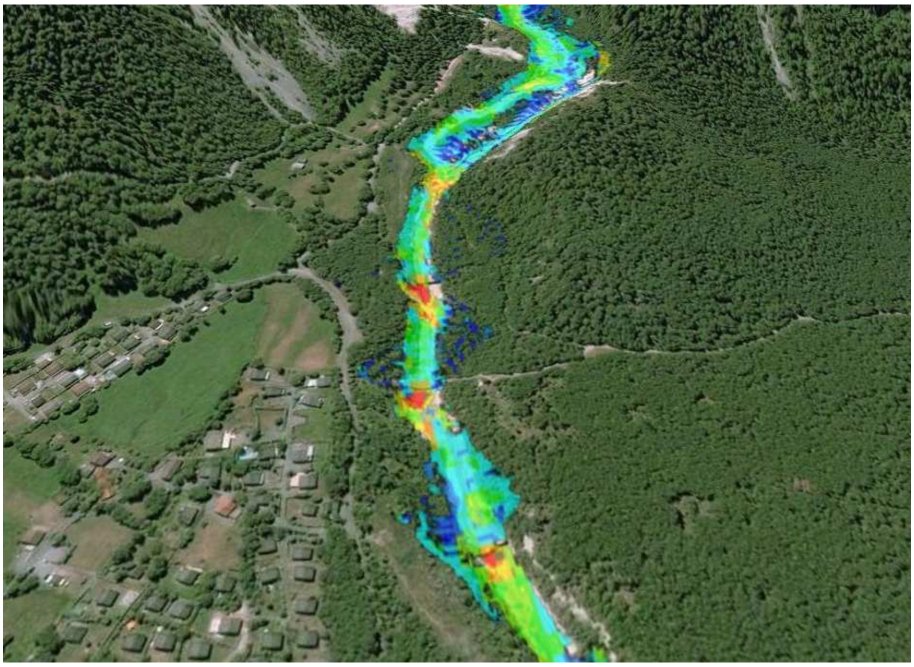

Figure 88. RAMMS simulation of the 28.05.2005 event. Distribution of flow velocities between check dam n°19 to check dam n°21. Light blue:3-4m/s, green:5.5-7m/s, red:9-10m/s

If the increase of flow velocities and the barrier effect of check dams on debris flow are clearly visible, the explanations for the overflows are probably due to two reasons:

- this area is still probably under the influence of the release zone height: as stated above, the release height doesn't have an influence if the area of interest is located far enough from the release area. If it is too close, then it has an influence.
- the debris flow was simulated with the erosion module, and by taking an initial release volume of 86'000 m^3. At this point the erosion volume added is around 20'000-30'000m^3. It means that the debris flow total volume at check dam n°20 is around 110'000m^3, which could explain the local overflows.

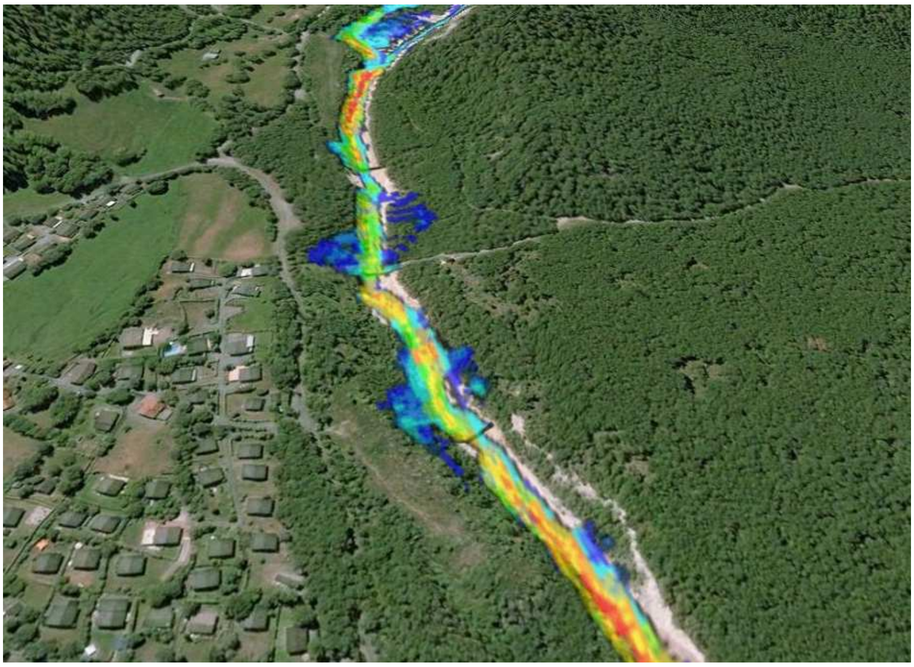

Figure 89. RAMMS simulation of the 28.05.2005 event. Distribution of flow heights between check dam n°19 and check dam n°21. Light blue:1.50-2.25m, yellow: 3.5-4.15m, red: 4.3-5m

5.3.5 Conclusions

RAMMS has been used associated with AVAL-1D to fix the friction parameters of the Voelly-Salm model for several recorded debris flow. We could see that the parameters fit in the range of values found in literature and with previous calculations made for Illgraben [71].

RAMMS is a powerful tool that allows the determination of debris flow features like flow height, flow velocity and spreading. It was able to correctly back calculate some debris flow events [54].

The erosion tool is very promising. By knowing more or less the zones prone to erosion (§4.6.2.3), the geotechnical features of the channel bed and on the basis of observed event, one has with this tool a very good way to backcalculate an event. This should allow to assess the initial volume of the debris flow (i.e. release area) and thus more realistically simulate the flow features all along the channel (i.e. diminishing the uncertainties provoked by an inappropriate release zone). This tool might be complementary to a field technique like the specific linear erosion assessment, as developped in [27]. But for the moment, it's not to efficiently evaluate its performance, as no published results are available.

6 CONCLUSIONS AND PERSPECTIVES

The Illgraben catchment have been studied for many years for its frequent debris flow occurrence, but there were no analysis done on the flood characteristics in Illgraben. This work brought new data on the large scale rainfall patterns influencing the hydrology of the catchment. Through a frequency analysis performed on the newest available data of ANETZ stations, we were able to build the IDF curve for Illgraben, making some assumptions that will have to be verified when the Illgraben raingauges will have sufficient data for doing the same analysis and thus determine if the methodology used could be applied to other catchments or if other assumptions have to be made.

The calculation of flood peak discharge, with a methodology recommanded by the BAFU, led to a wide range of results because of the many cases taken into account. Many assumptions are inherent to HAKESCH and field work is an important point in the methodology, especially to determine the runoff coefficent: as it is a very sensitive parameter, it could be good to analyse more into details the influence of subsurface runoff and infiltration in mountain catchments. It would also be good to look whether the values we got are in relation with what really happens in the catchment, by the mean of real-time measurements of flood discharges.

The check dams built all along the Illgraben fan play a major role in the reduction of erosion, and thus in the debris flow magnitudes. They have numerous purposes and that is the reason why in the 1970's, all over Europe, concrete check dams were constructed in the main torrents prone to debris flow activity. In Illgraben, the protection measures concept had a direct impact on the debris flow processes as they stopped for a few years; but debris flow started again after few years, and never stopped since then. Around 1/3 of these check dams collapsed, mainly due to geomorphological reasons. Indeed, if an appropriate structural design is clear, a study of the geomorphological and flow processes are of first importance. By studying the entire channel and more closely the check dams vicinity, we came to the conclusion that the different sediment transfert processes interact strongly between each other and the stability of the check dams might be evaluate considering several aspects like: the actual flow regime/period (aggrading or degrading phase, in relation with the concept of equilibrium slope), the level of the channel vs. maximum scour depth, the maximum sediment transport capacity of a given flood, which allow to determine which areas are subject to deposition and which to erosion. All the features give indication of the actual and probable evolution of the channel bed depending on the type of event that might occur. A further topic on research on the subject would be to analyse the influence of sediment transport in the total sediment transfer processes in Illgraben. Actually, only debris flow events are recorded and the bedload is the unknown part of the processes. A modelisation with continuous rainfall records would be interesting to study the evolution of runoff in the catchment and understand how the bedload evolves among the other processes. The other aim would be to evaluate the percentage of bedload compare to debris flow, and it could be interesting to understand the interactions and local/total sediment processes in the channel and its evolution in time.

Debris flow were modelled using two software developped at WSL: AVAL-1D and RAMMS. The former demonstrated its simple use and the short time needed to get results. It is probably the best tool among the two to parametrize the different parameters which are used in both model, because both developped on the

Voellmy theory. We tested the ability of AVAL-1D to reproduce flow behaviour at the vicinity of check dams, and it showed than the equations used in the model (friction parameters) reproduced quite well the open-channel hydraulics in such cases. An attempt have been done using extra energy losses, but the results showed that few differences could be found.

RAMMS is a much more powerful tool: it allows to model debris flows in 2D and recently, an erosion module was developped. We tried to use it but more in an experimental way. This tool, when knowing quite well the catchment, material properties as well as debris flow behaviour, could be powerful to backcalculate debris flow volumes and assessing the initial volume of an event. But for the moment, no paper is available on the subject and there would be the need for many trials before showing its real abilities.

7 REFERENCES

[1] Armanini, A., Dellagiacoma, F. & Ferrari, L. 1991. From the check dam to the development of functional check dams. *Lecture Notes in Earth Sciences* 37: 331-344.

[2] BAFU. 2006. HAKESCH 2.0 Methoden.

[3] Bardou E. 2002. *Methodologie de diagnostic des laves torrentielles sur un bassin versant alpin*. Phd thesis. EPFL. Lausanne.

[4] Bartelt, P., Salm, B. & Gruber U. 1999. Calculating dense-snow avalanche runout using a Voellmy-fluid model with active/passive longitudinal strain. *Journal of Glaciology* 45 (150): 242-254.

[5] Berti, M., Genevois, R., Simoni, A. & Tecca, P.R. 1999. Field observations of a debris flow event in the Dolomites. *Geomorphology* 29: 265-274.

[6] Bezzola, G.R. : " Flood protection measures: Debris-flow and protection measures", MAS in Hydraulic Engineering, Module D2, Submodule D2.3 Lecture Notes, EPFL

[7] Böll A. 1997. Wildbach- und Hangverbau. *Berichte der WSL* 343.

[8] Chen, H. & Lee, C.F. 2003. A dynamic model for rainfall-induced landslides on natural slopes. *Geomorphology* 51: 269-288.

[9] Chow, V.T, Maidment, D.R. & Mays, L.W. 1998. *Applied Hydrology*. McGraw-Hill Series in Water Resources and Environmental Engineering.

[10] Christen, M., Bartelt, P. & Gruber, U. 2002. AVAL-1D: An avalanche dynamics program for the practice. *International Congress INTERPRAEVENT 2002 in the Pacific Rim – Matsumoto / Japan*. Congress Publication 2: 715-725

[11] Christen, M., Bartelt, P. & Gruber, U. 2005. Numerical calculation of snow avalanche runout distance. *Computing in Civil Engineering*. *Proceedings of the 2005 International Conference, Cancun, Mexico.*

[12] Christen, M., Bartelt, P., Kowalski, J. & Stoffel, L. 2008. Calculation of dense snow avalanches in three-dimensional terrain with the numerical simulation program RAMMS. *Proceedings of the International Snow Science Workshop, Whistler, BC, Canada*: 709–716.

[13] Cunnane, C. 1978. Unbiased plotting positions – A review. *Journal of Hydrology* 37 (3-4): 205-202.

[14] De Kalbermatten, G. 1985. L'évolution dans la conception des barrages en torrents en Valais – L'exemple de la correction du Saint-Barthélémy. *Ingénieurs et architectes suisses* 7: 95-108.

[15] Coussot, P. 1996. Les laves torrentielles, Connaissance à l'usage du praticien. *Equipements pour l'eau et l'environnement* (25). Grenoble: CEMAGREF éditions.

[16] Cunnane, C. 1978. Unbiased plotting positions – A review. *Journal of Hydrology* 37 (3-4): 205-202.

[17] De Cesare, G., Schleiss, A. & Hermann, F. 2001. Impact of turbidity currents on reservoir sedimentation. *Journal of Hydraulic Engineering. January 2001.*

[18] Deymier, C., Tacnet, J-M. & Mathys, N. 1994. Conception et calcul de barrages de correction torrentielle. *Equipements pour l'eau et l'environnement* (18). Grenoble: CEMAGREF éditions.

[19] Fournier, F. 2000. *Dépôt de laves torrentielles dans le cône de l'Illgraben (VS).* Diplôme de géologie. Université de Genève.

[20] GHO. 1999. *Recommandations concernant l'estimation de la charge sédimentaire dans les torrents, Partie II*. Berne.

[21] Gibbons, J.D. & Chakraborti, S. 2003. *Nonparametric Statistical Inference*, 4th edition, Statistics : A Dekker series of textbooks and monographs, Marcel Dekker, New York.

[22] Graf, W.H. et al. 1993. *Hydraulique fluviale, Tome 1 : Ecoulement permanent uniforme et non uniforme*. Lausanne : PPUR.

[23] Gwerder, C. 2007. *Temporal and spatial variation of erosion processes in the Illgraben, an alpine debris flow catchment*. Diplomarbeit. ETHZ.

[24] Hager, W.H. 1984. A simplified hydrological rainfall-runoff model. *Journal of Hydrology* 74:151-170. Amsterdam:Elsevier Science Publishers B.V.

[25] Hirano, M. .*Prediction of Debris Flow for Warning and Evacuation*. Departement of Civil Engineering, Kyushu University.

[26] Hose, A. 2007. *Einfluss der Topographie auf die Murgangsimulation im Ablagerungsbereich und Implikationen auf die Gefahrenbeurteilung*. Diplomarbeit. Universität Stuttgart.

[27] Hungr, O., Morgan, G.C. & Kellerhals, R. 1984. Quantitative analysis of debris torrent hazards for design of remedial measures. *Canadian Geotech. Journal* 21: 663-677.

[28] Hürlimann, M., Rickenmann, D. & Graf, C. 2003. Field and monitoring data of debris-flow events in the Swiss Alps. *Canadian Geotech. Journal* 40: 161-175.

[29] Ingenieurbüro Cordonier N. & Rey G. SA. 2001. *Sanierung Illgraben – Schwellenzustand 2001*.

[30] Ingenieurbüro Teysseire & Candolfi AG. 2003. Schutzkonzept Illgraben, Bericht Nr. 1693 – 4.

[31] Jaeggi, M.N.R. Torrent Check dams and debris flow amplification. 1993. *Proc. XXV Congress of International Association of Hydraulic Research* (VIII), B-6-2:188-194.Tokyo

[32] Jaeggi, M.N.R. and Pellandini S. 1997. Torrent check dams as a control measure for debris flows. *Lecture Notes in Earth Sciences* 64: 186-207

[33] Jakob, M. & Hungr, O. 2005. *Debris-flow Hazards and Related Phenomena*. Springer Praxis Book/Geophysical Sciences.

[34] Knobel, R. 2006. Modellierung von Murgängen und Eislawinen in Nordossetien mit Hilfe des RAMMS-Modells und systematischen Testens von Satellitenbildern. Diplomarbeit. Geographisches Institut Universität Zürich.

[35] Lichtenhahn, C. 1971. Zwei Betonmauern: Die Geschieberückhaltesperre am Illgraben (Wallis) und die Staumauer des Hochwasserschutzbeckens an der Orlegna im Bergell (Graubünden). Bern

[36] Lenzi, M.A. & Comiti, F. 2003. Local scouring and morphological ajustments in steep channels with check-dam sequences. *Geomorphology* (55): 97-109.

[37] Lenzi, M.A., Comiti, F. & Marion,A. 2004. Local Scouring at Bed Sills in a Mountain River: Plima River, Italian Alps. *Journal of Hydraulic Engineering*. March 2009: 267-269.

[38] Liu, C.M. 1992. The effectiveness of check dams in controlling upstream channel stability in norteastern Taiwan. *Erosion, Debris Flows and Environment in Mountain Regions* 209: 423-428.

[39] Marion, A., Lenzi, M.A. & Comiti F. 2004. Effect of sill spacing and sediment size grading on scouring at grade-control structures. *Earth Surface Processes and Landforms* (29): 983-993.

[40] McArdell, B.W., Bartelt, P. & Kowalski, J. 2007. Field observations of basal forces and fluid pore pressure in a debris flow. *Geophysical Research Letters* 34: 1-4.

[41] McArdell, B.W., Zanuttigh, B. & Lamberti, A. & Rickenmann, D. 2003. Systematic comparison of debris flow laws at the Illgraben torrent, Switzerland. *Debris-Flow Hazards Mitigation :Mechanics, Prediction, and Assessment*. Rickenmann & Chen (eds): 647-657. Rotterdam: Millpress.

[42] Meunier, M. 1991. *Eléments d'hydrauliques torrentielles*. *Etude Montagne* (1). Grenoble: CEMAGREF éditions.

[43] Meylan, P., Favre, A.C. & Musy, A. 2008. *Hydrologie fréquentielle – une science prédictive*. Lausanne : PPUR.

[44] Minoia, R. 2009. *Réévaluation des dangers liés aux laves torrentielles du torrent de l'Illgraben (Loèche, Valais)*. MAS diploma thesis.EPFL.Lausanne.

[45] Nydegger, C. 2008. *Fluvial system dynamics in steep headwater basins*. Diploma thesis. ETHZ

[46] OFEG, 2003. Evaluation des crues dans les bassins versants de Suisse. *Rapports de l'OFEG, Série Eaux* 4. Berne.

[47] Osti, R. & Egashira, S. 2008. Method to improve the mitigative effectiveness of a series of check dams against debris flows. *Hydrological Processes* 22: 4986-4996.

[48] Perla, R., Cheng, T.T & McClung, D.M. 1980. A two-parameter model of snow-avalanche motion. *Journal of Glaciology* 26 (94): 197-207.

[49] Rickenmann, D. 1999. Empirical relationships for debris flow. *Natural Hazards* 19: 47-77.

[50] Rickenmann, D., Hürlimann, M., Graf, C. & Näf, D. 2001. *Studie Illgraben – Teil WSL: Simulation des Fliessverhaltens*. Überarbeitere Version. WSL.

[51] Rickenmann, D., Laigle, D., McArdell, B.W. & Hübl, J. 2006. Comparison of 2D debris-flow simulation models with field events. *Computational Geosciences*: 241-264.

[52] Rieder, P.A. 1987. *Entretien du seuil n°20 de l'Illgraben sur le territoire de la commune de Loèche*. Département des travaux publics du Canton du Valais.

[53] Rinderknecht, P. 2002. *Analyse der Wirkungsweise von Geschieberückhalte-Bauwerken in Wildbächen*. Diplomarbeit. ETHZ

[54] Scheuner, T. 2007. *Modellierung von Murgangereignissen mit RAMMS und Vergleich durch GIS-basiertes Fliessmodell*. Diplomarbeit. Geographisches Institut Universität Zürich.

[55] Schneider, D., Bartelt, P., Caplan-Auerbach, J., Christen, M., Huggel C. & McArdell, B.W. *Insights into rock-ice avalanche dynamics by combined analysis of seismic recordings and a numerical avalanche model*. (in prep.)

[56] Schnydrig, D. 2007. *Debris-Flow Processes in the Illgraben*. Diplomarbeit. Universität Bern.

[57] Service fédéral des routes et des digues. 1973. *Dimensionnement des barrages en torrents en béton et béton armé.* Berne.

[58] Shieh, C.-L., Jan, C.-D. & Tsai, Y.-F. 1996. A Numerical Simulation of Debris Flow and Its Application. *Natural Hazards* 13: 39-54.

[59] Spreafico, M. & Weingartner, R. 2001. *Atlas hydrologique de la Suisse*. OFEG (ed).

[60] Takahashi, T. 1991. Debris Flow. *IAHR monograph serie*. A.A. Balkema, Rotterdam.

[61] Takahashi, T. 2007. *Debris-flow, Mechanics, Prediction and Countermeasures*. Taylor & Francis Group.

[62] Tognacca, C. 1999. Beitrag zur Untersuchung der Entstehungsmechanismen von Murrgängen. VAW Mitteilungen n°164, Zürich.

[63] Tognacca, C., Bezzola, G.R. & Minor, H.-E. 2000. Threshold criterion for debris-flow initiation due to channel-bed failure. *Debris-Flow Hazards Mitigation*: *Mechanics, Prediction and Assessment:* 89-97.

[64] Veyrat-Charvillon, S. & Memier, M. 2006. Stereophotogrammetry of archive data and topographic approaches to debris-flow torrent measurements: calculation of channel-sediment states and a partial sediment budget for Manival torrent (Isère, France). *Earth Surf. Process. Landforms* 31 : 201–219. John Wiley & Sons, Ltd.

[65] Weidmann, M. 1998. *Notice explicative de la carte géologique de Sierre, feuille 1287. Pennique au Sud de la plaine du Rhône*.

[66] Wendeler, C., McArdell, B.W., Volkwein, A., Denk, M. & Gröner, E. *Debris Flow mitigation with flexible ring net barriers – field tests and case studies*. (in prep.)

[67] Wendeler, C., Roth, A. & Denk, M. (in prep.). *Dimensioning concept for GEOBRUGG UX/VX flexible debris flow barriers*. GEOBRUGG.

[68] Whittaker, J.G., Schaelchli, U. & Jaeggi, M.N.R.1985. Design problems with torrent check dams in Switzerland. *International Symposium on Erosion. Debris Flow and Disaster Prevention.September 3-5, 1985.* Tsukuba, Japan.

[69] Zeller, J., Geiger, H., & Röthlisberger, G. 1980. *Starkniederschläge des schweizerischen Alpen- und Alpenrandgebietes. Intensitäten und Häufigkeiten. Ausgewertete Periode 1901-1970*. Band 5 Wallis/Tessin. Eidgenössische Anstalt für das forstliche Versuchwesen.

[70] Zillgens, B., Merz, B., Kirnbauer, R. & Tilch, N. 2007. Analysis of the runoff response of an alpine catchment at different scales. *Hydrol. Earth Sci* 11: 1441-1454.

[71] Zimmermann & al. 1997. *Murganggefahr und Klimaänderung – ein GIS-basierter Ansatz.* Vdf. Hochschulverlag AG an der ETH Zürich.

[72] Zimmermann, M. & al. 2001. Illgraben – *Geomorphologie und Geschiebelieferung – Vorläufiger Bericht*. Bern und Visp, Oktober 2001.